Department of
Industry and Resources

EXPLANATORY NOTES

GEOLOGY OF THE ATLEY, RAYS ROCKS, AND SOUTHERN SANDSTONE 1:100 000 SHEETS

by S. F. Chen

1:100 000 GEOLOGICAL SERIES

Geological Survey of Western Australia

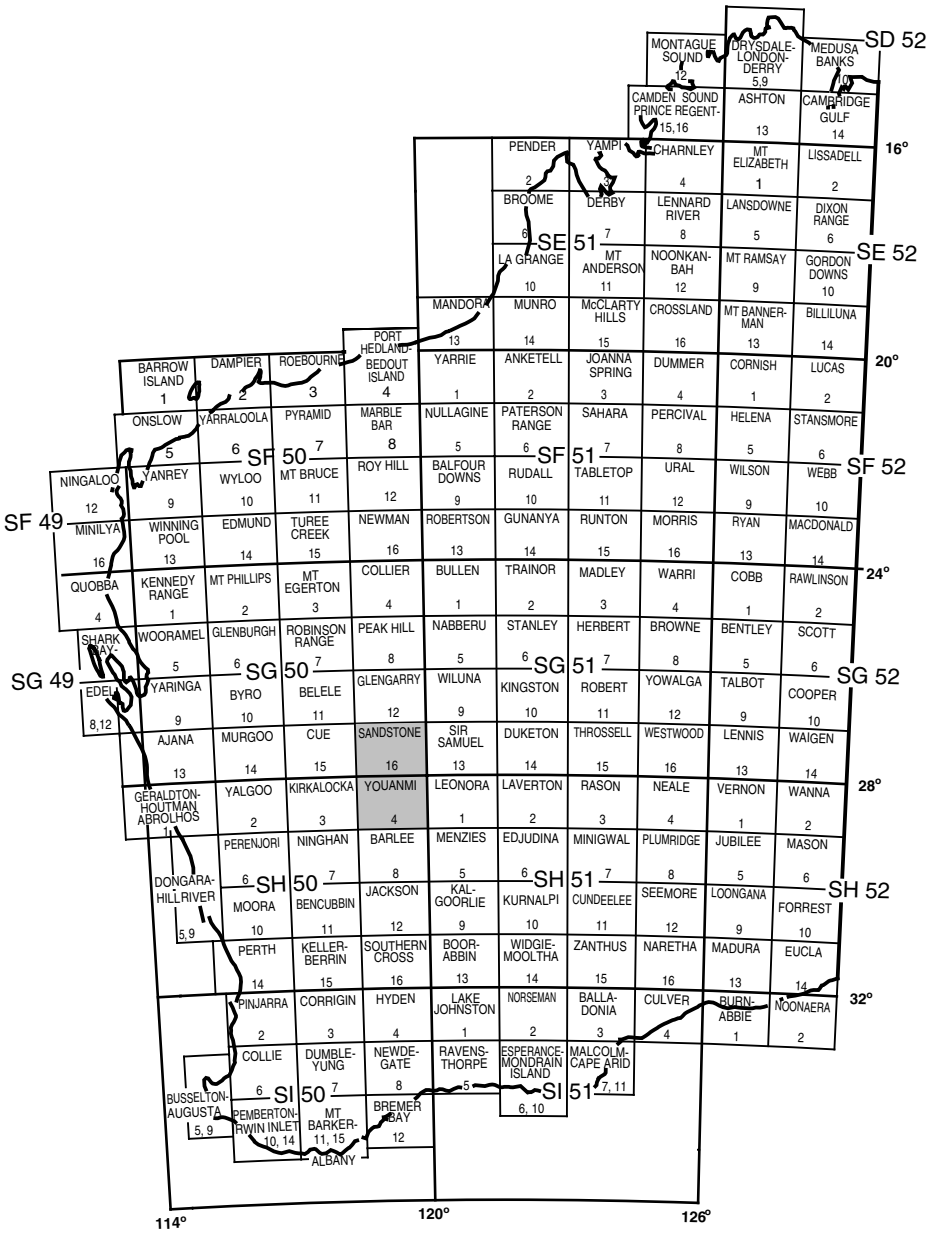

NOW THANNA 2643	YOUNO DOWNS 2743	MONTAGU 2843
SANDSTONE SG 50-16		
WOODLEY 2642	SANDSTONE 2742	LAKE MASON 2842
WINDIMURRA 2641	ATLEY 2741	EVERETT CREEK 2841
YOUANMI SH 50-4		
YOUANMI 2640	RAYS ROCKS 2740	RICHARDSON 2840

SFC118 12.11.04

GEOLOGICAL SURVEY OF WESTERN AUSTRALIA

GEOLOGY OF THE ATLEY, RAYS ROCKS, AND SOUTHERN SANDSTONE 1:100 000 SHEETS

by
S. F. Chen

Perth 2005

MINISTER FOR STATE DEVELOPMENT
Hon. Alan Carpenter MLA

DIRECTOR GENERAL, DEPARTMENT OF INDUSTRY AND RESOURCES
Jim Limerick

DIRECTOR, GEOLOGICAL SURVEY OF WESTERN AUSTRALIA
Tim Griffin

REFERENCE
The recommended reference for this publication is:
CHEN, S. F., 2005, Geology of the Atley, Rays Rocks, and southern Sandstone 1:100 000 sheets: Western Australia Geological Survey, 1:100 000 Geological Series Explanatory Notes, 42p.

National Library of Australia Card Number and ISBN 1 74168 007 7

ISSN 1321–229X

Grid references in this publication refer to the Geocentric Datum of Australia 1994 (GDA94). Locations mentioned in the text are referenced using Map Grid Australia (MGA) coordinates, Zone 50. All locations are quoted to at least the nearest 100 m.

Copy editor: M. J. Quinn
Cartography: S. Dowsett
Desktop publishing: K. S. Noonan

Published 2005 by Geological Survey of Western Australia
This Explanatory Note is published in digital format (PDF), and is available online at www.doir.wa.gov.au/gswa/onlinepublications. Laser-printed copies can be ordered from the Information Centre for the cost of printing and binding.

Further details of geological publications and maps produced by the Geological Survey of Western Australia are available from:
Information Centre
Department of Industry and Resources
100 Plain Street
EAST PERTH, WESTERN AUSTRALIA 6004
Telephone: +61 8 9222 3459 Facsimile: +61 8 9222 3444
www.doir.wa.gov.au/gswa/onlinepublications

Cover photograph:
London Bridge — a natural bridge developed in laterite about 3 km southeast of Sandstone (MGA 727518E 6899373N)

Contents

Abstract 1
Introduction 2
Location and access 2
Climate, physiography, and vegetation 2
Previous and current geological investigations 2
Archaean Yilgarn Craton 5
Regional geological setting 5
Southern Cross Granite–Greenstone Terrane 5
Sandstone greenstone belt 5
Metamorphosed ultramafic rocks (*Aur*, *Au*, *Auk*, *Aus*, *Aup*, *AmuxsYSA*) 10
Metamorphosed fine- to medium-grained mafic rocks (*Abv*, *Ab*, *Abf*, *Aba*, *Abk*, *Abr*, *Abt*, *Abg*) 11
Metamorphosed medium- to coarse-grained mafic rocks (*Aog*, *Aogf*, *Ao*) 12
Metamorphosed sedimentary rocks (*As*, *AshYSA*, *AmtqYSC*, *Acc*, *Aci*) 12
Metamorphosed fine-grained felsic rock (*Af*) 13
Geochemistry of ultramafic and mafic rocks in the Sandstone greenstone belt (by P. A. Morris) 14
Geophysical modelling of the Sandstone greenstone belt (by S. Shevchenko) 21
East Youanmi greenstone belt (*Aur*, *Aba*, *Aogf*, *Acc*, *Aci*) 22
Murchison Granite–Greenstone Terrane 23
Unaly Hill greenstone belt (*Aba*, *Aci*, *Aog*, *Aur*) 23
Granitic rocks (*Agm*, *Agf*, *Agmf*, *Agn*, *Ang*, *Ag*, *Agcm, Agb*) 23
Structural geology 24
First deformation event (D_1) 25
Second deformation event (D_2) 26
Third deformation event (D_3) 26
Post-D_3 deformation 29
Metamorphism 29
Veins and dykes (*q*, *g*, *gy*) 29
Proterozoic mafic to ultramafic dykes (*Ed*) 30
Cainozoic geology 30
Residual or relict units (*Rd*, *Rf*, *Rg*, *Rgp$_g$*, *Rk*, *Rz*, *Rzu*) 30
Depositional units (*C*, *Cf*, *Cg*, *Clc$_i$*, *Cq*, *W*, *Wf*, *A*, *A$_f$*, *A$_p$*, *A$_k$*, *L$_l$*, *L$_d$1*, *L$_m$*, *L$_d$2*, *S*, *Sl*) 31
Economic geology 31
References 33

Appendices

1. Gazetteer of localities on Atley, Rays Rocks, and southern Sandstone 36
2. Correlation of old and new rock codes for Atley, Rays Rocks, and southern Sandstone 37
3. Sample preparation and analysis for geochemistry 38
4. Recorded gold production from the Sandstone area 39
5. Gold resources in the Sandstone area 42

Figures

1. Regional geological setting of Atley, Rays Rocks, and southern Sandstone 3
2. Principal localities, roads, tracks, and physiographic features on Atley and Rays Rocks 4
3. Outline of the Yilgarn Craton, showing distribution of greenstone belts, granitic rocks, major shear zones, and faults 6
4. Interpreted bedrock geological map of the central-northern part of the Southern Cross Granite–Greenstone Terrane 7
5. Interpreted bedrock geological map of Atley and southern Sandstone 8
6. First vertical derivative aeromagnetic image of total magnetic intensity for Atley, Rays Rocks, and southern Sandstone 9
7. Lithostratigraphic column of the Sandstone greenstone belt 9
8. Relict platy and random olivine-spinifex textures in komatiite from the Bulchina openpit 11
9. Komatiite with a relict, random olivine-spinifex texture pseudomorphed by serpentine 11
10. Komatiite with a relict olivine-orthocumulate texture 11
11. Basalt with pillow-lava structures 12
12. Geochemical plots of mafic and ultramafic rocks on Atley 16
13. Geochemical plots of mafic and ultramafic rocks on Atley 18

14. Chondrite-normalized rare earth element chemistry for samples from the mafic-dominated succession 19
15. Chondrite-normalized rare earth element chemistry for samples from the ultramafic-dominated succession 20
16. Geochemical plots of mafic and ultramafic rocks on Atley 21
17. Gravity modelling across the southern Sandstone greenstone belt 22
18. Photomicrograph of amphibolite with a foliation defined by preferred alignment of hornblende and plagioclase 22
19. Shear-sense indicators in the Youanmi and Yuinmery Shear Zones 27
20. Sinistral shear-sense indicators in the Yuinmery Shear Zone 28
21. Photomicrograph of granophyric texture in granophyre 30
22. Large, angular block of syenogranite in granophyre 30

Tables

1. Representative analyses of mafic and ultramafic rocks from the Sandstone greenstone belt 15
2. Tectonic history of Atley, Rays Rocks, and southern Sandstone 25

Geology of the Atley, Rays Rocks, and southern Sandstone 1:100 000 sheets

by

S. F. Chen

Abstract

The ATLEY, RAYS ROCKS, and southern SANDSTONE 1:100 000 sheets lie predominantly in the central-northern part of the Southern Cross Granite–Greenstone Terrane of the Yilgarn Craton. ATLEY contains the majority of the Sandstone greenstone belt, which extends onto southern SANDSTONE, and a small part of the Unaly Hill greenstone belt. RAYS ROCKS contains a small part of the East Youanmi greenstone belt. The remainder of ATLEY, RAYS ROCKS, and southern SANDSTONE is occupied by granite and granitic gneiss.

The Sandstone greenstone belt has a triangular geometry and is characterized by widespread ultramafic rocks. It is bounded by the Youanmi and Edale Shear Zones to the northwest and northeast respectively, with its southern margin intruded by several large granite plutons. The Archaean lithostratigraphy of the Sandstone greenstone belt on ATLEY and southern SANDSTONE is largely controlled by the regional-scale Sandstone Syncline that was previously interpreted as a northerly plunging anticline. A mafic-dominated succession is preserved mainly on the limbs of the syncline, and contains abundant banded iron-formation, chert, and a major unit of tremolite–chlorite(–talc) schist. An ultramafic-dominated succession of mainly komatiites, and fine-grained clastic sedimentary rocks are located in the central-southern part and the northern apex of the Sandstone greenstone belt respectively. Both of them are structurally higher than, and appear to be discordant with, the mafic-dominated succession, but their exact stratigraphic relationship with the latter remains unclear due to poor exposure and structural complexity.

Archaean granitic rocks occupy or underlie much of ATLEY and southern SANDSTONE, and most of RAYS ROCKS. They are dominated by massive to weakly deformed monzogranite. Strongly deformed granitic rocks (foliated monzogranite, gneissic granite, and granitic gneiss) are commonly distributed along regional-scale ductile shear zones, or adjacent to granite–greenstone contacts, with some significant exceptions.

Three principal deformation events (D_1–D_3) have been recognized on ATLEY, RAYS ROCKS, and southern SANDSTONE. North–south compression during D_1 produced layer-parallel foliation, thrusts, and originally east-trending folds, particularly a regional-scale F_1 syncline that is outlined by a prominent unit of banded iron-formation and chert. East–west shortening during D_2 produced the regional-scale, doubly plunging Sandstone Syncline with a box-fold geometry, and other north- to north-northeast-trending, macroscopic to mesoscopic folds in greenstones, and a northerly trending gneissic banding in granitic gneiss. Progressive and inhomogeneous east–west shortening in D_3 produced the northwest-trending, sinistral Edale and Yuinmery Shear Zones, and the northeast-trending, dextral Youanmi Shear Zone.

All Archaean greenstones and granitic rocks on ATLEY, RAYS ROCKS, and southern SANDSTONE have been metamorphosed. In the Sandstone greenstone belt, the medium- to low-grade (amphibolite to mid-greenschist facies) marginal zones are characterized by high-strain, dynamic-style metamorphism, whereas the low- to very low grade central zone is characterized by low-strain, static-style metamorphism. Medium-grade, dynamic-style metamorphism has also affected the eastern margin of the East Youanmi greenstone belt. Most granitic rocks show evidence of only low-grade metamorphism, although medium- to high-grade metamorphism may have taken place in granitic gneiss.

The Sandstone greenstone belt on ATLEY and southern SANDSTONE has produced more than 25 t of gold.

KEYWORDS: Archaean, Yilgarn Craton, Southern Cross Granite–Greenstone Terrane, Sandstone greenstone belt, deformation, gold.

Introduction

These Explanatory Notes describe the ATLEY*, RAYS ROCKS, and the southern SANDSTONE 1:100 000 geological map sheets, in order to cover the whole Sandstone greenstone belt and associated granitic rocks.

Location and access

ATLEY (SH 50-4, 2741) lies in the central-northern part of the YOUANMI 1:250 000 sheet, and covers the area between latitudes 28°00' and 28°30'S and longitudes 119°00' and 119°30'E (Fig. 1). The map sheet is named after Atley Homestead† (Fig. 2). RAYS ROCKS (SH 50-4, 2740) occupies the central-southern part of the YOUANMI 1:250 000 sheet, and is bounded by latitudes 28°30' and 29°00'S and longitudes 119°00' and 119°30'E (Fig. 1). The map sheet is named after Rays Rocks (Fig. 2).

Access to ATLEY is provided by the Paynes Find – Sandstone road from Perth, and by the Menzies–Sandstone road from Kalgoorlie (Fig. 2). Pastoral tracks, connecting roads to the Atley, Dandaraga, and Blackhill (on EVERETT CREEK to the east) Homesteads, and mineral exploration grids provide access within ATLEY. The Paynes Find – Sandstone road across the northwestern corner of RAYS ROCKS, and two connecting roads to the Yuinmery Homestead provide access to RAYS ROCKS (Fig. 2). Pastoral tracks, and a connecting major track between the Yuinmery Homestead and Cashmere Downs Homestead (on RICHARDSON to the east) provide access within RAYS ROCKS. Landing grounds for light aircraft are near the Atley, Dandaraga, and Yuinmery Homesteads.

Climate, physiography, and vegetation

The region that includes ATLEY, RAYS ROCKS, and southern SANDSTONE has a semi-arid climate. Summers are dry and hot, with temperatures regularly higher than 30°C from January to March. Winters are mild to cold, with some frosty nights. Rain falls mainly in winter months from May to July. Tropical cyclones coming from the north-northwest result in occasional thunderstorms in summer months. Average annual rainfall in the region is similar to that of the township of Sandstone (Fig. 1; 247 mm; Commonwealth Bureau of Meteorology, 2004).

The topography of ATLEY, RAYS ROCKS, and southern SANDSTONE is typically flat to undulating. Altitude ranges from about 400 to 581 m above the Australian Height Datum (AHD) on ATLEY, and from about 400 to 526 m above AHD on RAYS ROCKS (Fig. 2). Like other parts of the central Yilgarn Craton, the landforms of ATLEY, RAYS ROCKS, and southern SANDSTONE are commonly controlled by the underlying rock types. Areas underlain by greenstones are characterized by subdued strike ridges and subrounded hills, whereas areas underlain by granite are characterized by rocky ground, flat pavements, well-developed breakaways up to 15 m high, and extensive sandplains. Although most of the prominent ridges are composed of banded iron-formation and chert, some are composed of mafic rocks (e.g. Black Range on ATLEY).

The present-day drainage on ATLEY and RAYS ROCKS is largely controlled by the Lake Noondie playa lake system. In the western and southern parts of ATLEY, intermittent surface water drains southwards into Lake Noondie on RAYS ROCKS, and in the central and eastern parts of ATLEY it drains eastwards into Lake Noondie on EVERETT CREEK (Riganti, 2003). On RAYS ROCKS, intermittent surface water drains into Lake Noondie (Fig. 2), except in the southeastern corner of the map sheet where it drains southwards into Lake Barlee. Both Lake Noondie and Lake Barlee form part of a series of salt lakes that drain southeasterly through the Raeside Palaeoriver (van de Graaff et al., 1977; Hocking and Cockbain, 1990). On southern SANDSTONE, intermittent surface water drains predominantly northwards into Lake Mason (Chen and Painter, in press).

ATLEY, RAYS ROCKS, and southern SANDSTONE lie within the Austin Botanical District (or Murchison Region) of the Eremaean Province (Beard, 1990). Vegetation in this region is dominated by mulga, a tall shrubland of *Acacia* species (*A. aneura* dominant), with local *Eremophila* and *Cassia* shrubs. Low woodlands of *Casuarina*, tall shrubs of *Eremophila*, and patches of *Eucalyptus* woodlands are found in greenstone hills and surrounding colluvial flats. Shrubby mulga (e.g. *Acacia aneura* and *A. quadrimarginea*) is common on granitic, rocky ground. Spinifex grass (*Triodia basedowii*) with sparse *Acacia* and *Eucalyptus* spp. covers sandplains. Mulga shrubland is typical of the alluvial plains, with denser thickets along drainage channels. Samphire (*Halosarcia halocnemoides*) and saltbush zones of *Atriplex, Maireana* and *Frankenia* are developed adjacent to, and locally within, Lake Noondie. Detailed descriptions of the ecosystems in the ATLEY – RAYS ROCKS – southern SANDSTONE and adjacent areas have been given by Beard (1976, 1990), the Biological Surveys Committee (1992), and Payne et al. (1998).

Previous and current geological investigations

In the region that includes ATLEY, RAYS ROCKS, and southern SANDSTONE, very few geological investigations or academic studies were carried out prior to 1970. The earliest geological sketch maps covering this region were produced by Talbot (1912). Historic gold mining centres and their production in the first half of the last century were documented by Gibson (1908), Maitland (1919), Clarke (1914), and Matheson and Miles (1947). Airborne magnetic and radiometric surveys of YOUANMI (1:250 000) were carried out by the Bureau of Mineral Resources (BMR, now Geoscience Australia) in 1968 (Gerdes et al., 1970). The ATLEY – RAYS ROCKS – southern SANDSTONE area was included in a regional petrochemical study by Hallberg (1976), and in the regional metamorphism studies by Binns et al. (1976) and Ahmat (1986). The first

* Capitalized names refer to standard 1:100 000 map sheets, unless otherwise indicated.

† MGA coordinates of localities mentioned in the text are listed in Appendix 1.

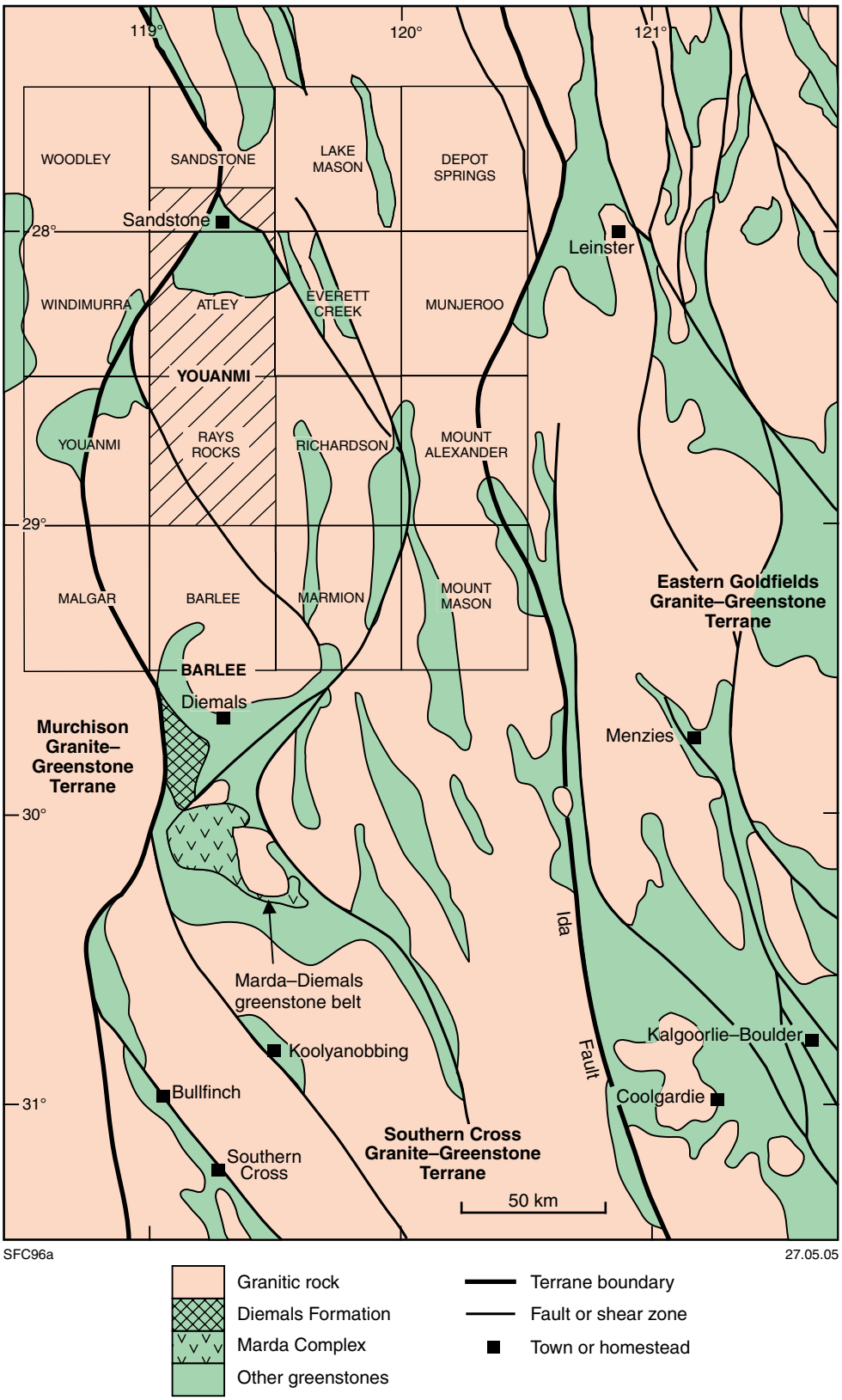

Figure 1. Regional geological setting of Atley, Rays Rocks, and southern Sandstone

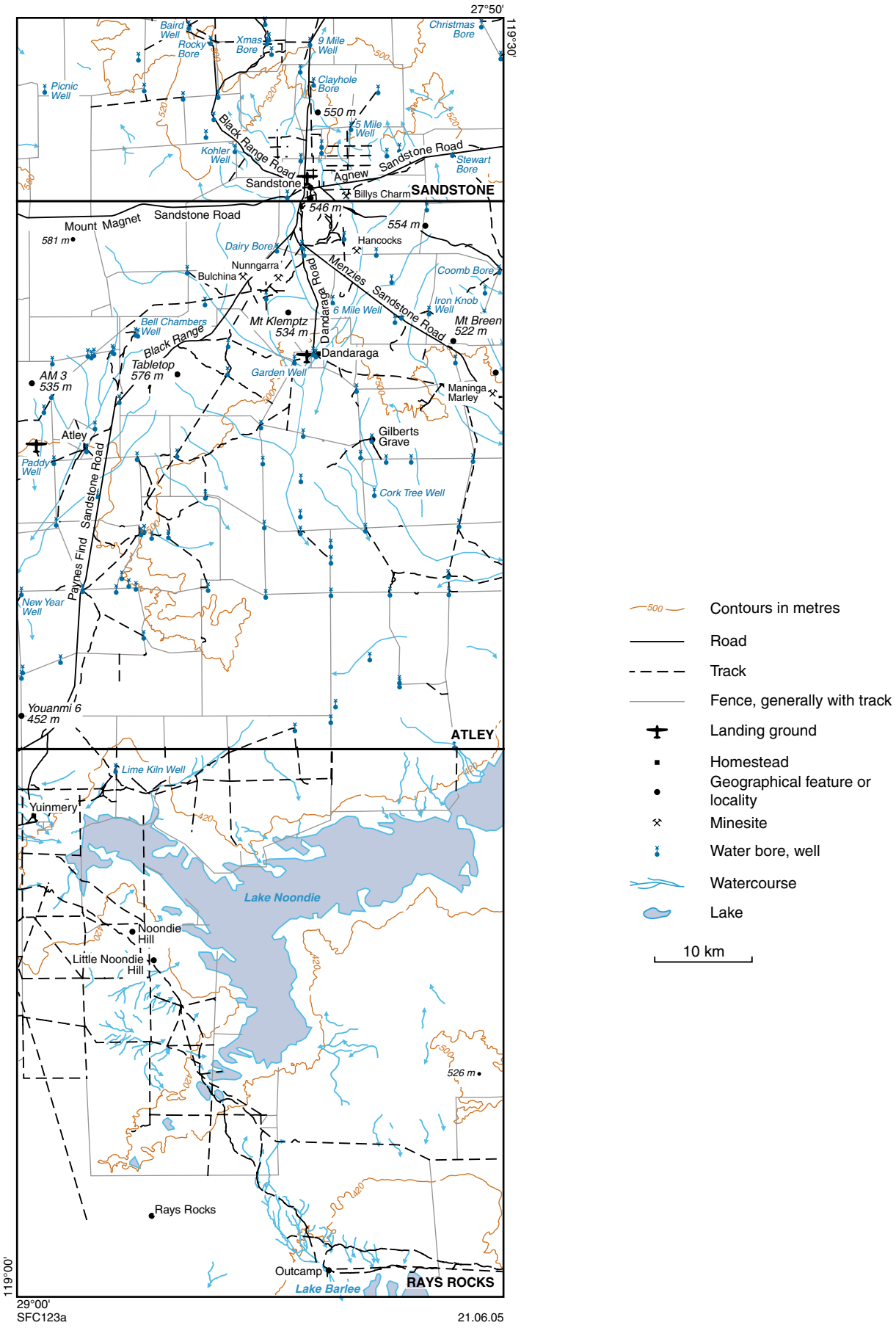

Figure 2. Principal localities, roads, tracks, and physiographic features on Atley and Rays Rocks

systematic regional geological mapping of the YOUANMI 1:250 000 sheet was carried out by the BMR and the Geological Survey of Western Australia (GSWA; Stewart et al., 1983).

The Sandstone greenstone belt on ATLEY and southern SANDSTONE (Figs 1 and 3) has undergone extensive mineral exploration since the late 1970s, which has resulted in significant gold discovery. Company reports are available through the Western Australian mineral exploration (WAMEX) open-file system at the Department of Industry and Resources (DoIR) in Perth, and at the Kalgoorlie Regional Office of GSWA. The index to this information and some of the reports are also available on the internet through <http://www.doir.wa.gov.au>.

The current work on ATLEY, RAYS ROCKS, and southern SANDSTONE forms part of the 1:100 000-scale regional geological mapping project in the central-northern part of the Southern Cross Granite–Greenstone Terrane of the Yilgarn Craton, that was initiated by GSWA in 1997. Fieldwork on ATLEY, RAYS ROCKS, and southern SANDSTONE was undertaken in 2001, 2002, and 2002–03 by using 1:25 000-scale colour aerial photographs that were taken in May 2000 (ATLEY), February 2002 (RAYS ROCKS), and May 2000 (SANDSTONE) respectively by the Department of Land Administration (DOLA; now Department of Land Information, DLI). Map compilation was assisted by Landsat Thematic Mapper (TM5) imagery. Interpretation of bedrock geology was assisted by aeromagnetic images that were derived from the 400 m line-spaced dataset collected mainly in 1999 by Kevron Geophysics Pty Ltd and Tesla Airborne Geoscience Pty Ltd; these are available from Geoscience Australia.

Archaean Yilgarn Craton

Regional geological setting

The Eoarchaean to Neoarchaean Yilgarn Craton is subdivided into five terranes from west to east (Fig. 3; Tyler and Hocking, 2001). The Narryer and South West Terranes are dominated by granite and granitic gneiss, whereas the Murchison, Southern Cross, and Eastern Goldfields Granite–Greenstone Terranes are composed of greenstone belts separated by extensive granite and granitic gneiss (Fig. 3). Currently available geochronological data suggest that greenstones in the Murchison and Southern Cross Granite–Greenstone Terranes are of similar age, and are generally older than those in the Eastern Goldfields Granite–Greenstone Terrane (Pidgeon and Wilde, 1990; Schiøtte and Campbell, 1996; Nelson, 1997, 1999, 2001, 2002; Pidgeon and Hallberg, 2000; Krapez et al., 2000; Chen et al., 2003; Blewett et al., 2004a). The Murchison and Southern Cross Granite–Greenstone Terranes share some common features in their lithostratigraphy and tectonic history, which are different from the younger greenstones and deformation events of the Eastern Goldfields Granite–Greenstone Terrane (Chen et al., 2003).

ATLEY, RAYS ROCKS, and southern SANDSTONE lie predominantly in the central-northern part of the Southern Cross Granite–Greenstone Terrane (Figs 1 and 3), and contain the Sandstone greenstone belt, and small parts of the Unaly Hill and East Youanmi greenstone belts (Figs 4 and 5; Griffin, 1990). The Sandstone and Unaly Hill greenstone belts are situated within the Southern Cross and Murchison Granite–Greenstone Terranes respectively. Although the East Youanmi greenstone belt has been assigned to the Southern Cross Granite–Greenstone Terrane by Tyler and Hocking (2001), it contains a layered mafic intrusion (Stewart et al., 1983) similar to those in the Murchison Granite–Greenstone Terrane. Further work is necessary to clarify the significance and location of the boundary between the Southern Cross and Murchison Granite–Greenstone Terranes.

Southern Cross Granite–Greenstone Terrane

No regional stratigraphy has been established for the central-northern part of the Southern Cross Granite–Greenstone Terrane, although local stratigraphy has been established in some greenstone belts, particularly the Marda–Diemals greenstone belt (1 in Fig. 3; Chen and Wyche, 2001, 2003; Wyche et al., 2001; Riganti and Chen, 2002; Greenfield, 2001; Chen et al., 2003; Riganti, 2003; Chen, 2004). Three principal deformation events have been recognized in the central-northern part of the Southern Cross Granite–Greenstone Terrane (Chen et al., 2001, 2003, 2004; Chen and Wyche, 2001, 2003; Greenfield, 2001; Wyche et al., 2001; Riganti and Chen, 2002; Riganti, 2003). D_1 north–south compression produced originally east-trending layer-parallel foliation, thrusts, and large- and small-scale folds in greenstones. D_2 east–west shortening produced the dominant north-trending upright folds in greenstones, and a northerly trending gneissic banding in granite, with local evidence for thrusting. D_3 progressive, inhomogeneous, east–west shortening produced northwest-trending sinistral and northeast-trending dextral shear zones, and regional-scale arcuate structures (Chen et al., 2001, 2003, 2004).

Sandstone greenstone belt

The Sandstone greenstone belt occupies a triangular area between the northeasterly trending Youanmi Shear Zone and the northwesterly trending Edale Shear Zone, with the northern apex of the triangle at the junction of the shear zones, and the southern margin disrupted by granite intrusions (Fig. 5). The triangle is approximately 40 km along its southern margin, and 35 km from south to north. Greenstones are locally well exposed in the western, eastern, and southeastern parts, with the best exposure in the Black Range (around MGA 712136E 6887178N). Exposure is poor in the centre and south, with extensive areas of laterite, colluvium, and sheetwash.

Stewart et al. (1983) interpreted a regional-scale, north-plunging anticline that largely defined the stratigraphy of the Sandstone greenstone belt. The lower part of their stratigraphic column was composed of ultramafic rocks and komatiitic basalt; the middle part consisted mainly of tholeiitic basalt, banded iron-formation, and chert, with minor gabbro and ultramafic rocks; and the upper part was

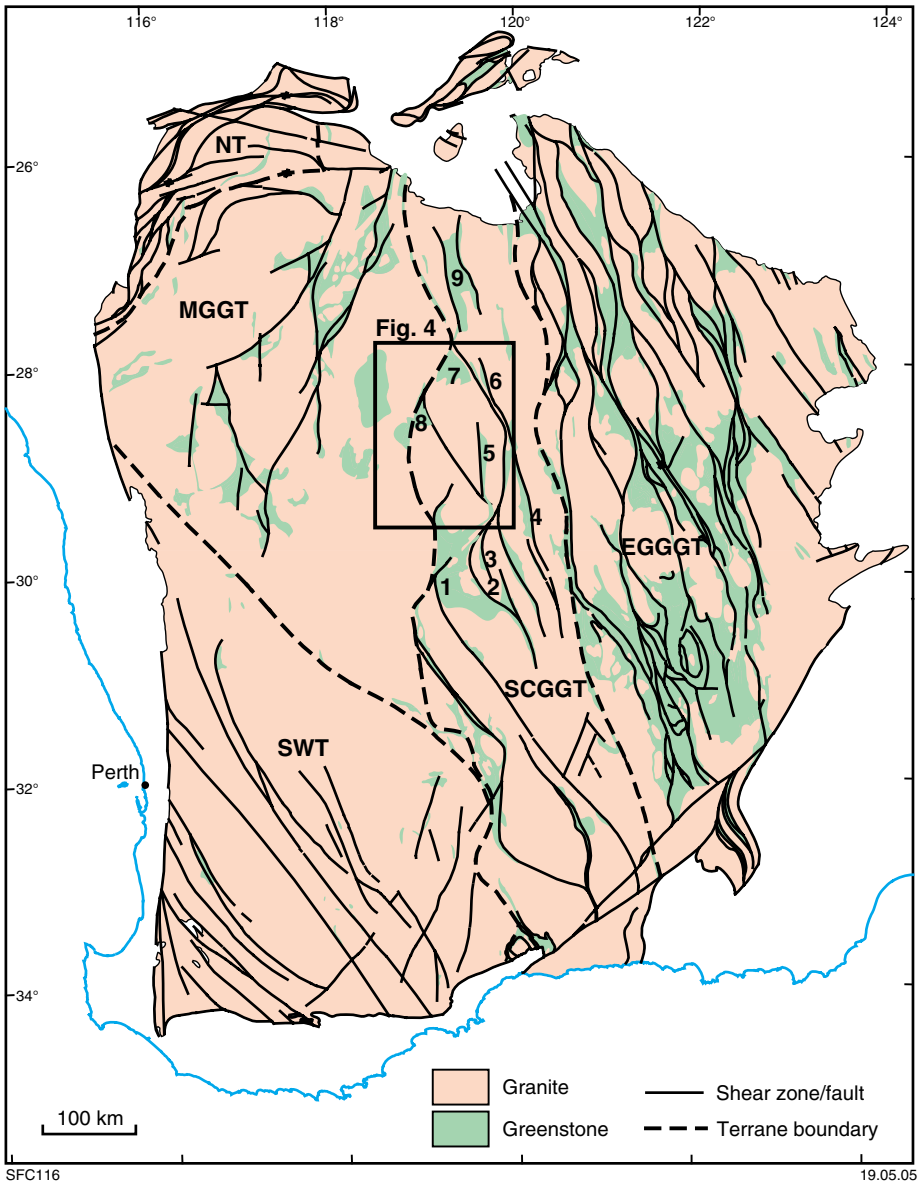

Figure 3. **Outline of the Yilgarn Craton, showing distribution of greenstone belts, granitic rocks, major shear zones, and faults. Geology is after Myers and Hocking (1998) and terrane subdivision is after Tyler and Hocking (2001): EGGGT—Eastern Goldfields Granite–Greenstone Terrane; MGGT—Murchison Granite–Greenstone Terrane; NT—Narryer Terrane; SCGGT—Southern Cross Granite–Greenstone Terrane; SWT—South West Terrane. Greenstone belts: (1) Marda–Diemals; (2) Hunt Range; (3) Mount Manning; (4) Illaara; (5) Mount Elvire; (6) Maynard Hill; (7) Sandstone; (8) East Youanmi; (9) Gum Creek**

dominated by shale, with minor gabbro and limestone. However, the recent geological mapping, combined with exploration drillhole data, and aeromagnetic image interpretation (Fig. 6), has caused this interpretation to be significantly revised. The northerly plunging anticline of Stewart et al. (1983) is reinterpreted as the northerly trending Sandstone Syncline (Fig. 5; see **Structural geology**) that largely defines the greenstone stratigraphy.

Structural complexity, poor exposure, and lack of geochronological data make it difficult to establish an overall stratigraphy for the Sandstone greenstone belt. A structurally lower, mafic-dominated succession is preserved mainly on the limbs of the regional-scale F_2 Sandstone Syncline, which is superimposed on an originally east-trending, macroscopic F_1 syncline (Fig. 5). The best exposed section through the stratigraphy is in the southwest of the greenstone belt (the Black Range area). Here, foliated basalt with local amphibolite, adjacent to the northwestern granite–greenstone contact, represent the structurally lowest exposed unit in the greenstone belt (Fig. 7). The basalt is less foliated away from the contact, and contains gabbro lenses. Above the basalt, poorly exposed, thin units of banded iron-formation and chert are intercalated with clastic sedimentary rocks, and are locally intruded by thick gabbroic sills. The sedimentary interval

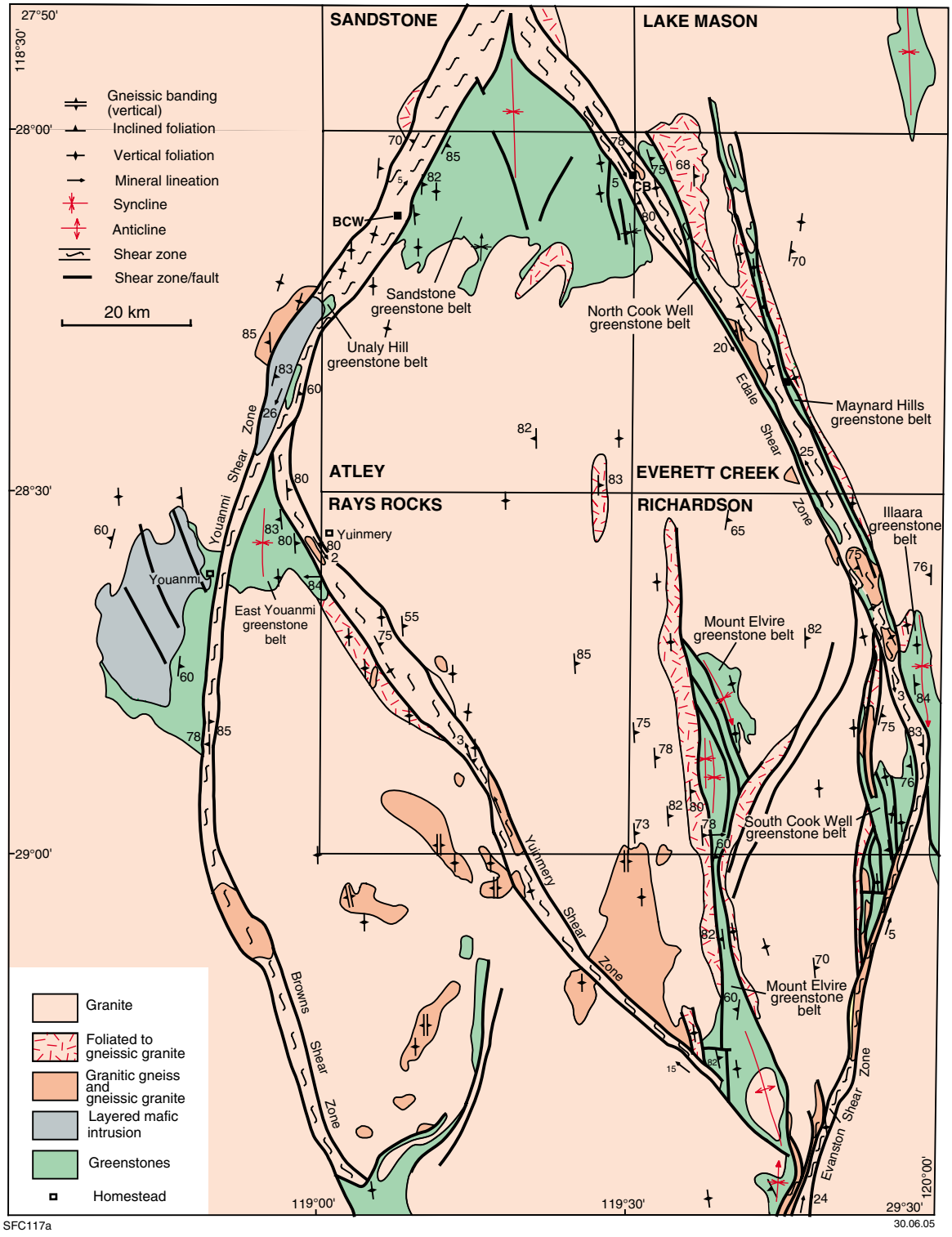

Figure 4. Interpreted bedrock geological map of the central-northern part of the Southern Cross Granite–Greenstone Terrane, compiled from published geological maps (Stewart et al., 1983; Riganti, 2002, 2003; Chen, 2004; Wyche, 2004; Atley, Rays Rocks, and southern Sandstone in these Explanatory Notes), and interpretation of aeromagnetic images. Locality names: BCW—Bell Chambers Well; CB—Coomb Bore

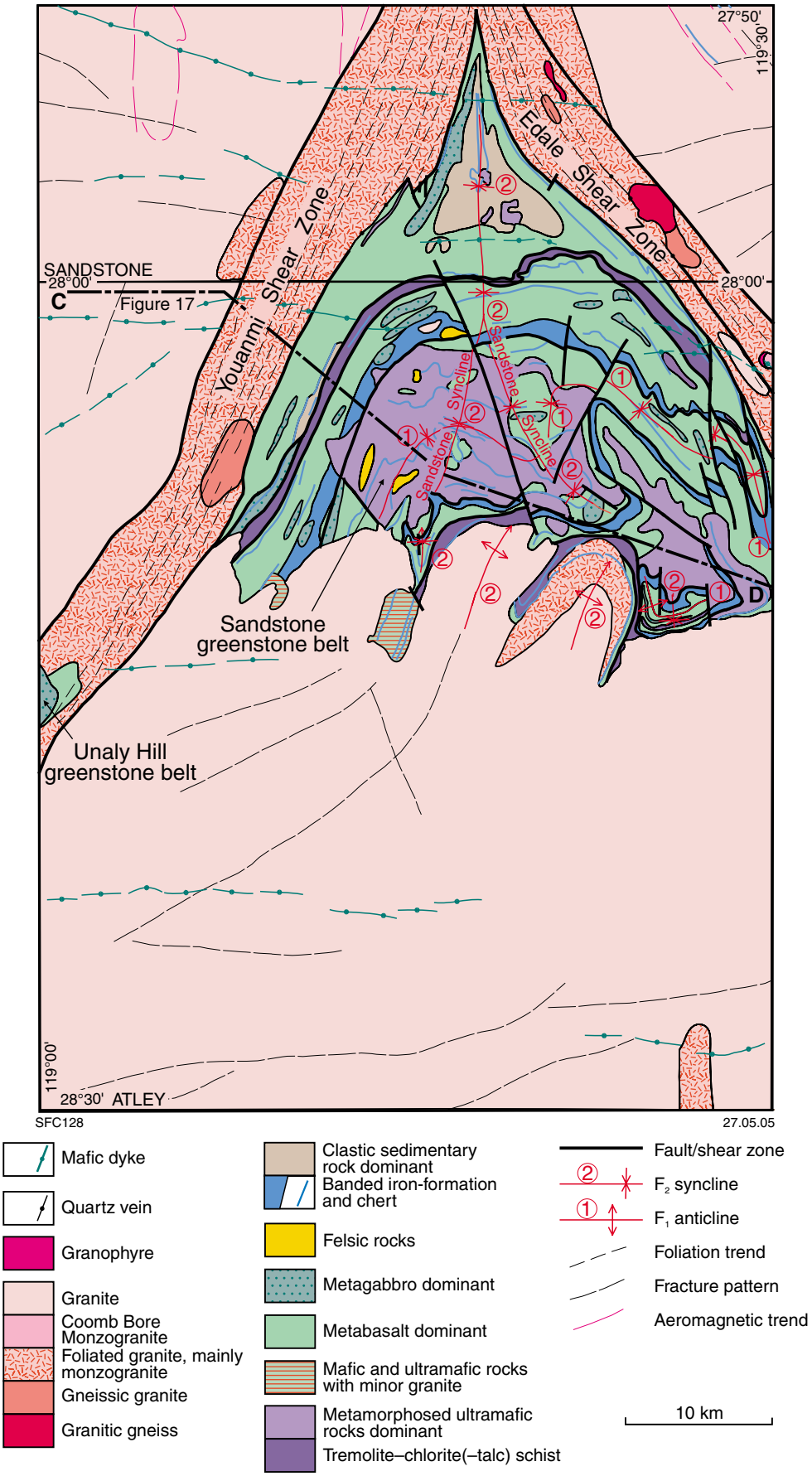

Figure 5. Interpreted bedrock geological map of Atley and southern Sandstone. C–D shows the position of the gravity traverse used in the geophysical modelling (see Fig. 17)

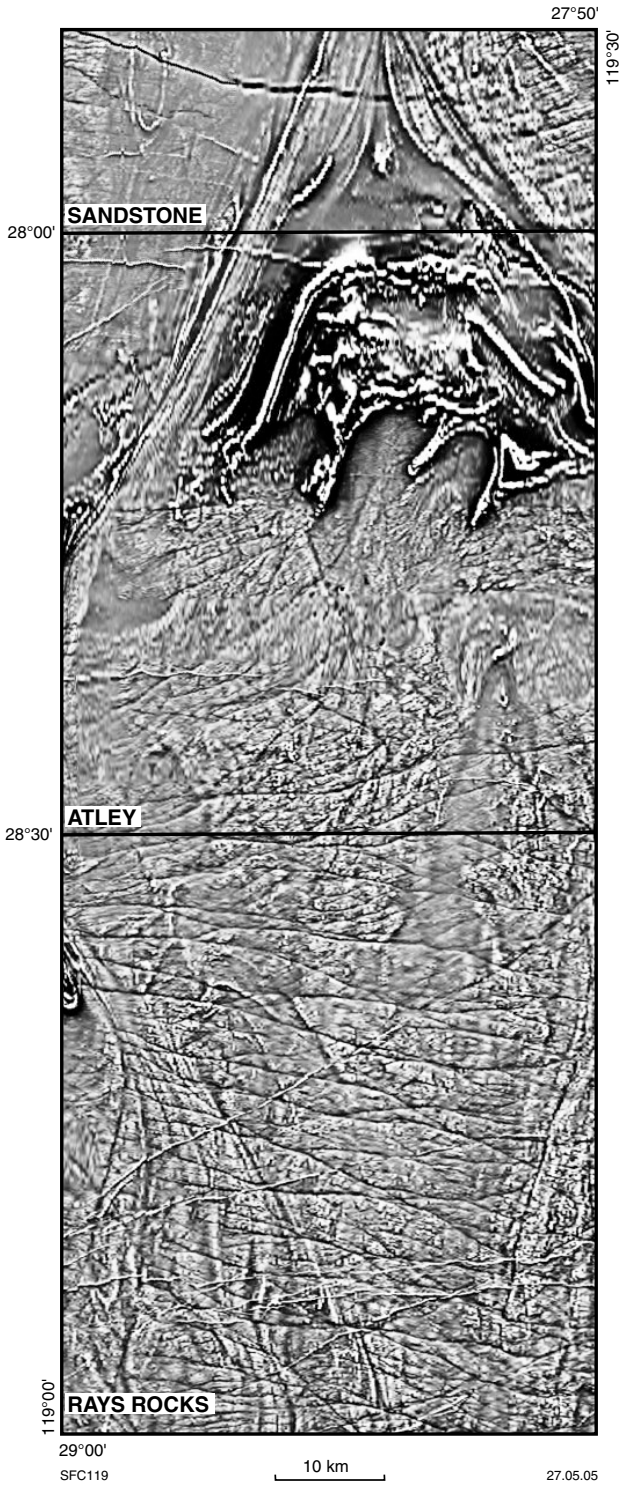

Figure 6. First vertical derivative aeromagnetic image of total magnetic intensity for ATLEY, RAYS ROCKS, and southern SANDSTONE (based mainly on 400 m line-spaced data)

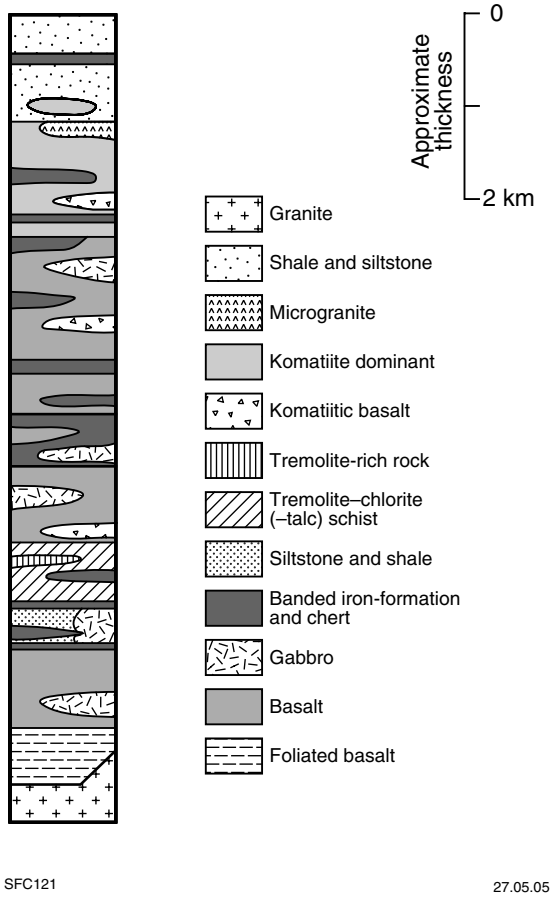

Figure 7. Lithostratigraphic column of the Sandstone greenstone belt

is overlain by a major unit of tremolite–chlorite(–talc) schist, with intercalated chert, and tremolite-rich rock possibly derived from komatiitic basalt (Fig. 7). This ultramafic unit is probably equivalent to similar rocks exposed near the northeastern and southern margins of the Sandstone greenstone belt on ATLEY (Fig. 5). The tremolite–chlorite(–talc) schist in the Black Range area is overlain by massive to weakly deformed tholeiitic basalt, with subordinate gabbro and komatiitic basalt. Above the basalt, a major interval (up to 500 m thick) of banded iron-formation and chert is locally intruded by gabbroic sills or intercalated with basalt, and is overlain by mafic rocks and thin units of banded iron-formation that are poorly exposed in the core of the Sandstone Syncline (Figs 5 and 7).

Although there is little fresh outcrop, extensive mineral exploration drillholes and areas of silica caprock indicate the presence of widespread ultramafic rocks (dominantly komatiite) in the central-southern part of the Sandstone greenstone belt. In addition subordinate banded iron-formation occupies the area. There is also evidence from drillholes and openpits for the presence of basaltic and sedimentary rocks, but these appear to be less abundant than ultramafic rocks. The stratigraphic relationship of this structurally higher, ultramafic-dominated succession with the structurally lower, mafic-dominated succession described above is uncertain due to the poor exposure. They may be unconformable with each other; or there may be a fault to separate them; or the ultramafic-dominated succession simply forms the intensely folded and thrusted top part of the mafic-dominated succession in this area. Nevertheless, this apparent abundance of ultramafic rocks is unusual for the Southern Cross Granite–Greenstone Terrane.

The structurally lower, mafic-dominated succession in the northern apex of the Sandstone greenstone belt is similar in character to that in the south. However, a lack of continuous outcrop between the northern and southern parts of the greenstone belt, and the absence of clear trends on published aeromagnetic images (Fig. 6), precludes direct correlation of units in the two areas. Structurally overlying the mafic-dominated greenstones in the northern apex area are fine-grained, clastic sedimentary rocks dominated by shale and siltstone, with intercalated banded iron-formation and chert (Fig. 5). They may be unconformable on, or structurally discordant with, the mafic-dominated succession. However, this relationship is not well exposed and remains uncertain. In the Gum Creek greenstone belt to the north (Fig. 3), there are abundant, fine-grained, clastic sedimentary rocks, with subordinate banded iron-formation and chert, at the stratigraphic top of greenstones (Tingey, 1985; Beeson et al., 1993).

The only geochronological data from within the Sandstone greenstone belt relate to a porphyritic microgranite that intrudes ultramafic rocks in the Bulchina openpit. This rock has a sensitive high-resolution ion microprobe (SHRIMP) U–Pb zircon age of 2731 ± 14 Ma (Nelson, 2004; GSWA 165364), and a SHRIMP U–Pb monazite age of 2731 ± 3 Ma (Nelson, in prep.; GSWA 165364).

The Sandstone greenstone belt straddles Atley and Sandstone (Fig. 5), with a small part extending east to Everett Creek (Fig. 1; Riganti, 2003). In the following description, old rock codes are used for Atley and Rays Rocks, and new rock codes, particularly of the rock types that are not present on Atley and Rays Rocks, are used for southern Sandstone. A correlation of old and new rock codes is shown in Appendix 2.

Metamorphosed ultramafic rocks (Aur, Au, Auk, Aus, Aup, Amuxs^{YSA})

Ultramafic rocks occupy extensive areas in the Sandstone greenstone belt (Fig. 5). Tremolite–chlorite(–talc) schist (*Aur*) on the limbs of the Sandstone Syncline is commonly conformable with bedding and igneous layering. Widespread ultramafic rocks (*Au, Auk, Aus*) in the central-southern part of the greenstone belt have been mainly revealed by recent mineral exploration drillhole data, and appear to have a discordant contact relationship with the underlying greenstones.

Tremolite–chlorite(–talc) schist (*Aur*) is exposed in areas adjacent to the northwestern, northeastern, and southeastern margins of the Sandstone greenstone belt on Atley, and probably extends to the southern margin of Sandstone (Fig. 5). A pervasive foliation within the schist is typically subparallel to the bedding of adjacent banded iron-formation and chert. Field observations, petrographic studies, and geochemical analyses indicate that the tremolite–chlorite(–talc) schist is derived from both ultramafic rocks and komatiitic basalt (*Abr* described in the next section).

In hand specimen, the tremolite–chlorite(–talc) schist derived from ultramafic rocks (*Aur*) is pale to dark green when fresh, and pale brown when weathered. In thin section, it is composed mainly of pale-green to colourless tremolite–actinolite with various amounts of chlorite, and locally contains olivine pseudomorphs. Tremolite–actinolite may form prismatic and fibrous aggregates, partly microspherulitic or fan-like, with lenses of schistose, aluminium-rich chlorite (MGA 731595E 6882851N), and accessory quartz and ilmenite. In some places (e.g. MGA 712618E 6886218N) abundant pale orange-brown vermiculite and phlogopite are probably derived from fine-grained (up to 0.5 mm across) olivine grains, forming a relict olivine-mesocumulate texture.

Massive to weakly deformed peridotite (*Aup*) is preserved locally within the tremolite–chlorite(–talc) schist (MGA 732000E 6882850N). It is greenish-grey to dark grey, with a relict olivine-cumulate texture pseudomorphed by medium- to coarse-grained serpentine.

Adjacent to the northwestern margin of the Sandstone greenstone belt (MGA 720693E 6906062N, on Sandstone), a thin unit of foliated pyroxenite (*Amuxs^{YSA}*), with intercalated serpentinite and komatiitic basalt, is bounded by amphibolite to the northwest, and by deeply weathered, undivided ultramafic rocks to the southeast. The medium- to coarse-grained pyroxenite consists mostly of tremolite–actinolite after pyroxene, with accessory plagioclase. Although the pyroxenite contains a steep, southeast-dipping foliation, a relict clinopyroxene cumulus texture is locally preserved (Tingey, 1985).

Recent mineral exploration drillhole data indicate that ultramafic rocks (*Au, Auk, Aus*) with minor intercalated komatiitic and tholeiitic basalts are widespread in the central-southern part of the Sandstone greenstone belt (Fig. 5). Although poorly exposed, the abundance of ultramafic rocks in this area is also indicated by the common silica caprock (*Rzu*). Deeply weathered ultramafic rocks have also been locally intersected by drillholes in the northern apex region of the Sandstone greenstone belt (Fig. 5).

Where preserved in outcrop (MGA 730969E 6884335N), komatiite (*Auk*) has a relict, random olivine-spinifex texture, with pseudomorphed olivine plates up to 2 cm long. Komatiite with platy and random olivine-spinifex textures (Fig. 8) is also exposed in the Bulchina openpit. Serpentinite (*Aus*) commonly preserves relict olivine-cumulate texture.

Petrographic studies, combined with geochemical analyses (see **Geochemistry of ultramafic and mafic rocks in the Sandstone greenstone belt**), indicate that the widespread ultramafic rocks intersected by mineral exploration drillholes in the central-southern part of the Sandstone greenstone belt are dominantly komatiite (*Auk*). In thin section, serpentine is abundant in some samples, but talc, tremolite, and phlogopite are the most abundant minerals. Accessory minerals include titanite, anatase, ilmenite, magnetite, goethite, and calcite. Relict olivine-spinifex and olivine-cumulate textures are locally well preserved. Random olivine-spinifex texture is mostly pseudomorphed by serpentine (Fig. 9) in a matrix composed of serpentine and tremolite. Olivine crystals in olivine orthocumulates have been altered to serpentine

SFC112 20.05.05

Figure 8. Relict platy and random olivine-spinifex textures in komatiite from the Bulchina openpit (at MGA 719337E 6893096N), with pseudomorphed olivine plates up to 5 cm long

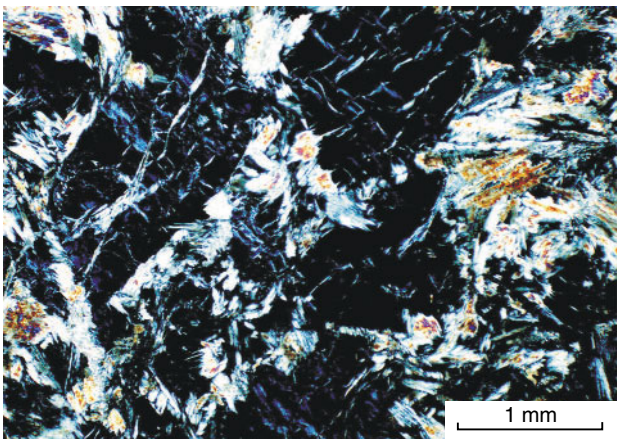

SFC126 20.05.05

Figure 10. Komatiite with a relict olivine-orthocumulate texture. Olivine grains are replaced by serpentine, and interstitial material is composed mainly of tremolite (cross-polarized light; GSWA 178342, MGA 719553E 6893605N)

(Fig. 10), talc, smectite, and vermiculite, with interstitial material composed of fine-grained tremolite, talc, and minor pyroxene. Olivine crystals in olivine mesocumulates have been pseudomorphed by phlogopite and talc, in a tremolite- or talc-rich groundmass.

Most of the ultramafic rocks intersected by mineral exploration drillholes have been altered to talc carbonate assemblages, or affected by near surface oxidation.

Metamorphosed fine- to medium-grained mafic rocks (Abv, Ab, Abf, Aba, Abk, Abr, Abt, Abg)

Metamorphosed fine- to medium-grained mafic rocks in the Sandstone greenstone belt are dominated by fine-grained metabasalt (*Abv*), and its weathered (*Ab*), deformed (*Abf*), and highly metamorphosed (*Aba*) equivalents. Komatiitic basalt (*Abk*), tremolite-rich and chlorite-rich rock (*Abr*), and mafic tuff (*Abt*) are less common. Interleaved mafic volcanic rocks with minor granite (*Abg*) outcrop along granite–greenstone contacts.

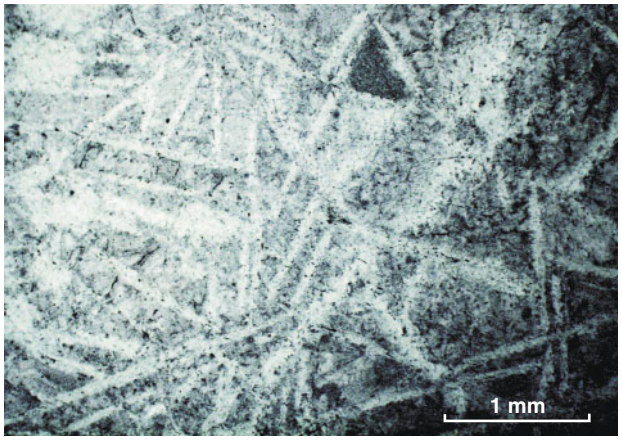

SFC125 20.05.05

Figure 9. Komatiite with a relict, random olivine-spinifex texture pseudomorphed by serpentine (plane-polarized light; GSWA 165378, MGA 738542E 6883050N)

Deeply weathered, fine-grained, massive rock with no primary quartz (*Ab*) is probably derived from metabasalt. It is yellow to brown, and locally contains pillow-lava structures.

Metabasalt (*Abv*) is typically fine- to very fine grained, and grey, with local green epidote alteration. It is generally massive to weakly foliated, and contains local, narrow, high-strain zones (commonly <30 m wide), particularly adjacent to granite–greenstone contacts. Metabasalt is typically aphyric, with rare plagioclase phenocrysts. Vesicles, and amygdales filled by quartz, calcite, and chlorite are locally abundant. Pillow-lava structures with unequivocal younging direction (Fig. 11) have only been identified in this mapping program near the eastern margin of Atley. However, Stewart et al. (1983) also recognized younging direction from pillow-lava structures 5 km northwest of Nunngarra.

In thin section, the primary minerals of basaltic rock (pyroxene and plagioclase) have been largely replaced by greenschist facies assemblages that consist of various proportions of actinolitic amphibole, albite, and chlorite. Accessory minerals include quartz, epidote, and opaque oxides (magnetite and ilmenite). Carbonate alteration of metabasalt is locally observed (e.g. near the Bulchina openpit).

Foliated basalt with minor amphibolite (*Abf*) is mainly distributed along the northwestern and northeastern margins of the Sandstone greenstone belt. Foliated basalt typically contains a pervasive foliation, and is weakly to moderately recrystallized. In thin section, it is composed mainly of greenschist facies assemblages (actinolite and plagioclase), with accessory chlorite, quartz, and

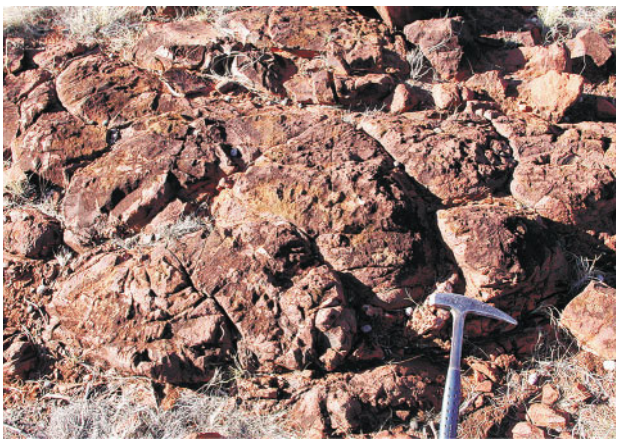

SFC113 20.05.05

Figure 11. Basalt with pillow-lava structures (MGA 744406E 6881307N)

opaque minerals. Hornblende is present in some samples that are transitional to amphibolite (e.g. MGA 710985E 6889148N).

Amphibolite (*Aba*) is a dark-grey, fine- to medium-grained, typically strongly foliated and recrystallized rock. It is derived mainly from basalt (e.g. MGA 737388E 6877519N and MGA 735967E 6880888N), and locally from dolerite (e.g. MGA 735766E 6880630N). In thin section, the amphibolite derived from basalt is composed of calcic plagioclase and blue-green hornblende, with accessory quartz and opaque minerals. Mineral segregation forms hornblende-rich and plagioclase-rich zones that are parallel to the foliation. In the amphibolite derived from dolerite, pyroxene has been largely replaced by hornblende, but some pyroxene crystals and a relict granular texture are locally preserved.

Mafic rocks that are interleaved with minor granite (*Abg*) outcrop along some granite–greenstone contacts. For example, near the southern margin of the Sandstone greenstone belt (MGA 720115E 6875987N), poorly exposed amphibolite and foliated basalt are irregularly intruded by medium- to coarse-grained, massive monzogranite.

Massive to weakly deformed komatiitic basalt (*Abk*) has a characteristic pyroxene-spinifex texture that is pseudomorphed by skeletal and acicular tremolite–actinolite (up to 10 mm long), in a fine-grained matrix composed of albite and tremolite–actinolite, with accessory chlorite, quartz, epidote, and opaque minerals (e.g. MGA 718868E 6897703N, and 729632E 6891866N).

Although some of the thin units of tremolite- and chlorite-rich rock (*Abr*), locally with a relict pyroxene-spinifex texture, have been separated from tremolite–chlorite(–talc) schist (*Aur*), many cannot be resolved at 1:100 000 scale. In thin section, tremolite- and chlorite-rich rock typically contains minor plagioclase, and locally contains phlogopite lamellae (e.g. MGA 713174E 6888130N).

A unit of mafic tuff (*Abt*; MGA 712932E 6888144N), about 10 m thick, is well exposed between komatiitic basalt and medium- to coarse-grained gabbro. The mafic tuff is grey to pale grey, and thinly bedded to laminated, with individual layers ranging from less than 1 mm to several millimetres in thickness. In thin section, the mafic tuff is composed of fine grained amphibole and chlorite, and fine- to very fine grained plagioclase and quartz, with accessory muscovite. Bedding is defined by the variation in composition and grain size.

Metamorphosed medium- to coarse-grained mafic rocks (Aog, Aogf, Ao)

Metamorphosed, medium- to coarse-grained mafic rocks are dominated by massive to weakly deformed, medium- to coarse-grained gabbro (*Aog*), with less abundant foliated gabbro (*Aogf*), and deeply weathered gabbro (*Ao*). They are commonly intercalated with banded iron-formation, chert, basalt, and amphibolite. Most gabbroic sills are conformable with bedding and igneous layering, but some gabbroic bodies appear to have intruded across stratigraphy (e.g. MGA 733500E 6885500N). Thin lenses of dolerite and gabbro, ranging from 20 to 100 m in thickness are locally contained within thick metabasalt.

Deeply weathered, medium- to coarse-grained rocks with no primary quartz are probably derived from metagabbro (*Ao*). They are typically massive, and reddish-brown to yellowish-brown. In these rocks, the original mineralogy has been altered, but a medium- to coarse-grained granular texture is locally preserved.

Pale- to dark-grey metagabbro (*Aog*) is medium to coarse grained, and massive to weakly deformed. Metamorphosed, pale-grey gabbro contains more abundant plagioclase than dark-grey metagabbro. A granular texture is commonly preserved in massive to weakly deformed metagabbro, although primary pyroxene has been largely replaced by amphibole and chlorite. Plagioclase is typically finer grained, and interstitial to amphibole and chlorite grains. Accessory minerals in metagabbro include quartz (up to 5%) and iron oxides.

Adjacent to the southeastern margin of the Sandstone greenstone belt (MGA 737388E 6877519N), a unit of heterogeneously deformed metagabbro (*Aogf*) is intercalated with amphibolite (*Aba*). It is medium to coarse grained, and contains a weak to moderate foliation dipping steeply to the north. Within the Youanmi Shear Zone, a small unit of amphibolite (*Aba* at MGA 708680E 6890462N) is derived from strongly foliated and metamorphosed dolerite, in which pyroxene has been largely replaced by hornblende, but the granular texture of former pyroxene is partly preserved.

Metamorphosed sedimentary rocks (As, Amtq$_{YSC}$, Acc, Aci, Ash$_{YSA}$)

Metasedimentary rocks in the Sandstone greenstone belt include locally exposed, thin units of clastic sedimentary rocks (*As*, *Amtq$_{YSC}$*), widespread chemical sedimentary rocks (*Acc*, *Aci*), and extensive, poorly exposed, fine-grained clastic sedimentary rocks (*Ash$_{YSA}$*) in the north on SANDSTONE.

Thin units of undivided clastic sedimentary rocks (*As*) on ATLEY are dominated by siltstone and shale, with minor mudstone, and fine-grained sandstone (e.g. around MGA 716400E 6899100N, and 714200E 6892000N). They are pale to darker grey, and weather to yellowish- and purplish-brown. Although they are commonly weathered and foliated, bedding defined by grain size variation can be locally recognized. These clastic sedimentary rocks are typically conformable with the intercalated banded iron-formation and chert, and are most abundant in the northwestern part of the Sandstone greenstone belt on ATLEY. Thin units of shale and siltstone (*AshYSA*) on SANDSTONE are intercalated with chert, or mafic volcanic rocks (e.g. MGA 722500E 6906400N).

On SANDSTONE, clastic metasedimentary rocks of dominantly shale and siltstone, with minor sandstone and felsic volcaniclastic rock (*AshYSA*) are widespread in the northern part of the Sandstone greenstone belt (Fig. 5), and appear to discordantly overlie the mafic-dominated greenstones. They are intercalated with thin units of chert and banded iron-formation that are at least partly derived from silicification and ferruginization of shale and siltstone, probably due to weathering. Local dolomitic shale formed by carbonate alteration was reported by Tingey (1985) on the western side of the Sandstone–Meekatharra Road.

Shale and siltstone are grey to black when fresh, and weather to yellow and brown. Most of these rocks have been moderately to deeply weathered. Fresh shale and siltstone have been found only in mineral exploration drillhole chips, some of which are graphitic (e.g. MGA 726486E 6908536N). Although locally well exposed, the widespread, fine-grained clastic metasedimentary rocks (*AshYSA*) on SANDSTONE are typically poorly exposed, with small outcrops scattered in colluvial gravel and debris.

In thin section, shale is composed mainly of very fine grained sericite(–chlorite), and clay minerals, with thin (commonly <1 mm) layers of quartz parallel to a pervasive slaty cleavage (e.g. MGA 726278E 6910508N and MGA 726242E 6909453N). Some coarser quartz grains are strongly flattened and elongated along the cleavage. Iron oxides are disseminated throughout the samples, but are mainly concentrated along the cleavage, and along later fractures perpendicular to the cleavage. Siltstone is composed mainly of fine- to very fine grained quartz, with lesser amounts of sericite(–chlorite), clay minerals, and accessory feldspar, that are stained by iron oxides (e.g. MGA 726514E 6910552N and MGA 726267E 6910704N).

The widespread, fine-grained, clastic, metasedimentary rocks (*AshYSA*) on SANDSTONE are commonly foliated. In some places, a northerly trending foliation has obliterated bedding. In other places, the millimetre- to centimetre-scale rhythmic layering of shale and siltstone represents bedding that is defined by variation in colour and grain size, and is typically subparallel to the foliation (e.g. MGA 726267E 6910704N). Where visible, a northerly trending bedding is subvertical, or dips steeply to both the east and west.

A single unit of quartzite (*AmtqYSC*), with intercalated quartz-rich sandstone and siltstone, is present in strongly foliated monzogranite, about 3.5 km east of the Sandstone greenstone belt (MGA 730701E 6914202N on SANDSTONE). The quartzite is pale grey to white, and massive to well bedded. Bedding is generally parallel to the foliation in the adjacent monzogranite, and is locally deformed into mesoscopic, variously plunging folds with wavelengths of 20–40 cm. The stratigraphic relationship of this quartzite unit with the Sandstone greenstone belt is uncertain, although it may be similar to the quartzites at the stratigraphic base of the Maynard Hills and Illaara greenstone belts to the south (Riganti, 2003; Chen, 2004; Wyche et al., 2004).

In thin section, the quartzite is composed of fine- to medium-grained quartz (>90%), with minor fine- to very fine grained muscovite, and accessory plagioclase and iron oxides. Most quartz grains are clean, and some contain deformation lamellae and fractures. Some coarser grained quartz crystals have reaction margins, indicating recrystallization. Plagioclase grains are partly sericitized. Muscovite is generally aligned parallel to bedding in finer grained beds, and is disseminated in coarser grained beds.

Widespread chemical metasedimentary rocks in the Sandstone greenstone belt include banded iron-formation (*Aci*) and chert (*Acc*) that form most of the prominent ridges on ATLEY and RAYS ROCKS. They are at various stratigraphic levels, particularly in the middle part of the greenstone stratigraphy (Fig. 5). Individual units of banded iron-formation and chert are typically less than 50 m thick, but a composite thickness of several closely spaced units may be over 500 m. Banded iron-formation and chert are intercalated with various rock types, particularly gabbro sills and basalt, and locally with ultramafic and clastic sedimentary rocks.

Both banded iron-formation (*Aci*) and chert (*Acc*) are well bedded and laminated at millimetre- to centimetre-scale. Banded iron-formation typically has a high magnetite content, and is visible as strong, typically linear anomalies on aeromagnetic images (Fig. 6). It may change into chert along strike, reflecting variations in iron content.

In thin section, banded iron-formation (*Aci*) comprises alternating bands of iron oxides and fine-grained quartz. Compared to banded chert that is dominated by quartz, banded iron-formation is composed mainly of iron oxides (magnetite, and hematite).

Metamorphosed chert (*Acc*) is typically well banded, and consists of white, pale-grey, and brown bands less than 1 mm thick. Most chert units are ferruginous to some degree. In thin section, light-coloured bands consist mainly of microcrystalline and recrystallized quartz, whereas darker bands consist of iron oxides and cryptocrystalline quartz.

Metamorphosed fine-grained felsic rock (Af)

Metamorphosed, fine-grained felsic rock (*Af*) includes porphyritic microgranite that locally intrudes the Sandstone greenstone belt, but outcrop is rare. Moderately weathered, foliated porphyritic microgranite (*Af*) is exposed in a small area (MGA 721978E 6894702N) about 3 km northeast

of the Bulchina openpit. It is pale grey to yellowish, and contains visible quartz and feldspar grains in a fine- to very fine grained quartzofeldspathic groundmass. About 400 m to the south (MGA 721929E 6894310N), fine-grained, massive to weakly deformed felsic rock or porphyritic microgranite is deeply weathered, and partly altered to kaolinite. Similar rock has also been intersected in some drillholes (e.g. MGA 718449E 6888793N, and 720141E 6890044N).

Porphyritic microgranite in the Bulchina openpit is quartz- and feldspar-phyric, and has an irregular intrusive relationship with the surrounding mafic–ultramafic rocks. It contains quartz (1–2%) and feldspar (1%) phenocrysts, up to 2 mm long, in a fine-grained, quartzofeldspathic, and sericite-altered groundmass, with accessory leucoxene, and carbonate. A sample from the microgranite has yielded a SHRIMP U–Pb zircon age of 2731 ± 14 Ma (Nelson, 2004; GSWA 165364), and a SHRIMP U–Pb monazite age of 2731 ± 3 Ma (Nelson, in prep.; GSWA 165364).

Geochemistry of ultramafic and mafic rocks in the Sandstone greenstone belt (by P. A. Morris)

Forty-two mafic and ultramafic rock samples from the Sandstone greenstone belt on ATLEY have been analysed. Representative analyses are presented in Table 1 and the complete set of data are available for download from the department's website at <http://www.doir.wa.gov.au>. Sample preparation and analytical conditions are discussed in Appendix 3. Each sample has been analysed for major element oxides and some trace elements by XRF, and for the remaining trace elements and rare earth elements (REE; La–Lu) by ICP-MS. FeO was determined by titration, and volatile loss by gravimetry. In the following, all oxide concentrations discussed are those derived by recalculating measured values to 100% volatile-free. Measured loss-on-ignition (LOI) values range from 0.22 to 10.8 in basalts, 3.9 to 5.4 in komatiitic basalts (apart from GSWA 192447; 18.3%), and 4.2 to 18.3% in komatiites.

Of the 42 samples, 14 are from the mafic-dominated succession, and 28 from the ultramafic-dominated succession. They are divided into basalt, komatiitic basalt, and komatiite, based on MgO contents, after recalculating the major element oxide values to 100% on a volatile-free basis. It is now generally accepted that komatiites have >18% MgO (e.g. Kerr and Arndt, 2001), but the MgO content for separation of basalt and komatiitic basalt is more arbitrary. A value of 12% MgO is used here.

Based on MgO contents, there are seven basalt samples, three komatiitic basalt samples, and four komatiite samples (two with MgO about 18% and two with MgO about 27%) from the mafic-dominated succession, and 27 komatiite samples (MgO contents ranging from 19 to 26%), and one komatiitic basalt sample (GSWA 192447) from the ultramafic-dominated succession.

In order to further examine compositional differences between the mafic- and ultramafic-dominated successions, and use geochemical data to comment on petrogenesis, it is necessary to assess the extent of element mobilization. Petrographic examination shows that the samples are variably serpentinized, carbonated and chloritized, as well as being deformed and probably weathered. The presence of feldspar in rocks with spinifex texture, and biotite in tremolite-bearing rocks is indicative of alteration. Sproule et al. (2002) made an assessment of alteration for komatiites from the Abitibi greenstone belt in Canada. They noted that published studies of komatiites suggested that high field-strength elements (HFSE: Nb, Ta, Zr, Hf), Th, and the heavy REE (HREE; Gd–Lu) can remain in their igneous concentrations if the rocks have been hydrated but not carbonated or deformed. In a study of ultramafic rocks from northern Labrador, Collerson et al. (1991) argued that the immobility of Y and the HREE could be demonstrated by constant Y/Ho close to the primitive mantle value of 28. For the ATLEY samples, komatiites from the mafic-dominated succession have average Y/Ho of 28 (range 23 to 32), whereas those from the ultramafic-dominated succession have an average of 27 (range 23 to 34), consistent with a lack of mobility of Y and the HREE. In a study of mafic and ultramafic rocks from the Pilbara Craton, Arndt et al. (2001) noted the correlation of REE (except Eu) and HFSE, suggesting immobility. They also noted that Al, Ti, and Fe plotted on coherent trends, and SiO_2 and CaO correlated with MgO for some, but not all, suites. The alkalis generally showed some scatter. From this study, they concluded that the REE, HFSE and Ni were immobile.

Transition elements, such as Cr, V, Sc, Mn, Fe, Mg, Co, and Ni, which are retained in either igneous or metamorphic minerals can also remain relatively immobile during hydration (Sproule et al., 2002). In contrast, large ion lithophile elements (LILE: Cs, Rb, K, Na, Sr, Ba, and Eu^{2+}) are commonly remobilized; these elements are typically found in labile phases (e.g. glass, feldspar). In addition, silica is viewed as mobile during alteration and metamorphism. A further complicating issue is the low concentrations of key elements such as Ta, Nb, and Hf in komatiites, and the difficulty of obtaining accurate and precise analysis of these elements, which are normally found at levels close to that of analytical detection.

A plot of LOI vs MgO (Fig. 12a) shows a broad positive correlation in that basaltic rocks in the mafic-dominated succession have lower MgO contents and appear to be less susceptible to alteration (taking LOI as an indication of alteration) than komatiites. Komatiitic basalts and komatiites from the ultramafic-dominated succession (e.g. GSWA 192447 and 178332) have significantly higher LOI values (up to 18%) than other samples with similar MgO.

In terms of MgO vs SiO_2 (Fig. 12b), there is a clear separation of basalts and komatiitic basalts in the mafic-dominated succession, from komatiites in both the mafic- and ultramafic-dominated successions in terms of MgO, but no correlation between SiO_2 and MgO.

Labile components, such as Na_2O and K_2O, are generally in low concentrations in komatiites, and predictably higher in mafic rocks. Exceptions are samples such as GSWA 192447, which has Na_2O = 1.70% and K_2O = 0.32%. There is, however, little correlation between LOI contents and Na_2O and K_2O.

Table 1. Representative analyses of mafic and ultramafic rocks from the Sandstone greenstone belt

		Mafic-dominated succession				*Ultramafic-dominated succession*		
GSWA no.	*DL*	*178345*	*165383*	*165392*	*165394*	*178341*	*165379*	*165388*
Rock type		*basalt*	*komatiitic basalt*	*komatiite*	*komatiite*	*komatiite*	*komatiite*	*komatiite*
					Percentage			
SiO_2	0.01	53.51	50.62	42.53	48.53	47.06	46.79	45.70
TiO_2	0.01	0.84	0.92	0.28	0.57	0.59	0.31	0.49
Al_2O_3	0.01	14.78	7.41	6.10	7.50	6.56	8.18	5.54
Fe_2O_3	0.01	1.86	4.57	1.74	1.44	6.25	6.78	1.11
FeO	0.01	6.88	7.37	7.20	8.84	4.75	2.99	8.55
MnO	0.01	0.21	0.18	0.13	0.17	0.11	0.12	0.12
MgO	0.01	7.11	13.199	24.44	17.88	18.32	19.95	23.02
CaO	0.01	11.36	7.54	5.49	8.17	5.12	4.77	4.97
Na_2O	0.01	2.15	1.64	0.05	1.26	0.51	0.77	0.06
K_2O	0.01	0.12	0.05	0.01	0.04	0.07	0.09	0.02
P_2O_5	0.01	0.09	0.06	0.02	0.06	0.07	0.01	0.05
SO_3	0.01	0.03	<0.01	0.16	0.01	0.0	<0.01	0.01
LOI	0.01	0.22	5.36	10.47	4.26	9.45	8.02	8.85
Total		**99.16**	**98.92**	**98.62**	**98.73**	**98.86**	**98.78**	**98.49**
Fe_2O_3 (T)	0.01	9.51	12.76	9.74	11.27	11.52	10.10	10.61
					Parts per million (unless otherwise indicated)			
Ag	0.01	0.04	<0.01	0.05	0.02	0.03	<0.01	0.02
As	0.5	<0.5	2.2	2.9	2.2	<0.5	1.5	4.4
Ba	10	32	23	24	32	16	31	20
Be	0.1	0.1	0.3	<0.1	0.2	<0.1	<0.1	<0.1
Bi	0.1	0.2	0.2	<0.1	<0.1	<0.1	<0.1	<0.1
Cd	0.1	<0.1	0.03	0.06	0.06	<0.1	0.04	0.02
Ce	0.1	7.47	3.08	0.99	4.88	4.51	2.06	8.89
Cr	2	223	2 363	2 723	2 371	3 397	3 497	2 751
Cs	0.01	0.16	0.27	0.16	0.19	0.18	0.17	0.2
Cu	1	55	78	24	66	60	104	56
Dy	0.01	3.09	3.28	1.18	2.27	2.44	1.43	1.64
Er	0.01	1.92	2.06	0.79	1.38	1.39	0.88	0.95
Eu (ppb)	1	811	736	130	458	512	198	204
F	50	201	365	<50	142	236	115	110
Ga	0.2	13.9	10.5	6.5	9.9	8.8	7.9	7.5
Gd	0.01	2.72	3.07	0.84	2.11	2.09	1.16	1.56
Ge	0.1	1.3	2.1	1.4	1.7	1.8	1.5	1.5
Hf	0.1	1.6	1.8	0.4	1.2	1.2	0.7	0.9
Ho	0.01	0.68	0.69	0.26	0.48	0.49	0.29	0.32
La	0.02	2.91	1.44	0.32	2.19	1.99	0.88	3.72
Lu	0.01	0.29	0.23	0.09	0.18	0.2	0.09	0.1
Mo	0.1	1.3	0.4	0.4	2.5	0.7	0.6	0.2
Nb	0.1	2.1	3.8	0.1	1.9	1.7	0.8	1.4
Nd	0.01	6.72	3.51	0.99	4.28	4.88	2.22	5.54
Ni	2	110	596	1 305	924	1 506	1 391	1 496
Pb	0.5	<0.5	1	0.7	<0.5	<0.5	<0.5	<0.5
Pr	0.01	1.09	0.57	0.15	0.81	0.81	0.4	1.13
Rb	1	<1	<0.3	<0.3	<0.3	<1	0.8	<0.3
Sb	0.1	<0.1	0.3	0.6	<0.1	<0.1	0.2	0.3
Sc	2	46	41	26	29	29	26	23
Sm	0.01	2.13	1.63	0.2	1.19	1.49	0.65	1.03
Sn	0.5	1	1.6	<0.5	0.6	0.9	<0.5	<0.5
Sr	1	93.8	64.4	56.2	43.4	46.2	47	49.2
Ta	0.1	0.2	0.2	<0.1	<0.1	0.1	<0.1	<0.1
Tb	0.01	0.49	0.59	0.17	0.37	0.37	0.22	0.27
Th	0.1	0.4	0.7	<0.1	0.4	0.4	0.3	0.2
U	0.1	0.11	0.15	<0.01	0.14	<0.1	0.05	0.08
V	5	296	218	151	191	131	132	162
Y	0.5	18.1	21	7.2	13.8	13.7	7.1	9.2
Yb	0.01	1.74	1.83	0.73	1.35	1.28	0.66	0.8
Zn	1	77	90.9	54.8	74.1	77	67.3	66.1
Zr	1	45	65	8	40	34	17	27
MgO*		7.19	14.11	27.73	18.93	20.49	21.98	25.68
Ti/Zr		113	91	236	90	117	119	120
$(La/Sm)_{CN}$		0.88	0.57	1.03	1.19	0.86	0.87	2.33
Al_2O_3/TiO_2		17.59	8.06	21.93	13.24	11.09	26.66	11.43
$(Al_2O_3/TiO_2)_{MN}$		0.79	0.36	0.99	0.59	0.50	1.20	0.51
Zr/Nb		21.43	17.11	80.00	21.05	20.00	21.25	19.29

Table 1. (continued)

GSWA no.	DL	Mafic-dominated succession				Ultramafic-dominated succession		
Rock type		178345 basalt	165383 komatiitic basalt	165392 komatiite	165394 komatiite	178341 komatiite	165379 komatiite	165388 komatiite
		Parts per million (unless otherwise indicated)						
La_{CN}		12.28	6.08	1.35	9.24	8.40	3.71	15.70
$(La/Yb)_{CN}$		1.20	0.56	0.31	1.16	1.12	0.96	3.34
$(Gd/Yb)_{CN}$		1.293	1.387	0.951	1.293	1.350	1.454	1.613
$(Gd/Yb)_{MN}$		1.262	1.360	0.932	1.267	1.323	1.424	1.580
Eu/Eu*		1.03	1.01	0.97	0.88	0.89	0.70	0.49
Y/Ho		27	30	28	29	28	24	29
Nb/Th		5	5		5	4	3	7
			ADK	AUDK	ADK	ADK	AUDK	ADK

NOTES:
DL detection level
Fe_2O_3 (T) total Fe as Fe_2O_3.
LOI loss-on-ignition (i.e. sample weight loss after heating to about 1000°C)
MgO* MgO recalculated loss-on-ignition free, with analytical total of 100%
CN chondrite-normalized, using C1 chondrite values of Sun and McDonough (1989)
MN mantle-normalized, using primitive mantle (pyrolite) values of McDonough and Sun (1995)

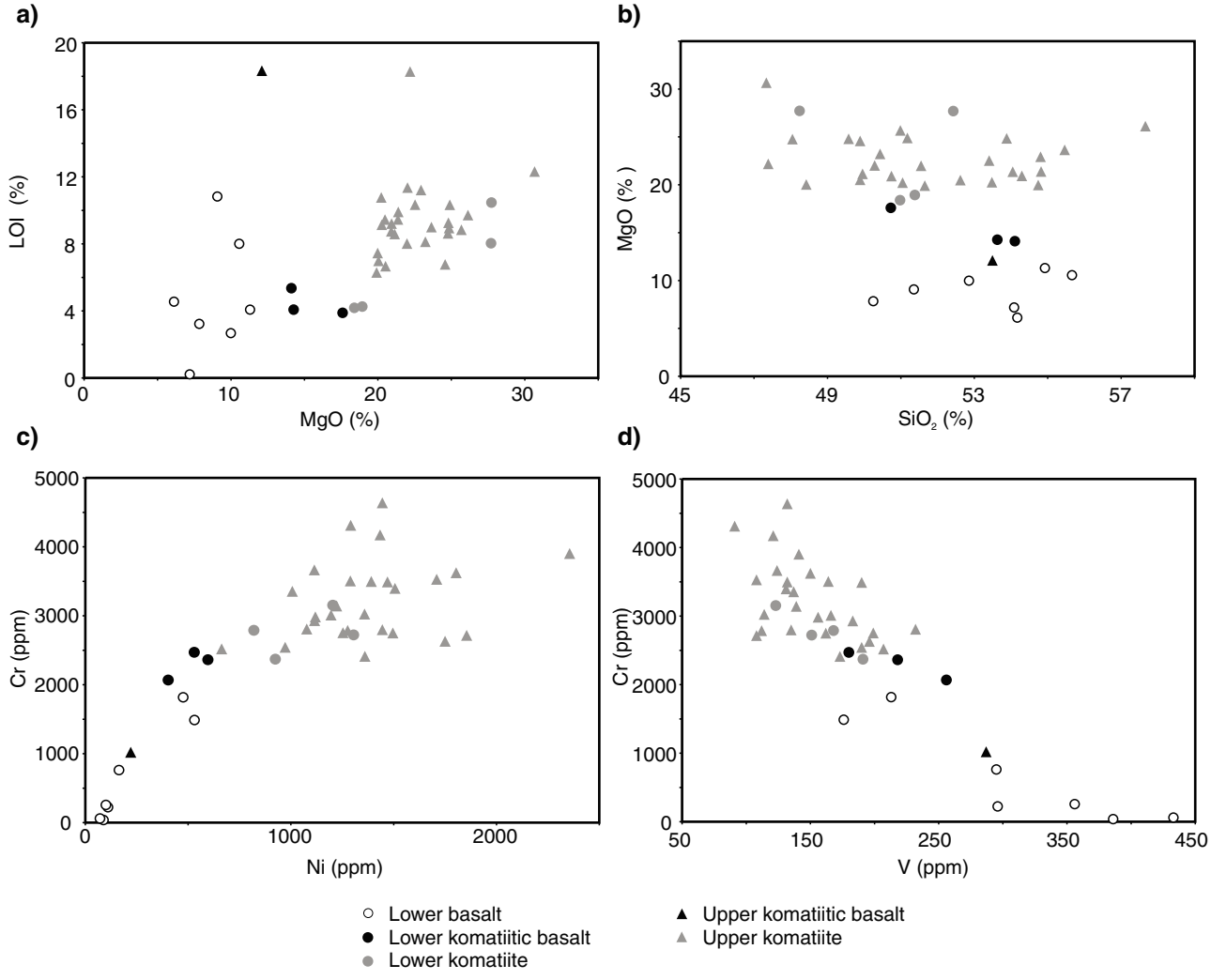

Figure 12. Geochemical plots of mafic and ultramafic rocks on Atley. Oxide values have been recalculated to 100% on a volatile-free basis: a) loss-on-ignition (LOI) vs MgO; b) MgO vs SiO_2; c) Cr vs Ni; d) Cr vs V. Lower basalt, lower komatiitic basalt, and lower komatiite samples are from the mafic-dominated succession; upper komatiitic basalt and upper komatiite samples from the ultramafic-dominated succession

The transition elements Cr and Ni show a positive correlation, although there is some scatter amongst komatiites (Fig. 12c). There is no separation of komatiites in terms of stratigraphic position, with most komatiites having Cr >2500 ppm and Ni >1000 ppm. Chromium and V show a broad negative correlation (Fig. 12d), with some scatter amongst komatiites, and lower Cr and higher V in komatiitic basalts and basalts.

Rubidium contents are generally low in most rocks, and are commonly less than the detection level (0.3 ppm) in komatiites. Strontium (Sr) concentrations in komatiites are generally <60 ppm, and show no correlation with either LOI or SiO_2, although one komatiite sample from the ultramafic-dominated succession (GSWA 178332) has high Sr (193.4 ppm) and LOI (18.28%). Barium (Ba) contents of komatiites are normally <40 ppm and do not correlate with LOI. Basaltic rocks have predictably higher contents of LILE compared to komatiites.

The relative immobility of the HFSE is confirmed by the strong correlation of Ti and Zr (r = 0.97; Fig. 13a) and Zr and Nb (r = 0.98; Fig. 13b). The average Zr/Nb of 23 for the Sandstone greenstone belt lies approximately midway between a normal mid-ocean-ridge basalt (N-MORB) average of 32 (Sun and McDonough, 1989) and a primitive mantle value of 16 (McDonough and Sun, 1995). There is no discernible separation of samples from the mafic- and ultramafic-dominated successions. A plot of Ti/Zr vs LOI (Fig. 13c) shows no correlation, and most Ti/Zr values lie in the range 90 to 120, comparable to a primitive mantle value of 115 (McDonough and Sun, 1995), and an N-MORB value of 102 (Sun and McDonough, 1989). Several samples (e.g. GSWA 165392, 165380, 165381, and 165384) have notably higher Ti/Zr. It is possible that these higher values result from small amounts of oxide, possibly titanomagnetite (7% in GSWA 165381) or leucoxene (GSWA 165392), or problems with analytical uncertainty at concentrations close to detection level for elements contained in phases that may be incompletely dissolved during preparation for ICP-MS analysis. This is well illustrated by samples with significantly high Zr/Nb, such as GSWA 165392, which has Zr = 8 ppm, but Nb = 0.1 ppm. Zirconium (Zr) and Y are also well correlated (Fig. 13d), apart from two samples from the mafic-dominated succession (GSWA 165389 and 165368) which have higher Y contents. Collerson et al. (1991) noted that komatiites commonly have Nb/Th between 7 and 15. Komatiite samples from the ultramafic-dominated succession on Atley have Nb/Th from 2 to 7, whereas most komatiite samples from the mafic-dominated succession have Nb/Th<5. Collerson et al. (1991) ascribed low Nb/Th in komatiites to crustal contamination. This may also be the case for komatiites in the Sandstone greenstone belt, as decreasing Nb/Th is accompanied by an increase in Th (Fig. 13e).

Basalts from the mafic-dominated succession have flat chondrite-normalized REE patterns ($(La/Yb)_{CN}$ = 1.1 to 1.9) with $(La)_{CN}$ from 12 to 25, and almost no Eu anomalies (Eu/Eu* = 0.9 to 1; Fig. 14a). Exceptions are GSWA 165368 and 165389, which are light REE (LREE)-enriched ($(La)_{CN}$ = 214 and 111) and have higher total REE contents. GSWA 165389 has a well-developed negative Ce anomaly, and both samples have weakly developed negative Eu anomalies (Eu/Eu* = 0.84 and 0.92). REE patterns are correspondingly steeper ($(La/Yb)_{CN}$ = 10 and 4). Both of these samples do not have unusually high LOI contents (8.0 and 4.1%), but both have high volatile-corrected SiO_2 contents near 55%.

Komatiitic basalts from the mafic-dominated succession have weakly enriched to slightly LREE-depleted patterns ($(La/Yb)_{CN}$ = 0.6–1.8), with generally lower LREE contents than basalts ($(La)_{CN}$ = 6–15), and no Eu anomalies (Fig. 14b). As such, their REE patterns show some overlap with basalts. GSWA 192447 has a weakly enriched REE pattern ($(La/Yb)_{CN}$ 1.3) with $(La)_{CN}$ = 12, and Eu/Eu* = 1.

Komatiites from the mafic-dominated succession have weakly enriched to LREE-depleted patterns ($(La/Yb)_{CN}$ = 0.3–1.4) with $(La)_{CN}$ from 1.4 to 11 (Fig. 14c). Some samples have slight negative Eu anomalies with Eu/Eu* as low as 0.8. GSWA 165392 has an aberrant REE pattern and notably higher Ti/Zr (240). This sample has poor textural preservation, significant carbonate, and disseminated primary and secondary opaque oxide, the latter possibly resulting in higher TiO_2 content. Komatiites from the ultramafic-dominated succession (Fig. 15a–d) have $(La/Yb)_{CN}$ from 0.6 to 5 and $(La)_{CN}$ from 1 to 20. Although Eu/Eu* in some samples is as high as 1.5, most values are <1. Both samples 178338 and 165375 have high LOI values (10.77 and 9.14 %) and well-developed negative Eu/Eu*, and it is likely that negative Eu anomalies are due to mobility of Eu during alteration. GSWA 165380 has low REE concentrations and an erratic REE pattern, which is likely to be be due to analytical problems.

It is possible that LREE enrichment, and the development of negative Ce and positive or negative Eu anomalies are due to alteration. A plot of $(La/Sm)_{CN}$ vs MgO (Fig. 16a) shows that most samples have $(La/Sm)_{CN}$ <2, although several komatiite samples from the ultramafic-dominated succession and two basalt samples from the mafic-dominated succession have higher $(La/Sm)_{CN}$.

Komatiites can be divided into Al-depleted (ADK; Barberton type) and Al-undepleted (AUDK; Munro type) based on their Al_2O_3/TiO_2 ratio and HREE chemistry. Al_2O_3/TiO_2 ranges for AUDK are 15 to 25, and <15 for ADK (e.g. Sproule et al., 2002). As some komatiite samples from the Sandstone greenstone belt have feldspar, it is possible that Al_2O_3/TiO_2 ratios could partly reflect alteration. In terms of Al_2O_3/TiO_2 vs LOI (Fig. 16b), samples fall into two broad groupings, with a break at about 15 (i.e. on the ADK–AUDK boundary). Samples are not separated on stratigraphic grounds, and there is no correlation between Al_2O_3/TiO_2 and LOI, although samples with lower Al_2O_3/TiO_2 show a slightly greater range in LOI. If Al_2O_3 was mobilized and TiO_2 immobile (which seems likely, given results on HFSE from previous studies, confirmed below), a positive correlation would be expected with LOI. Al_2O_3/TiO_2 does not correlate with SiO_2, with both groups of samples showing a similar range in SiO_2. Similarly, there is no correlation with MgO. From these variations, it is possible that komatiites from both the mafic- and ultramafic-dominated successions consist of both AUDK and ADK types.

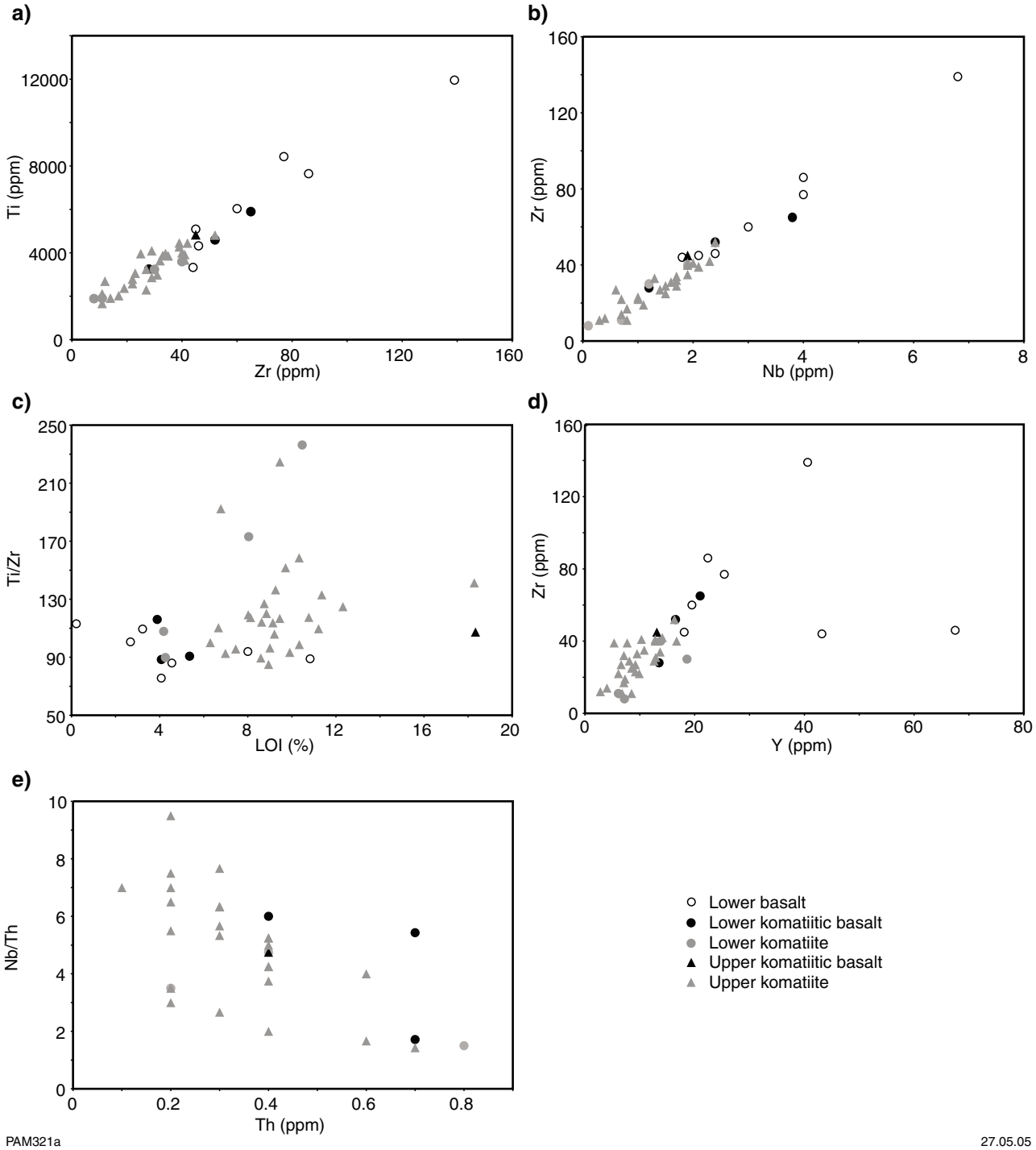

Figure 13. Geochemical plots of mafic and ultramafic rocks on ATLEY. Oxide values have been recalculated to 100% on a volatile-free basis: a) Ti (converted from TiO_2) vs Zr; b) Zr vs Nb; c) Ti/Zr (Ti calculated from TiO_2) vs LOI; d) Zr vs Y; e) Nb/Th vs Th. Decreasing Nb/Th with increasing Th is consistent with crustal contamination. Lower basalt, lower komatiitic basalt and lower komatiite samples are from the mafic-dominated succession; upper komatiitic basalt and upper komatiite samples from the ultramafic-dominated succession

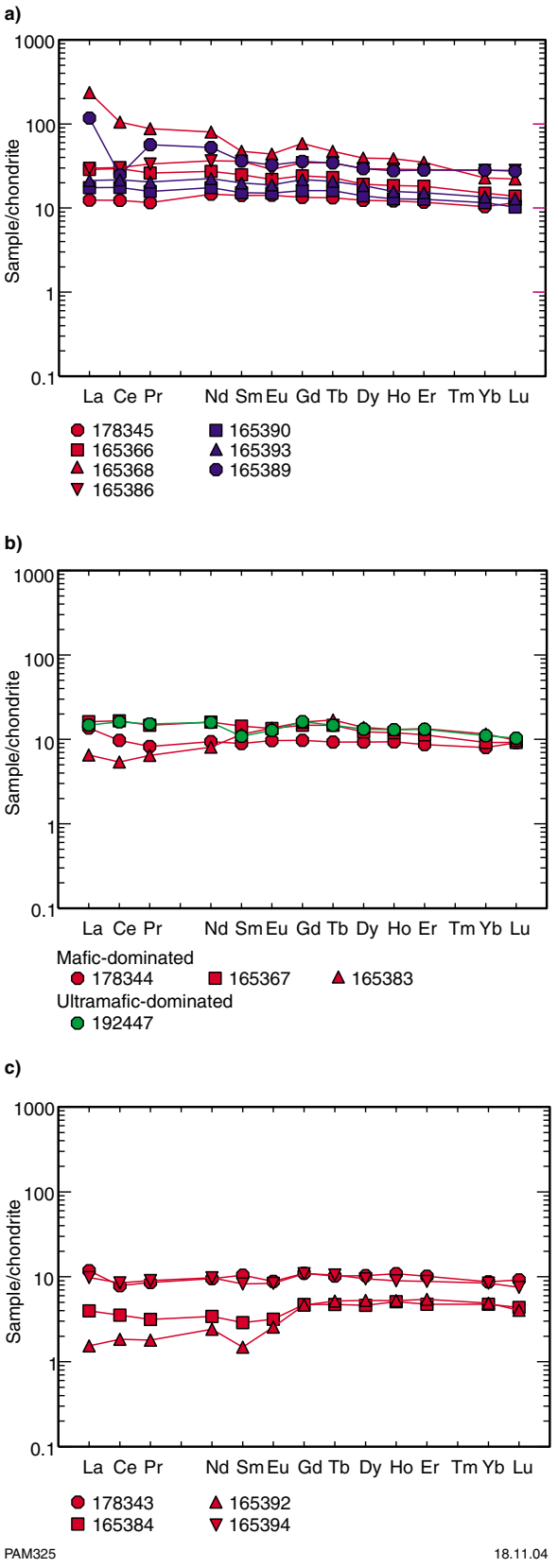

Figure 14. Chondrite-normalized rare earth element chemistry for samples from the mafic-dominated succession. Normalization factors are C1 chondrite from Sun and McDonough (1989): (a) basalt; (b) komatiitic basalt (includes GSWA 192447 from the ultramafic-dominated succession); (c) komatiite

A plot of mantle-normalized Al_2O_3/TiO_2 vs Gd/Yb (Fig. 16c) shows a broad negative correlation. Both Al and Yb are more strongly partitioned into garnet than either Ti or Gd, meaning that samples with lower $(Al_2O_3/TiO_2)_{MN}$ and higher $(Gd/Yb)_{MN}$ are from a source in which garnet has been retained, or represent a melt from which garnet has crystallized. If the variation in Al_2O_3/TiO_2 reflected alteration, then the relationship with $(Gd/Yb)_{CN}$ would not be expected. It is clear from this diagram that komatiites in the Sandstone greenstone belt form a series from AUDK to ADK, but there is no division according to stratigraphy. As Al is more strongly partitioned into garnet than Ti, ADK are indicative of melting at higher pressure where garnet is retained in the source or where majorite garnet is a fractionating phase (Arndt and Lesher, 1992; Gruau et al., 1990). AUDK represent melting at shallower depths or melting of a garnet-depleted source. Several authors (e.g. Arndt and Lesher, 1992) have suggested that the preponderance of ADK in the early Archaean, and AUDK in the late Archaean results from early extraction of garnet at higher pressure followed by melting of a depleted source in the late Archaean. Another possibility is a greater depth of melt segregation for ADK compared to AUDK (dynamic melting), which could explain the occurrence of both komatiite types in the same greenstone succession. It was noted that c. 2900 Ma komatiites from the Forrestania area of the Southern Cross Granite–Greenstone Terrane (Perring et al., 1996) also consist of both AUDK and ADK, although komatiites from lower in the stratigraphy are ADK, whereas, AUDK are found at higher stratigraphic levels. Perring et al. (1996) argued that this could be attributed to less retention of garnet in the source over time, as well as progressively shallower depths of melting.

Several conclusions can be made from the above discussion:

1. Despite notable alteration visible in thin section, and dominance of metamorphic mineralogy, HFSE, REE (apart from La, Ce and Eu in some cases), transition elements such as Cr, Ni, and V, and possibly MgO, have remained relatively immobile in the Sandstone greenstone belt. Most komatiites are LREE-depleted, and as LREE enrichment in komatiites of the Sandstone greenstone belt is normally accompanied by development of an Eu anomaly and, less commonly, a negative Ce anomaly, it is unlikely that LREE enrichment results from crustal contamination, although this cannot be assessed due to alteration. However, as Th is probably less mobile, decreasing Nb/Th with increasing Th contents is consistent with crustal contamination. Alkaline earth elements, such as Na, K, Rb, Sr, and Ba, have been mobilized.

2. Variations in Cr vs MgO, Cr vs Ni, and Cr vs V show that the chemistry of komatiites and komatiitic basalts is in part controlled by fractional crystallization. The chemistry of basalts from the mafic-dominated succession is similar to Archaean tholeiites from elsewhere, with flat to slightly LREE-enriched REE patterns and Ti/Zr ratios close to 100.

3. Geochemical analysis has confirmed the presence of widespread komatiites in the central–southern part of

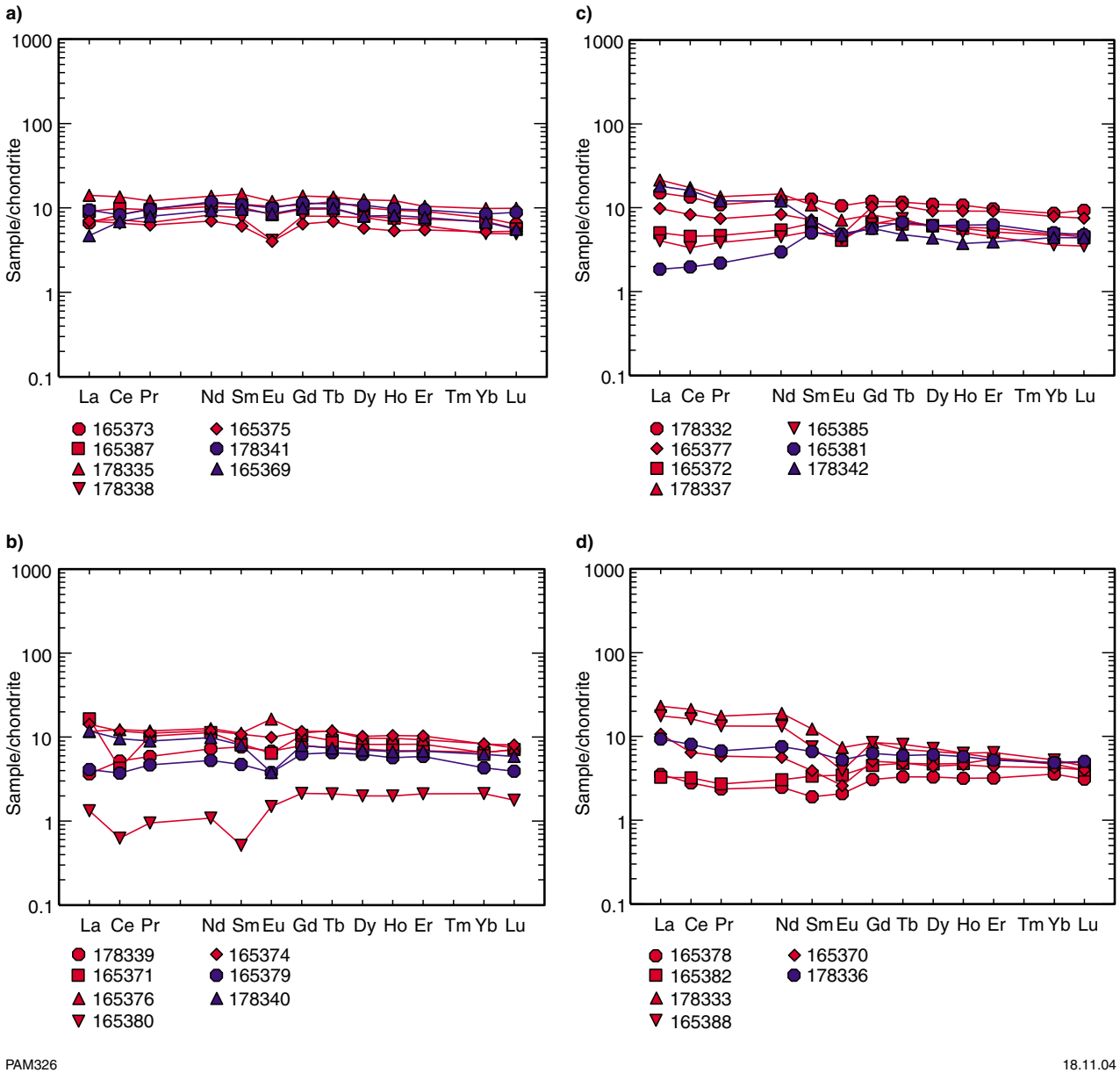

Figure 15. Chondrite-normalized rare earth element chemistry for samples from the ultramafic-dominated succession: a) komatiites with 19.91–20.52% MgO; b) komatiites with 20.91–22.02% MgO; c) komatiites with 22.19–24.77% MgO; d) komatiites with 24.80–30.67% MgO. Oxide values have been recalculated to 100% on a volatile-free basis. Normalization factors are C1 chondrite from Sun and McDonough (1989)

the Sandstone greenstone belt. The chemical similarity of komatiites from the mafic- and ultramafic-dominated successions suggests that the komatiites may belong to the same magma type, but not necessarily the same magma batch (but see argument about Al_2O_3/TiO_2 vs Gd/Yb below).

4. Mantle-normalized Al_2O_3/TiO_2 – Gd/Yb shows that komatiites in the Sandstone greenstone belt span the ADK–AUDK fields, with no separation into either AUDK or ADK according to stratigraphic levels. Based on previously published work, it is likely that ADK represent melting at higher pressure, where garnet was either retained in the source or fractionated from the melt. Alternatively, ADK probably represent melting of a garnet-depleted source at shallower depths. One way to accommodate both AUDK and ADK in the same succession is by dynamic melting, where different melt fractions are produced simultaneously. More speculatively, if this process involved a mantle plume (commonly invoked for komatiites), initial melting of the asthenosphere by the rising plume head could account for basalts and komatiitic basalts in the mafic-dominated succession, and their paucity in the ultramafic-dominated succession, representing the komatiite tail (cf. Campbell et al., 1989).

Geophysical modelling of the Sandstone greenstone belt (by S. Shevchenko)

A semi-regional gravity traverse was carried out from Atley to western Everett Creek to determine the thickness of greenstones and to define the geometry of granite–greenstone contacts in the southern part of the Sandstone greenstone belt. The gravity data, which were collected with a variable station spacing along the traverse, are shown in Figure 17. The station spacing is about 1 km over the granite and greenstones, with a closer station spacing of 250–500 m across granite–greenstone contacts, and in areas with predictable gravity gradients. An observed gravity line profile obtained from the traverse was used for 2D forward geophysical modelling.

Airborne magnetic data with 200 m line spacing were collected by World Geoscience Corporation in 1985. A magnetic intensity profile was extracted from the gridded data, along the same locations as the gravity profile, and used as a magnetic channel in the modelling. The geophysical modelling package Model Vision Pro was used to perform the modelling. A number of limited length polygonal prisms were created and assigned petrophysical properties for the construction of the 2D greenstone model.

Physical properties for the rocks shown in Figure 17 were taken from publications in which similar granite–greenstone terranes have been modelled (House, 1996; Lane et al., 2003; Blewett et al., 2004b).

The gravity data was the primary method used to model the geometry of greenstones, whereas magnetic data were used to model the high-intensity magnetic bodies of probable banded iron-formation within the greenstones. The best fit of the observed and modelled curves indicates inward-dipping granite–greenstone contacts on both sides of the model, with an average depth of 4 km. Two positive gravity anomalies, A and B in Figure 17, were modelled as high-density rocks of likely banded iron-formation or amphibolite, although data collected with closer gravity station spacing and information on the physical properties of these rocks would be needed for more reliable

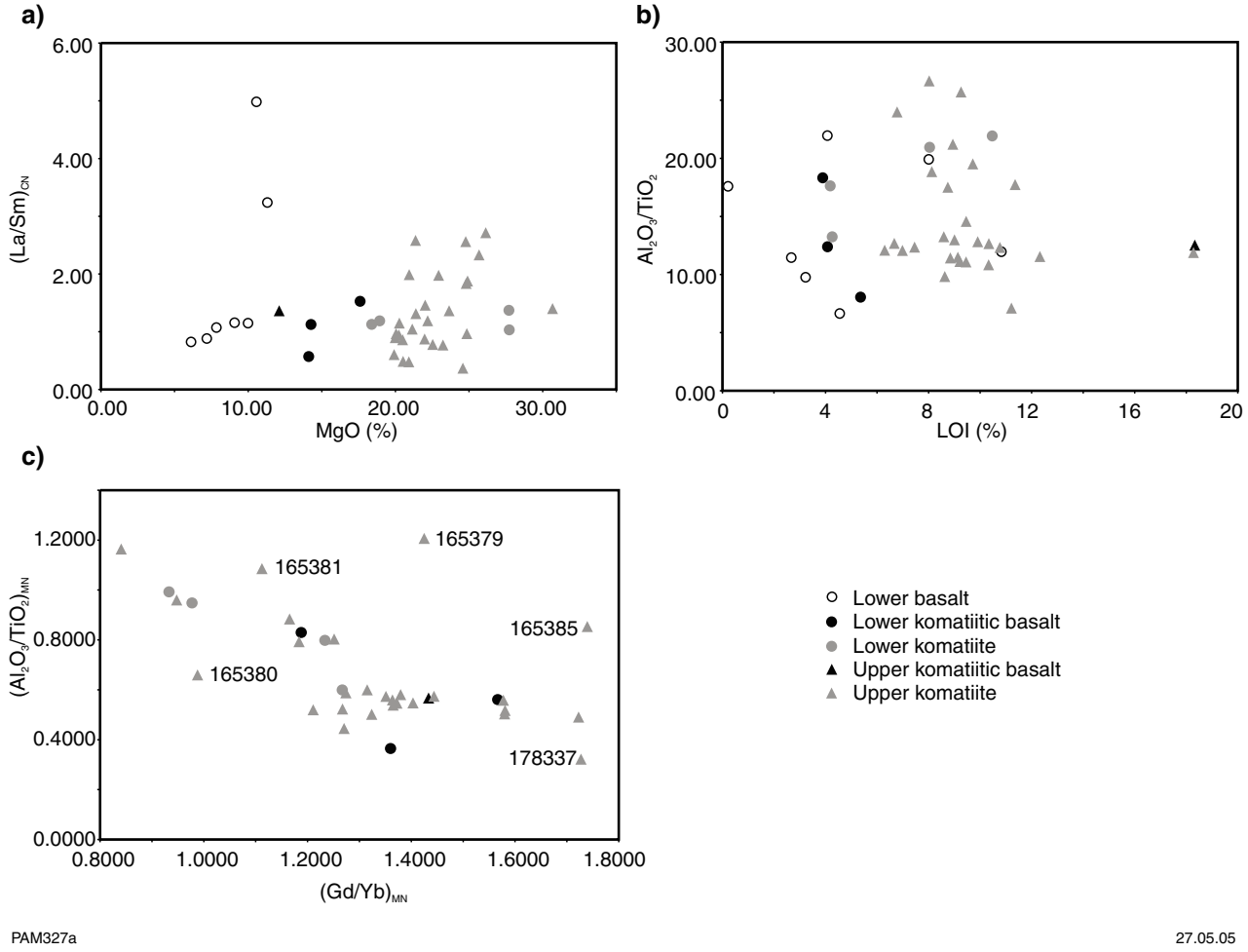

Figure 16. Geochemical plots of mafic and ultramafic rocks on Atley. Oxide values have been recalculated to 100% on a volatile-free basis: a) chondrite-normalized (La/Sm) vs MgO. Normalization factors are C1 chondrite from Sun and McDonough (1989); b) Al_2O_3/TiO_2 vs LOI; c) mantle-normalized Al_2O_3/TiO_2 vs (Gd/Yb) for komatiitic basalts and komatiites only. Mantle normalization values are pyrolite values from McDonough and Sun (1995). Lower basalt, lower komatiitic basalt and lower komatiite samples are from the mafic-dominated succession; upper komatiitic basalt and upper komatiite samples from the ultramafic-dominated succession

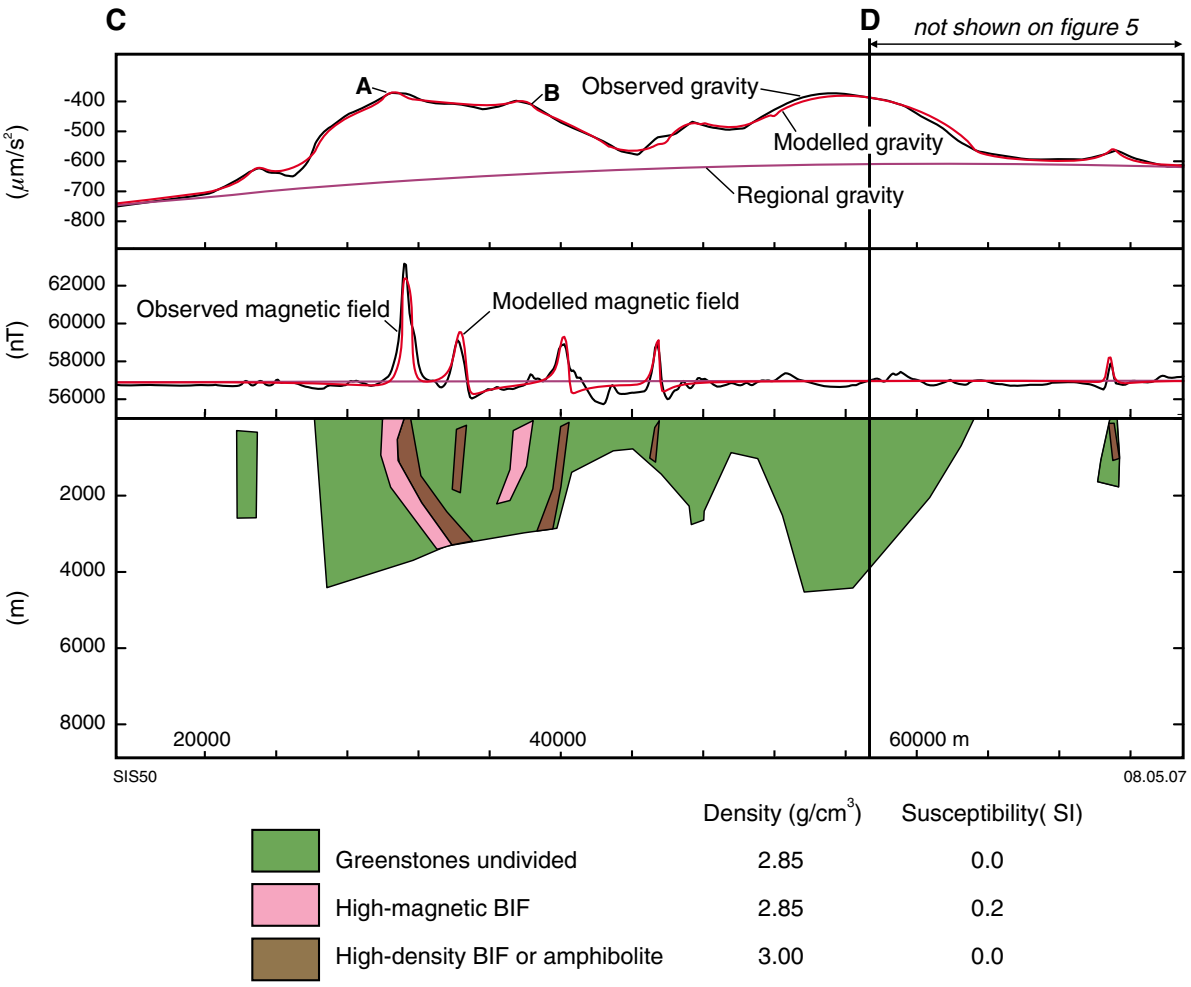

Figure 17. Gravity modelling across the southern Sandstone greenstone belt. A and B represent positive gravity anomalies. See Figure 5 for location

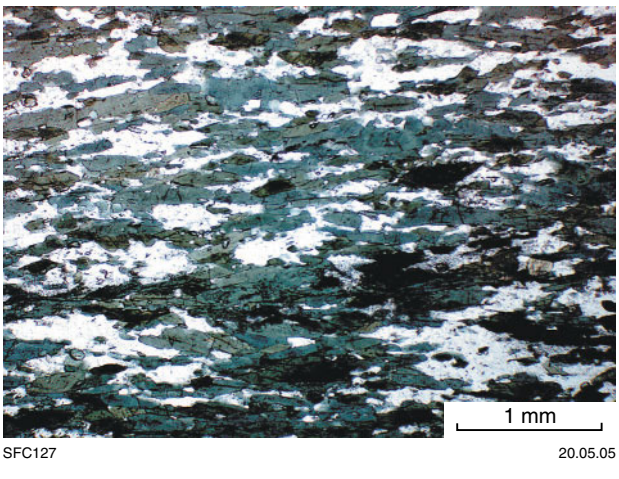

Figure 18. Photomicrograph of amphibolite with a foliation defined by preferred alignment of hornblende and plagioclase (plane-polarized light; GSWA 178365, MGA 96016E 6832965N)

modelling. A small 'blind' greenstone body was also modelled in the western part of the gravity traverse.

East Youanmi greenstone belt (*Aur, Aba, Aogf, Acc, Aci*)

A small part of the East Youanmi greenstone belt (Griffin, 1990) is preserved near the western margin of Rays Rocks (Fig. 4), where ultramafic (*Aur*), mafic (*Aba*, *Aogf*), and chemical sedimentary (*Acc*, *Aci*) rocks are exposed in a synclinal structure. These rocks are similar to those in the Sandstone greenstone belt.

Tremolite–chlorite(–talc) schist (*Aur*), up to 500 m thick, contains a pervasive foliation that is folded around the syncline. In thin section, it is composed of pale-green to colourless tremolite–actinolite, with minor chlorite, and accessory opaque minerals.

Amphibolite (*Aba*) is a dark grey, fine- to medium-grained mafic rock derived from basalt. It is typically strongly recrystallized and foliated, with a pervasive foliation defined by segregation and preferred alignment of hornblende and plagioclase (Fig. 18). Flattened pillow-

lava structures with a westward younging direction are locally preserved in relatively less foliated, but strongly recrystallized amphibolite (MGA 695679E 6833316N). A thin unit of strongly foliated, medium-grained gabbro (*Aogf*, MGA 696679E 6831178N) is intercalated with banded iron-formation.

Several units of metamorphosed chert (*Acc*) and banded iron-formation (*Aci*), up to 20 m thick, outline the synclinal structure on aeromagnetic images. Banded chert consists of microcrystalline to recrystallized quartz and minor iron oxides, while banded iron-formation consists mainly of blue or steel-grey to black magnetite–hematite-rich bands, with subordinate quartz bands.

Murchison Granite–Greenstone Terrane

Unaly Hill greenstone belt (*Aba, Aci, Aog, Aur*)

Within the Youanmi Shear Zone near the western margin of Atley, fine- to medium-grained, dark-grey, strongly foliated amphibolite (*Aba*, around MGA 698223E 6875469N), with minor metagabbro, is intercalated with several horizons of metamorphosed banded iron-formation (*Aci*). To the south and west, medium- to coarse-grained metagabbro (*Aog*), and tremolite–chlorite(–talc) schist (*Aur*) were intersected by mineral exploration drillholes. These rocks form part of the Unaly Hill greenstone belt (Figs 4 and 5), which is dominated by the Atley layered mafic intrusion (Stewart et al., 1983), and is mainly exposed to the southwest on Windimurra.

Granitic rocks (*Agm, Agf, Agmf, Agn, Ang, Ag, Agcm, Agb*)

Although Archaean granitic rocks are typically poorly exposed, they occupy or underlie the majority of the area covered by Atley, Rays Rocks, and southern Sandstone (Figs 4 and 5). They are dominated by monzogranite (*Agm*), with subordinate granodiorite that is mainly present in gneissic granite and granitic gneiss, and has not been mapped separately. Strongly deformed granitic rocks (*Agf*, *Agmf*, *Agn*, *Ang*) are most commonly within, and adjacent to, regional-scale shear zones (e.g. the Youanmi, Edale, and Yuinmery Shear Zones), although there are some significant exceptions (Figs 4 and 5).

Undivided granitic rocks (*Ag*) include deeply weathered rocks, and remote outcrops that are interpreted from aerial photographs and Landsat images, with no compositional and structural data. Deeply weathered granitic rocks (*Ag*) are typically poorly exposed and locally capped by siliceous duricrust. They have a relict granular texture and quartzofeldspathic mineralogy, but their original composition cannot be ascertained.

Weathered and foliated granite (*Agf*) is typically found within or adjacent to major shear zones. For example, moderately to deeply weathered, and foliated granite is poorly exposed in large areas adjacent to the southwestern margin of the Yuinmery Shear Zone on Rays Rocks (around MGA 706000E 6814000N). The weathered granite has a medium- to coarse-grained, granular texture, and contains a steep to subvertical, northerly trending foliation. In some places, a moderate to intense foliation is preserved in relatively less weathered granite below breakaways, but has been completely obliterated in siliceous duricrust (*Rd*) directly above the breakaways.

Like other areas in the central Yilgarn Craton, monzogranite (*Agm*) is the most common granite type on Atley, Rays Rocks and southern Sandstone. It is typically massive to weakly deformed, and locally has a northerly trending, steep to subvertical foliation in narrow high-strain zones (commonly <50 m wide). The fine- to coarse-grained monzogranite is typically equigranular, and locally feldspar-phyric, with K-feldspar phenocrysts ranging from 5 to 20 mm in size. Pegmatite dykes and stocks with irregular geometry occur locally within monzogranite. Small patches of massive granodiorite (e.g. MGA 714991E 6879079N), up to 100 m wide, cannot be separated at 1:100 000 scale.

In thin section, monzogranite (*Agm*) is composed of microcline, plagioclase, quartz, and biotite, with accessory muscovite, chlorite, hornblende, and opaque oxides. Sericitization of plagioclase is common in some samples (e.g. MGA 709013E 6869876N). Some plagioclase grains are completely replaced by sericite, whereas others only have a sericitized core. Quartz is typically finer grained than microcline and plagioclase, and some coarser grained quartz crystals are fractured. Mafic minerals in monzogranite are dominated by biotite (1–8% of the rock) that is partly altered to chlorite, and minor hornblende is locally found in monzogranite.

About 4.6 km north of the Yuinmery Homestead on Rays Rocks, fine- to medium-grained, massive, biotite monzogranite with minor microgranodiorite is exposed in large tors. A sample taken from the microgranodioritic phase has yielded a SHRIMP U–Pb zircon crystallization age of 2688 ± 11 Ma (Nelson, in prep.; GSWA 178052, MGA 697330E 6843460N).

On southern Sandstone, several small plutons (<200 m across), composed of medium-grained, massive monzogranite (*Agm*), have intruded foliated monzogranite. A sample taken from one of these plutons yielded a SHRIMP U–Pb zircon crystallization age of 2664 ± 10 Ma (Nelson, in prep.; GSWA 178061, MGA 730380E 6929450N). About 300 m to the south, a sample taken from the foliated monzogranite yielded a SHRIMP U–Pb zircon crystallization age of 2697 ± 6 Ma (Nelson, in prep.; GSWA 178062, MGA 730380E 6929130N).

The Coomb Bore Monzogranite (*Agcm*) in the northeastern corner of Atley is a small intrusion that straddles Atley and Everett Creek. It forms a northwesterly elongated, weakly to moderately foliated pluton, which is enclosed by strongly foliated monzogranite in the Edale Shear Zone. Although the surrounding strongly foliated monzogranite forms pavements and low-lying outcrops, the Coomb Bore

Monzogranite forms prominent bornhardts with a distinctive airphoto pattern.

The Coomb Bore Monzogranite intrusion (*Agcm*) is dominated by monzogranite, with minor syenogranite and granodiorite. The various lithological phases of the intrusion are typically medium grained, equigranular to porphyritic, and vary from dark pinkish-grey to pale red. The change in colour results mainly from clay alteration and iron-staining of K-feldspar and plagioclase, and partly from an increase in K-feldspar content (Riganti, 2003). Two samples taken from a granodioritic phase of the Coomb Bore Monzogranite yielded SHRIMP U–Pb zircon crystallization ages of 2691 ± 3 Ma (Nelson, 2002; GSWA 169070, MGA 746410E 6893600N on Everett Creek), and 2686 ± 5 Ma (Nelson, 2004; GSWA165365, MGA 745650E 6894870N on Atley).

Strongly foliated monzogranite (*Agmf*) has a similar mineralogy and composition to the massive monzongranite (*Agm*). It contains a pervasive foliation that is defined by grain size reduction, the preferred alignment of quartz and feldspar, and segregation of biotite from quartzofeldspathic minerals. It is widely distributed in the Youanmi, Edale, and Yuinmery Shear Zones (Figs 4 and 5), along the southern margin of the Sandstone greenstone belt (around MGA 735000E 6878000N), and within a northerly trending high-strain zone that straddles Atley and Rays Rocks (around MGA 740000E 6847000N). A sample from strongly foliated to locally gneissic monzogranite (*Agmf*) within the Yuinmery Shear Zone yielded a SHRIMP U–Pb zircon crystallization age of 2718 ± 13 Ma (Nelson, in prep.; GSWA 178050, MGA 719790E 6805440N).

Where granite and minor mafic rocks cannot be separated at 1:100 000 scale, they were mapped as a composite unit (*Agb*). On the northeastern margin of the Sandstone greenstone belt (MGA 744206E 6890999N), medium- to coarse-grained monzogranite is interleaved with small patches of dark-grey, fine- to medium-grained amphibolite crosscut by thin granitic dykes. The monzogranite contains a pervasive, steep west-southwesterly dipping foliation, and the amphibolite is strongly recrystallized but weakly to moderately foliated.

Granitic gneiss (*Ang*) and gneissic granite (*Agn*) are mainly distributed within or adjacent to regional-scale ductile shear zones on Atley, Rays Rocks, and southern Sandstone, although some significant outcrops of these rock types appear to be unrelated to any major shear zones (e.g. granitic gneiss in the southwestern part of Rays Rocks). Granitic gneiss (*Ang*) consists of alternating leucocratic and mesocratic bands of mainly monzogranite to granodiorite. The well-developed gneissic banding is defined by variation in grain size and biotite content, and by numerous pegmatite dykes, and less commonly, aplite and schlieren lenses. Individual compositional bands have sharp to diffuse contacts, and range from a few millimetres up to 30 cm in thickness. Gneissic granite (*Agn*) is a transitional rock type between granitic gneiss (*Ang*) and strongly foliated monzogranite (*Agmf*). It contains a pervasive foliation and locally prominent gneissic banding.

In the northwest- and northeast-trending ductile shear zones, granitic gneiss (*Ang*) contains a northerly trending gneissic banding that has been progressively rotated to become subparallel with the shear zones (Chen et al., 2004). Two samples from granitic gneiss within the Yuinmery Shear Zone yielded SHRIMP U–Pb zircon crystallization ages of 2701 ± 8 Ma (Nelson, 2002; GSWA 169068, MGA 695710E 6837960N), and 2681 ± 4 Ma (Nelson, in prep.; GSWA 178051, MGA 695950E 6835460N). One sample from granitic gneiss in the Edale Shear Zone yielded a SHRIMP U–Pb zircon crystallization age of 2683 ± 8 Ma (Nelson, in prep.; GSWA 178060, MGA 731420E 6914200N on Sandstone).

In the southwestern part of Rays Rocks, a northerly trending (355–005°), steep to subvertical gneissic banding is well developed in the fine- to coarse-grained granitic gneiss (*Ang*), in which mesocratic bands are less common than leucocratic bands. Most pegmatite dykes (2–10 cm thick) are parallel to the banding, and some are deformed into symmetric folds with axial planes parallel to the banding. Strongly flattened quartzofeldspathic grains or grain aggregates (e.g. MGA 715517E 6790482N), and symmetric porphyroclasts of feldspar (e.g. MGA 714855E 6791214N) are aligned along the gneissic banding. Similar granitic gneiss at Willow Bore to the south on Barlee yielded a SHRIMP U–Pb zircon crystallization age of 2714 ± 10 Ma (Nelson, 2002; GSWA 168972, MGA 706760E 6779780N).

Gneissic granite (*Agn*) is mainly distributed within or adjacent to the Youanmi and Yuinmery Shear Zones. For example, in the Bell Chambers Well area within the Youanmi Shear Zone, gneissic granite contains a locally prominent, north- to north-northeast-trending gneissic banding, with individual compositional bands ranging from less than 1 cm up to 1 m in thickness. Two samples from the gneissic granite in this area yielded SHRIMP U–Pb zircon crystallization ages of 2667 ± 8 Ma (Nelson, 2002; GSWA 169069, MGA 708100E 6888160N), and 2674 ± 9 Ma (Nelson, in prep.; GSWA 178054, MGA 709810E 6889310N).

Structural geology

Table 2 outlines the tectonic history of the study area. Like other areas in the central Yilgarn Craton (Dalstra et al., 1999; Greenfield and Chen, 1999; Chen et al., 2001, 2003, 2004; Wyche et al., 2001; Riganti and Chen, 2002; Riganti, 2003; Chen and Wyche, 2001, 2003; Chen, 2004), three principal deformation events have been recognized on Atley, Rays Rocks, and southern Sandstone, based on overprinting relationships, deformation styles, and structural orientations.

The timing of the three major deformation events (D_1–D_3) on Atley, Rays Rocks, and southern Sandstone is not well constrained (Table 2). On a regional-scale, there are no direct constraints on the age of D_1 other than that it pre-dates emplacement of the Marda Complex rhyolite to the south at c. 2730 Ma (Chen and Wyche, 2001; Riganti and Chen, 2002; Chen et al., 2003).

Table 2. Tectonic history of Atley, Rays Rocks, and southern Sandstone

Age (Ma)	*Deformation event*	*Geology*
<c. 3130		Deposition of greenstones
	D_1	North–south compression: layer-parallel foliation, thrusts, and large- and small-scale folds in greenstones Possible deposition of clastic sedimentary rocks in the northern part of the Sandstone greenstone belt
c. 2730 – c. 2680	D_2	East–west shortening: northerly trending folds (e.g. Sandstone Syncline) in greenstones Granite intrusion and formation of north-trending gneissic banding Peak metamorphism
c. 2680 – c. 2665	D_3	Progressive and inhomogeneous east–west shortening: northeast- and northwest-trending ductile shear zones (Youanmi, Edale, and Yuinmery Shear Zones) Intrusion and deformation of granite Metamorphism near shear zones
	Post-D_3	Development of brittle faults and fractures Intrusion of mafic dykes

Regional structural studies combined with geochronological dating in the central Yilgarn Craton recognized that D_2 was probably active between c. 2730 and c. 2680 Ma, and D_3 between c. 2680 and c. 2655 Ma (Chen and Wyche, 2001; Chen et al., 2001, 2003, 2004). On Atley, Rays Rocks, and southern Sandstone, strongly deformed granitic rocks that were affected by D_2 or D_3 (or both) within regional-scale ductile shear zones yielded SHRIMP U–Pb zircon ages ranging from c. 2718 to c. 2667 Ma. In the Waukenjerrie Hill area on southern Sandstone, a small, undeformed monzogranite pluton that has intruded monzogranite with northwest- and northeast-trending S_3 foliations yielded a SHRIMP U–Pb zircon age of 2664 ± 10 Ma (Nelson, in prep.; GSWA 178061). This age is within error of the 2667 ± 8 Ma date (Nelson, 2002; GSWA 169069) obtained for gneissic granite within the Youanmi Shear Zone, and probably represents the minimum age of D_3 in this area.

The Youanmi Shear Zone contains gneissic granite with SHRIMP U–Pb zircon ages of 2667 ± 8 Ma (Nelson, 2002; GSWA 169069) and 2674 ± 9 Ma (Nelson, in prep.; GSWA 178054). The sheared Coomb Bore Monzogranite in the Edale Shear Zone has SHRIMP U–Pb zircon ages of 2691 ± 3 Ma (Nelson, 2002; GSWA 169070) and 2686 ± 5 Ma (Nelson, 2004; GSWA 165365), and granitic gneiss in the shear zone has a SHRIMP U–Pb zircon age of 2683 ± 8 Ma (Nelson, in prep.; GSWA 178060). In the Yuinmery Shear Zone, granitic gneiss has SHRIMP U–Pb zircon ages of 2701 ± 8 Ma (Nelson, 2002; GSWA 169068) and 2681 ± 4 Ma (Nelson, in prep.; GSWA 178051), and strongly foliated to locally gneissic monzogranite has a SHRIMP U–Pb zircon age of 2718 ± 13 Ma (Nelson, in prep.; GSWA 178050).

First deformation event (D_1)

North–south compression in D_1 produced layer-parallel foliation, thrust faults, and large- and small-scale folds that are overprinted by D_2 structures. In the East Youanmi greenstone belt on Rays Rocks (Fig. 4), a layer-parallel S_1 foliation in tremolite–chlorite–(talc) schist (*Aur*) is folded around the hinge zone of a large-scale F_2 syncline, where the S_1 foliation trends nearly easterly and dips 40–50° to the north (MGA 695496E 6832257N). Similarly, in the Sandstone greenstone belt on Atley, a layer-parallel S_1 foliation and D_1 thrusts in tremolite–chlorite(–talc) schist are folded by the northerly trending F_2 Sandstone Syncline, and by two north-northeasterly trending F_2 anticlines adjacent to the southern margin of the greenstone belt (Fig. 5). The layer-parallel S_1 foliation was developed during D_1 north–south thrusting, and the S_1 foliation and D_1 thrusts were then folded in D_2.

In the area northwest of Dandaraga Homestead on Atley, many units of banded iron-formation (*Aci*) trend nearly east and dip shallowly to moderately towards the north. Some show evidence for D_1 folding (e.g. mesoscopic, east-trending, and shallowly plunging F_1 folds at MGA 724585E 6890061N, and 726010E 6890266N). A moderately north-dipping D_1 thrust is associated with south-verging F_1 folds in its hangingwall (MGA 724583E 6888726N), indicating a southward-thrusting direction. The D_1 south-directed thrusting may have also resulted in structural repetition of banded iron-formation units in the area northwest of Dandaraga Homestead.

In the central-southern part of the Sandstone greenstone belt, a regional-scale, originally east-trending F_1 syncline is outlined by a prominent unit of banded iron-formation and chert (Figs 5 and 6). Bedding dips predominantly to the south on its northern limb, and to the north on its southern limb. Its eastern hinge zone was reoriented during D_2. Here, bedding dips moderately (35–45°) to the north (MGA 745455E 6882732N), and pillow-lava structures in basalt indicate a northward-younging direction (MGA 744406E 6881307N). This regional-scale F_1 syncline is overprinted by the F_2 Sandstone Syncline, and has been significantly disrupted by brittle faults and granite intrusion.

Second deformation event (D_2)

As in other areas of the central Yilgarn Craton (Chen et al., 2001, 2003, 2004; Wyche et al., 2001; Riganti and Chen, 2002), east–west shortening in D_2 produced macroscopic and mesoscopic folds with a local axial-planar foliation in greenstones, and a northerly trending gneissic banding and foliation in granitic rocks on ATLEY and RAYS ROCKS.

Stewart et al. (1983) interpreted a regional-scale, northerly plunging anticline in the Sandstone greenstone belt, based on a predominantly northerly plunge of minor folds, and a northerly dip of east-trending banded iron-formation. They also recognized northerly facings in pillow-lavas 5 km northwest of Nunngarra, and 3 km west-northwest of Maninga Marley, that indicate a northward-younging greenstone stratigraphy (Stewart et al., 1983).

New field observations, combined with aeromagnetic image interpretation, suggest that the regional-scale, northerly trending fold (the anticline of Stewart et al., 1983) is a doubly plunging F_2 syncline with a box-fold geometry (the Sandstone Syncline in Fig. 5) that is superimposed on an originally east-trending F_1 syncline. The new interpretation takes account of the following observations:

1. On ATLEY, north-dipping bedding and northerly plunging mesoscopic folds in banded iron-formation and chert were found predominantly in the southern hinge zone of the Sandstone Syncline that was disrupted by granite intrusion, whereas south-dipping bedding and southerly plunging mesoscopic folds were found mainly in the northern hinge zone of the syncline (e.g. MGA 729222E 6897422N).

2. On ATLEY, bedding in banded iron-formation and chert dips predominantly to the southeast on the northwestern limb of the Sandstone Syncline, and to the southwest on its northeastern limb.

3. On southern SANDSTONE, most bedding attitudes of banded iron-formation and chert also coincide with a northerly trending, doubly plunging syncline rather than a northerly plunging anticline (Chen and Painter, in press).

4. On ATLEY, the north-facing pillow-lava structures in basalt near Maninga Marley (Fig. 11) are consistent with an F_1 syncline that was reoriented in D_2. The northwest-facing pillow-lava structures in basalt 5 km northwest of Nunngarra (not found during 1:100 000-scale mapping) can be explained by local stratigraphic overturn resulting from D_1 folding and thrusting.

Adjacent to the southern margin of the Sandstone greenstone belt, two macroscopic, north-northeast-trending anticlines with granite in their cores are considered to be F_2 folds (Fig. 5) that have folded an S_1 foliation in tremolite–chlorite–(talc) schist (*Aur*). Strongly foliated to locally gneissic monzogranite (*Agmf*) in the core of one anticline contains a pervasive foliation that is generally parallel to the granite–greenstone contact, with a locally prominent down-dip mineral lineation (e.g. MGA 734778E 6880411N, and 734374E 6882854N). To the east, a northerly trending F_2 fold outlined by banded iron-formation is superimposed on a large-scale F_1 fold (Fig. 5). Type 1 interference folding (Ramsay, 1967) between mesoscopic, north-trending F_2 folds and east-trending F_1 folds is evident in banded iron-formation to the northwest of Dandaraga Homestead (e.g. around MGA 724583E 6888726N).

A northerly trending, steep to subvertical S_2 foliation that is axial planar to the F_2 Sandstone Syncline is well developed in fine-grained clastic metasedimentary rocks in the northern apex region of the Sandstone greenstone belt. A northerly trending gneissic banding in granitic gneiss (*Ang*) and gneissic granite (*Agn*) was predominantly developed during D_2, and locally in syn-D_3 granite intrusions (Chen et al., 2004). Within a northerly trending D_2 high-strain zone, about 13.5 km long and up to 2.5 km wide, that straddles ATLEY and RAYS ROCKS, medium- to coarse-grained, strongly foliated monzogranite (*Agmf*) contains a northerly (355–005°) trending, steep to subvertical S_2 foliation.

Third deformation event (D_3)

Progressive and inhomogeneous east–west shortening in D_3 (Chen et al., 2001, 2004) produced the northeast-trending, dextral Youanmi Shear Zone, and the northwest-trending, sinistral Edale and Yuimery Shear Zones on ATLEY, RAYS ROCKS, and southern SANDSTONE. The Youanmi and Edale Shear Zones form the northwestern and northeastern margins of the Sandstone greenstone belt respectively, and the Yuinmery Shear Zone is developed mainly in granitic rocks (Figs 4 and 5).

The northeastern section of the Youanmi Shear Zone, adjacent to the Sandstone greenstone belt, is a 5 – 8.5 km wide, high-strain zone (Figs 4 and 5) in strongly foliated monzogranite (*Agmf*), foliated and weathered granite (*Agf*), and gneissic granite (*Agn*). In the western part of the shear zone, a northerly trending foliation is dextrally displaced by a moderately developed, northeast-trending foliation (Chen et al., 2001, 2004). In the shear zone centre, a discontinuous, C'-type shear band cleavage (Fig. 19a; cf. Passchier and Trouw, 1996) dextrally offsets a dominant foliation that is subvertical or dips steeply to the northwest. Numerous asymmetric feldspar porphyroclasts (e.g. Fig. 19b) indicate a dextral shear sense, and a consistently shallow-plunging mineral lineation (Fig. 19c) suggests a dominant strike-slip shear component. The southeastern boundary of the shear zone coincides with the granite–greenstone contact. Strongly foliated basalt (*Abf*) and local amphibolite east of the contact contain both northerly and northeasterly trending foliations that dip steeply to the east.

The southwestern section of the Youanmi Shear Zone contains several major quartz veins in poorly exposed, foliated granite, mafic–ultramafic schist, and layered mafic intrusion (Chen et al., 2001, 2004). Asymmetric feldspar porphyroclasts in granite, and Z-shaped asymmetric folds with an axial-planar foliation in mafic schist indicate a dextral shear sense (Chen et al., 2004). Where the strike of the shear zone changes to north–south, a northerly trending

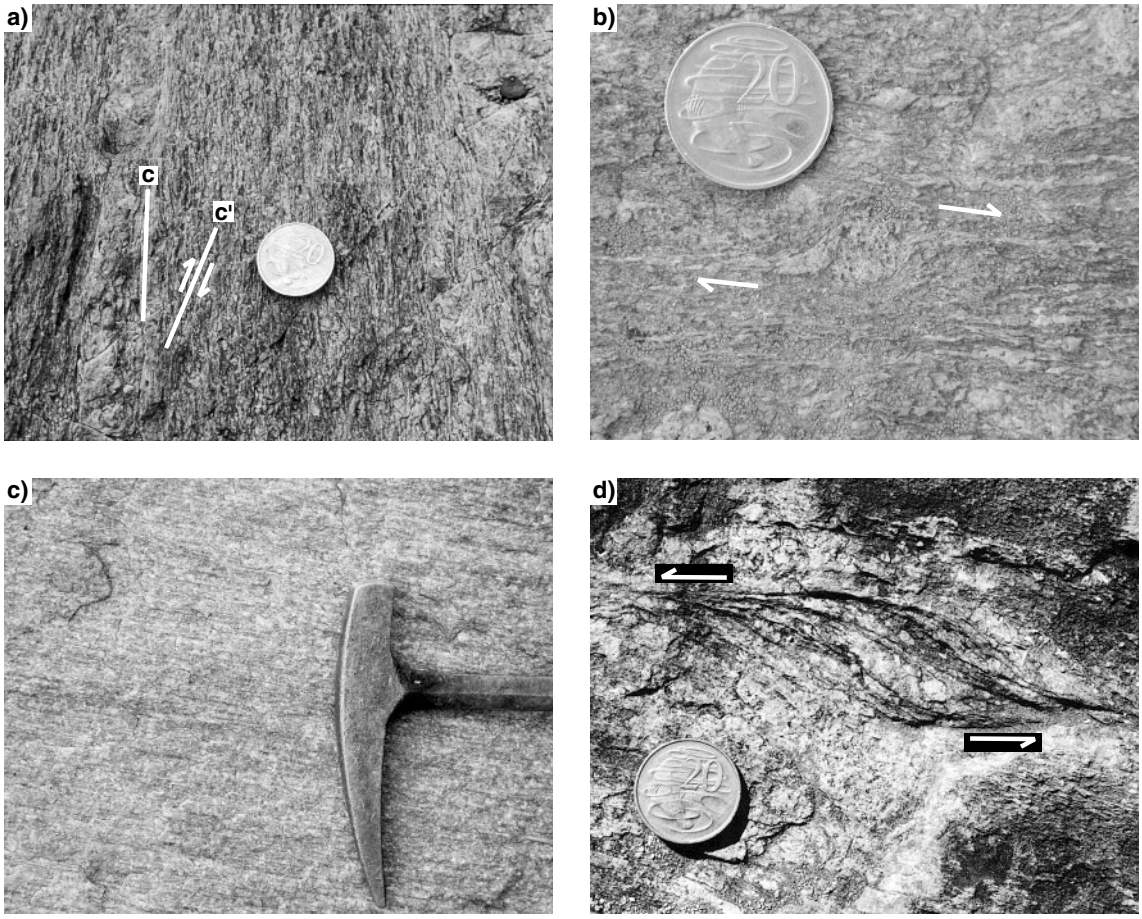

Figure 19. Shear-sense indicators in the Youanmi and Yuinmery Shear Zones: a) C'-type shear band cleavage in gneissic granite (MGA 709800E 6889300N); b) asymmetric porphyroclasts of feldspar with strongly attenuated tails, indicating a dextral shear sense (MGA 709800E 6889300N); c) shallowly plunging mineral lineation in gneissic granite (MGA 707760E 6888410N); d) a small-scale restraining jog bound by northwest-trending, right-stepping discrete shear zones in strongly foliated monzogranite. The curvature of internal foliation and shear zones against the bounding shear zones indicates a sinistral shear sense (MGA 695883E 6834391N)

foliation is wrapped around flattened and symmetric feldspar porphyroclasts (Eisenlohr et al., 1993).

The northwestern section of the 4–6 km wide Edale Shear Zone is on the northeastern margin of the Sandstone greenstone belt (Figs 4 and 5; Chen et al., 2004). The shear zone is mainly developed in strongly deformed granitic rocks that locally enclose less deformed monzogranite. Strongly foliated monzogranite and granitic gneiss contain a pervasive, northwest-trending foliation, with a shallowly (2–20°) plunging mineral lineation. The foliation dips steeply to the southwest adjacent to the greenstone margin, and towards the northeast away from the margin. A northerly trending foliation within the shear zone locally contains a steeply (60–75°) plunging to down-dip mineral lineation (e.g. MGA 745087E 6896594N). S–C fabrics, C'-type shear band cleavage (e.g. MGA 745466E 6895712N), and locally abundant asymmetric feldspar porphyroclasts (e.g. MGA 730255E 6914206N on Sandstone) indicate a sinistral shear sense. Structures in the North Cook Well greenstone belt east of the shear zone (Fig. 4), and in strongly foliated monzogranite farther east on Everett Creek (Riganti, 2003), include a northerly (345–010°) trending foliation that is axial planar to macroscopic folds in the greenstone belt, and that curves into the shear zone with an apparent sinistral sense (Eisenlohr et al., 1993).

In the middle section of the Edale Shear Zone on Everett Creek (Riganti, 2003) and Richardson (Chen, 2004), a northerly trending gneissic banding is parallel to numerous pegmatite dykes, some of which are strongly boudinaged. Asymmetric feldspar porphyroclasts, quartzofeldspathic aggregates with strongly attenuated tails, S–C fabrics and C'-type shear band cleavage in granitic gneiss and quartz–muscovite schist, and S-shaped asymmetric folds in quartzite provide unequivocal evidence of sinistral shear (Chen et al., 2001, 2004; Riganti, 2003). Where the shear zone curves into a north–south orientation at the southern end on Richardson, a well-developed, north-trending foliation wraps around flattened and symmetric feldspar porphyroclasts, and deformation is characterized by flattening or pure shear. Several north-northeast-trending shear zones splaying off the Edale Shear Zone (Fig. 4) are dominated by flattening

with a subsidiary strike-slip shear component (Chen et al., 2001, 2004; Chen, 2004).

The northwestern section of the Yuinmery Shear Zone is a 2–3 km wide high-strain zone developed mainly in granitic rocks along the northeastern margin of the East Youanmi greenstone belt (Fig. 4). Across the strike of the shear zone from east to west, a steep foliation gradually changes from northwest to due north in strike, and from northeast to west in dip direction. The plunge of a prominent mineral lineation on the foliation surface also gradually becomes steeper from east to west. Locally developed S–C fabrics, C'-type shear band cleavage, and the geometry of small-scale restraining jogs (Fig. 19d) indicate a sinistral shear sense (Chen and Wyche, 2001; Chen et al., 2004).

The middle section of the Yuinmery Shear Zone is developed entirely within foliated granite and granitic gneiss on Rays Rocks, and the shear zone boundaries (particularly the southwestern boundary) are poorly defined. In some places, the Yuinmery shear zone is a composite structure made up of at least two shear zones (1.5–2 km wide), showing simple-shear-related deformational features, which are separated and flanked by zones of pure shear (Chen et al., 2004). The simple shear zones are characterized by a well-developed, northwest-trending, steep foliation that contains a prominent, shallowly plunging mineral lineation. This foliation sinistrally offsets northerly (345–005°) trending gneissic banding and foliation. The northerly trending foliation (S-fabric) has been rotated progressively to become subparallel with the northwest-trending foliation (C-fabric) towards the shear zone centre (Fig. 20a). Well-developed S–C fabrics (Fig. 20b), C'-type shear band cleavage (Fig. 20c), and abundant asymmetric porphyroclasts of feldspar and quartzofeldspathic aggregates (Fig. 20d) consistently indicate sinistral movement in the simple shear zones. In contrast, the pure shear zones characterized by flattening only contain moderate to intense northerly trending foliation and gneissic banding with associated symmetric feldspar porphyroclasts (e.g. MGA 723498E 6793382N). They generally lack the northwest-trending foliation and S–C fabrics, although their boundaries with simple shear zones are typically gradational (Chen et al., 2004).

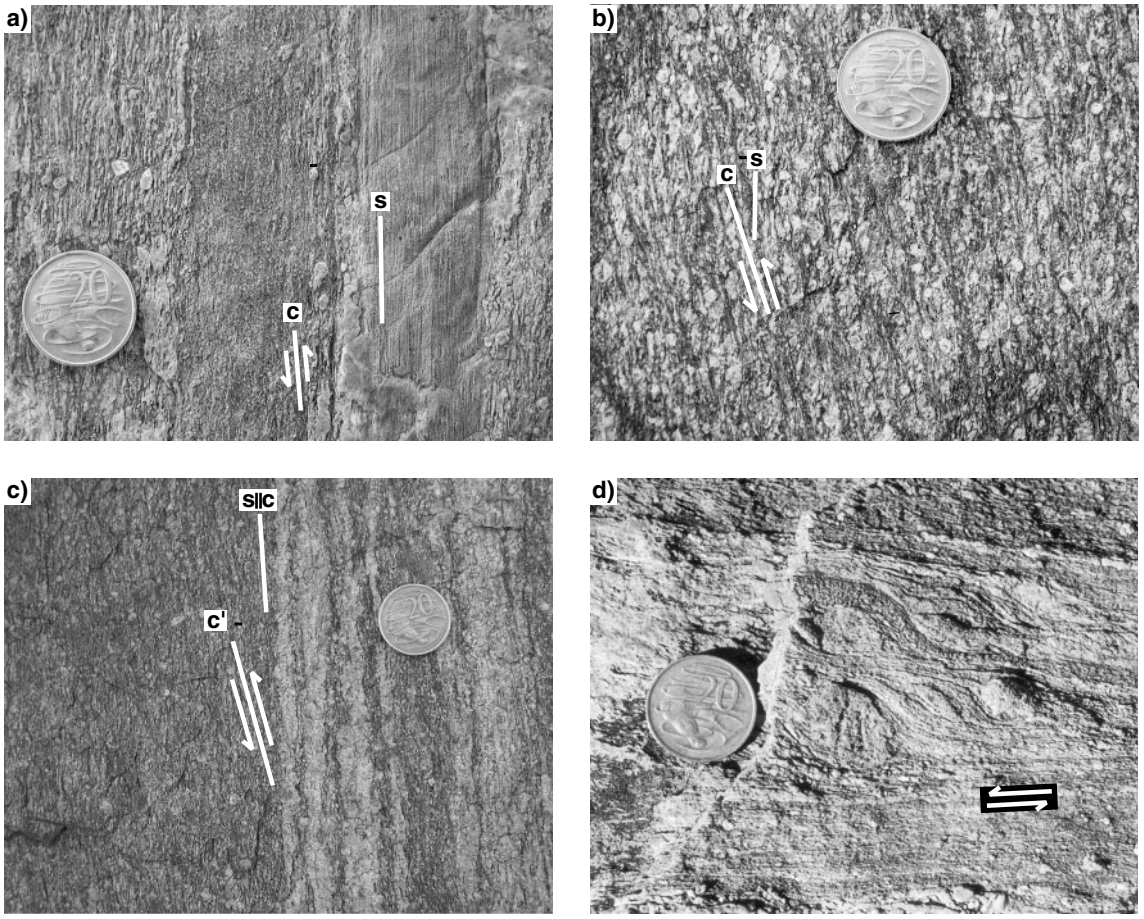

Figure 20. Sinistral shear-sense indicators in the Yuinmery Shear Zone: a) S-fabric is subparallel to C-fabric that is associated with asymmetric feldspar porphyroclasts in gneissic granite (MGA 722997E 6798479N); b) S–C fabrics in strongly deformed granite (MGA 723307E 6798242N); c) C'-type shear band cleavage in gneissic granite (MGA 723747E 6798108); d) asymmetric porphyroclasts of feldspar and quartzofeldspathic aggregates in gneissic granite (MGA 723354E 6797758N)

The southeastern section of the Yuinmery Shear Zone truncates the southern end of the Mount Elvire greenstone belt (Fig. 4), and is locally well exposed in granite with a pervasive northwest-trending foliation. Asymmetric porphyroclasts of feldspar and S-shaped asymmetric folds of gneissic banding indicate a sinistral shear sense (Chen, 2004; Chen et al., 2004).

Post-D_3 deformation

Post-D_3 structures on ATLEY and RAYS ROCKS include widespread easterly, east-northeasterly, east-southeasterly, northeasterly, and northwesterly trending brittle faults or fractures, some of which are filled by quartz veins (e.g. MGA 708498E 6818488N) or mafic dykes (e.g. MGA 740659E 6896124N). These later structures crosscut D_2 and D_3 structures. Other post-D_3 structures include locally preserved, east-trending, small-scale open folds (e.g. MGA 726267E 6910704N on SANDSTONE), and variously oriented kink folds.

Metamorphism

The regional metamorphic study of Binns et al. (1976) introduced the concept of static and dynamic metamorphic styles in the central and eastern Yilgarn Craton. The static-style, lower grade metamorphism in the centres of wide greenstone belts is characterized by lack of preferred mineral orientation, and preservation of primary textures. The dynamic-style, higher grade metamorphism along the margins of greenstone belts is characterized by development of penetrative structural fabrics, and obliteration of primary textures. Stewart et al. (1983) recognized static metamorphism in the interior of the Sandstone greenstone belt and dynamic metamorphism along its margins, but their metamorphic grades do not correlate with those recognized by Binns et al. (1976). Stewart et al. (1983) also recognized two episodes of regional metamorphism in granitic gneiss — medium- to high-grade progressive metamorphism followed by low-grade, retrogressive metamorphism.

In a regional metamorphic study of the central Yilgarn Craton, Ahmat (1986) showed relatively narrow, medium- and low-grade metamorphic zones adjacent to the margins of the Sandstone greenstone belt, and a wide, very low grade metamorphic zone in the centre of the greenstone belt. He also showed a medium-grade metamorphic zone on the northeastern margin of the East Youanmi greenstone belt. The medium- and low-grade marginal zones are characterized by high-strain, dynamic-style metamorphism, whereas the very low grade central zone is characterized by low-strain, static-style metamorphism (Ahmat, 1986).

The current 1:100 000-scale geological mapping on ATLEY, RAYS ROCKS, and southern SANDSTONE has confirmed the conclusions of previous studies by Binns et al. (1976) and Ahmat (1986). The metamorphic grade of greenstone belts decreases towards their centres, with amphibolite (*Aba*) distributed mainly along the southeastern, northeastern, and northwestern margins of the Sandstone greenstone belt, and the northeastern margin of the East Youanmi greenstone belt. Amphibolite in these areas is strongly recrystallized and pervasively foliated. The foliation is defined by preferred alignment of hornblende, and by segregation of hornblende and plagioclase (Fig. 18).

Strongly foliated metabasalt (*Abf*) of mid-greenschist to low-amphibolite facies along the northwestern and northeastern margins of the Sandstone greenstone belt is composed mainly of actinolite and albite. The metabasalt has a pervasive foliation, but is typically weakly to moderately recrystallized. Greenstones in the central part of the Sandstone greenstone belt are characterized by low- to very low grade metamorphism of low-greenschist to prehnite–pumpellyite facies (Ahmat, 1986). In massive to weakly foliated metabasalt (*Abv*), primary igneous features are commonly preserved, but primary mineralogy is typically replaced by metamorphic assemblages of actinolite, epidote, chlorite, and rare prehnite.

Although medium- to high-grade metamorphism in granitic gneiss was reported by Stewart et al. (1983), most of the massive and foliated monzogranite on ATLEY and RAYS ROCKS exhibit evidence of only low-grade metamorphism, with secondary minerals dominated by sericite and chlorite.

Veins and dykes (*q, g, gy*)

Quartz veins (*q*) are most abundant in regional-scale ductile shear zones, and in easterly, east-southeasterly and east-northeasterly trending brittle faults. Along the northwestern margin of the Sandstone greenstone belt, prominent quartz veins up to 80 m wide (e.g. MGA 711990E 6892819N) are concentrated along the granite–greenstone contact, parallel to the Youanmi Shear Zone. In the centre of the Edale Shear Zone, a 3–5 m wide quartz vein (e.g. MGA 740568E 6900223N), occurs intermittently for about 10 km from ATLEY to SANDSTONE, parallel to the shear zone. Short, nearly east-trending quartz veins crosscut northeasterly and northwesterly trending foliations in the Youanmi and Edale Shear Zones. In strongly deformed granite on RAYS ROCKS, several east-southeasterly trending quartz veins up to 10 m wide (e.g. MGA 712024E 6817634N, and 708498E 6818488N) are parallel to brittle faults that cut across the Yuinmery Shear Zone. Minor quartz veins are scattered in greenstones, and massive to weakly deformed granite.

Granitic dykes (*g*), 1–3 m wide, are composed of fine- to coarse-grained, massive to moderately foliated monzogranite. They are predominantly distributed in greenstones near the southern margin of the Sandstone greenstone belt (e.g. MGA 709876E 6880901, and 738800E 6877400N).

In the northeastern corner of ATLEY, a small body of granophyre (*gy*) was distinguished from the Coomb Bore Monzogranite (*Agcm*) by its characteristic granophyric texture (Fig. 21). The granophyre contains numerous milky quartz blebs up to 10 cm in size, and angular fragments and blocks up to 70 cm × 40 cm in size (Fig. 22) that are composed of syenogranite, pegmatite, monzogranite, and vein-quartz. In thin section, the granophyric rock

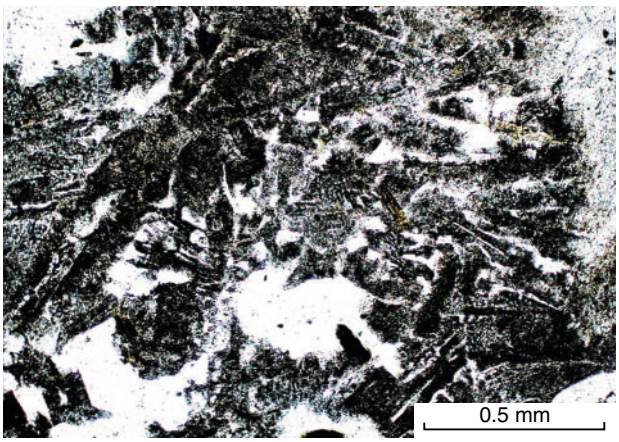

SFC114 20.05.05

Figure 21. Photomicrograph of granophyric texture in granophyre (crossed nicols; GSWA 180605, MGA 745148E 6894854N)

appears to have a remelted texture (MGA 745056E 6894852N). It contains fritted residual plagioclase and lenses of recrystallized quartz that are separated by zones of euhedral, partly skeletal plagioclase laths and abundant granophyric intergrowths, as well as brown hornblende, and biotite. A sample taken from the granophyre body yielded a SHRIMP U–Pb zircon crystallization age of 2689 ± 6 Ma (Nelson, in prep.; GSWA 178056, MGA 745070E 6894850N), similar to the Coomb Bore Monzogranite (2691 ± 3 Ma, Nelson, 2002; GSWA 169070; 2686 ± 5 Ma, Nelson, 2004; GSWA 165365).

Proterozoic mafic to ultramafic dykes (*Pd*)

On Atley, Rays Rocks, and southern Sandstone, several prominent easterly and east-northeasterly trending aeromagnetic features that cut across greenstones, granite, and all other structural trends (Figs 5 and 6) are interpreted as brittle fractures or faults filled by mafic to ultramafic dykes (*Pd*). They are normally concealed, but one of them corresponds to local exposures of a gabbroic dyke, and extends from northeastern Atley to the east-southeast across Everett Creek. On Atley (MGA 740659E 6896124N), the dyke is composed of medium- to coarse-grained, grey, massive gabbro; at Mount Holmes near the eastern edge of Everett Creek, the dyke has a flat, sheet-like geometry, and consists of fine- to medium-grained, medium- to dark-grey, massive rocks ranging from gabbro to norite (Riganti, 2003). Hallberg (1987) suggested that the crosscutting mafic and ultramafic dykes in the Yilgarn Craton were emplaced between 2.4 and 2.0 Ga, post-dating cratonization.

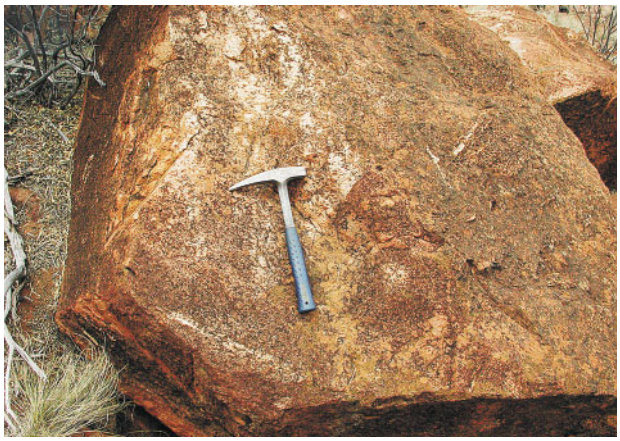

SFC115 20.05.05

Figure 22. A large, angular block of syenogranite in granophyre (MGA 745056E 6894852N)

Cainozoic geology

Extensive regolith deposits on Atley, Rays Rocks, and southern Sandstone were mapped by combining field observations with interpretation of aerial photographs and Landsat Thematic Mapper (TM5) imagery. Regolith deposits were classified according to the RED (Residual–Erosional–Depositional) scheme of Anand et al. (1993) that was extended and modified by Hocking et al. (2001). In addition to the erosional regime of bedrock exposures, regolith deposits can be broadly subdivided into two groups: (1) residual or relict units represented by siliceous and ferruginous duricrust; and (2) depositional units that include colluvial, sheetwash, alluvial, and lacustrine deposits. Sandplains may be either depositional (eolian) or residual. A comprehensive review of regolith geology of the Yilgarn Craton is given by Anand and Paine (2002).

Residual or relict units (*Rd, Rf, Rg, Rgp$_g$, Rk, Rz, Rzu*)

Undivided duricrust (*Rd*) is either siliceous or ferruginous. It commonly overlies granite and is typically exposed above breakaways and on low hills. In some areas underlain by granitic rocks, undivided duricrust (*Rd*) is covered by a veneer of yellow sand with variable amounts of ferruginous granules, silcrete debris, silt, and clay (*Sl*). Ferruginous or lateritic duricrust (*Rf*) comprises nodular or massive ferricrete, and is readily identified by its dark brown to black tone on aerial photographs. It is extensively distributed in the deeply weathered parts of the Sandstone greenstone belt on Atley.

Quartzofeldspathic sand over granitic rocks (*Rg*) contains scattered, deeply weathered granite outcrops, with local silcrete. Quartzofeldspathic sand with sparse granitic outcrops (*Rgp$_g$*) is typically distributed below breakaways or in the areas adjacent to granite exposures. Quartz and silcrete clasts are locally abundant in these areas.

A few patches of white, massive to nodular calcrete (*Rk*) in small areas away from drainages are distinguished from the calcrete deposited within or adjacent to alluvial channels (*Ak*). Silcrete (*Rz*) is a siliceous duricrust

overlying granite. Pale-brown silica caprock over ultramafic rocks (*Rzu*) is widespread in the Sandstone greenstone belt. It locally contains a strong foliation (after tremolite–chlorite–talc schist), or relict olivine-spinifex and olivine-cumulate textures (after komatiite).

Depositional units (*C*, *Cf*, *Cg*, *Clc$_i$*, *Cq*, *W*, *Wf*, *A*, *A$_f$*, *A$_p$*, *A$_k$*, *L$_l$*, *L$_d$1*, *L$_m$*, *L$_d$2*, *S*, *Sl*)

Depositional regolith units are widely distributed on Atley and Rays Rocks, and include colluvial (*C, Cf, Cg, Clc$_i$, Cq*), sheetwash (*W, Wf*), alluvial (*A, A$_f$, A$_p$, A$_k$*), lake (*L$_l$, L$_d$1, L$_m$, L$_d$2*), and sandplain (*S, Sl*) deposits. In general, colluvial units are proximal to granite and greenstone outcrops, whereas sheetwash and lacustrine units represent distal deposits.

Undivided colluvium (*C*) includes lithologically mixed boulder, gravel, sand, and silt on steep to gently sloping ground, particularly in areas adjacent to greenstone outcrops, and granite–greenstone contacts. Further subdivisions distinguish colluvium with talus and debris that are derived predominantly from one lithotype. Coarse talus from banded iron-formation and chert (*Clc$_i$*) is distributed on the flanks of prominent ridges, and grades downslope into finer ferruginous colluvium (*Cf*). Talus from granitic rocks (*Cg*) includes granite or gneiss fragments, with abundant quartzofeldspathic sand, silt, and subordinate silcrete and quartz clasts. Colluvium dominated by quartz debris (*Cq*) is typically derived from adjacent quartz veins.

Sheetwash deposits (*W*) consist of sand, silt, and clay on gently sloping to flat ground. Ferruginous sheetwash (*Wf*) is characterized by locally abundant fine, ferruginous grit.

Alluvium consisting of sand, silt and gravel (*A*) is distributed along ephemeral channels and watercourses. Floodplain deposits (*A$_f$*) are dominated by clay and silt, with various proportions of sand and gravel. They are distributed in broad areas in which alluvial channels dissipate during flooding seasons. Calcrete developed in, and adjacent to, alluvial channels were shown as *Ak*. All drainage systems are ephemeral on Atley and Rays Rocks, but water can persist for longer periods in claypans (*A$_p$*) that contain a veneer of clay and silt.

Both the Lake Noondie and Lake Barlee playa lake systems form part of the Raeside Palaeoriver (van de Graaff et al., 1977; Hocking and Cockbain, 1990). Lake Noondie occupies the northern and central parts of Rays Rocks. Lake Barlee extends from Barlee (Riganti, 2002) in the south to the southeastern corner of Rays Rocks. Saline playa lake deposits (*L$_l$*) contain mud, silt, and sand, with a veneer of halite and gypsum, and are locally vegetated. Barren to poorly vegetated, active dunes (*L$_d$1*) are composed of sand and evaporite, whereas vegetated and stabilized dunes (*L$_d$2*) consist mainly of sand and silt, with lesser amounts of evaporitic material. The areas immediately adjacent to the playa lakes have mixed alluvial, eolian and lacustrine deposits (*L$_m$*).

On Atley, Rays Rocks, and southern Sandstone, extensive sandplain deposits (*S*) occur in areas underlain by granite. The quartz-rich, yellow sand is derived predominantly from disintegration of underlying granitic rocks, but its deposition has involved significant eolian processes, as indicated by the presence of numerous sand dunes. Yellow to reddish-yellow sand (*Sl*) over undivided duricrust (*Rd*) contains locally abundant ferruginous and siliceous granules, and may represent a mixture of eolian and residual deposits.

Economic geology

Appendix 4 summarizes gold production statistics for the Sandstone greenstone belt on Atley and southern Sandstone, which has a recorded gold production of 25 120.23 kg since 1903, with a further gold resource of 14 783.8 kg (Appendix 5). No gold production and resource were recorded for the East Youanmi and Unaly Hill greenstone belts on Atley and Rays Rocks.

The Sandstone greenstone belt has been extensively explored for gold and base metals using magnetic surveys, soil and stream sampling, and rotary air-blast (RAB), reverse circulation (RC), and diamond drilling. Open-file statutory mineral exploration reports (from the WAMEX database) and mines and mineral deposits information (from the MINEDEX database) are held at the Western Australian Department of Industry and Resources in Perth, and at the Kalgoorlie Regional Office of the Geological Survey of Western Australia, and are accessible online.

In the Sandstone greenstone belt, gold deposits are hosted by various rock types such as quartz veins in basaltic rocks at Bellchambers mine; ultramafic rocks in the Nunngarra area; basalt, dolerite, and banded iron-formation in the Sandstone, Maninga Marley, and Hancocks areas; basalt and chert at Raffertys Patch; and quartz veins in komatiitic basalt around Six Mile Well (Stewart et al., 1983). Near Sandstone township, the most important orebody is the northerly trending Sandstone Reef that is composed of crumbly and friable quartz and abuts a 'jasper bar' (banded iron-formation; Maitland, 1919). Another important ore horizon near Sandstone township is the northerly trending Black Range Reef that also consists of quartz and has a spatial association with banded iron-formation (Maitland, 1919; Tingey, 1985).

Opencut mining at Bulchina (MGA 719337E 6893096N), that started in 1999 and ceased in April 2004, represents the only gold operation in the Sandstone greenstone belt during this period of time, and has produced 7152.37 kg of gold (Appendix 4; Minmet Australia Pty Ltd, 2004). Gold mineralization is hosted by mafic and clastic sedimentary rocks in the western part of the openpit, and porphyritic microgranite and ultramafic rocks in the eastern part. Gold mineralization is related to quartz veining. The orebody (approximately 4 m wide) typically follows steep to subvertical quartz veins that trend 010–020°, whereas shallowly to moderately dipping quartz veins are not mineralized.

Two significant new gold deposits (Lord Henry and Lord Nelson) have been discovered near the eastern edge of ATLEY, and they have a total inferred resource estimated at 3 673 000 t grading 2.7 g/t gold, with contained gold of 9922 kg (Troy Resources NL, 2004). The Lord Henry gold deposit is hosted by altered, medium- to coarse-grained granodiorite. It consists of a series of shallowly (20–30°) north-dipping, near-surface gold lodes, and has been defined by extensive drilling along strike for about 400 m and to a vertical depth of 60 m (Troy Resources NL, 2004). Most of the gold mineralization is confined to a central zone of sericite–quartz–carbonate–pyrite altered granodiorite. This zone contains multiple quartz–carbonate–pyrite–galena veins that vary from massive to laminated to brecciated (Troy Resources NL, 2004).

The Lord Nelson gold deposit is hosted by sheared basaltic and granitic rocks, close to or along the contact with a steeply dipping ultramafic unit. The north-northwest-trending mineralization attains a maximum surface width of 180 m and a strike length of 460 m (Troy Resources NL, 2004). Two principal north-northwest-trending zones of mineralization have been defined at Lord Nelson. A central zone of oxidized and supergene mineralization extends to 60–80 m depth; the East Lode of primary mineralization is hosted in quartz–carbonate–pyrite veins in westerly dipping, brittle–ductile shear zones (Troy Resources NL, 2004).

Ultramafic rocks in the Sandstone greenstone belt have been explored for nickel, and were found to contain normal background amounts of nickel with no economic concentrations (Stewart et al., 1983), although the widespread ultramafic rocks in the central–southern part of the greenstone belt were only revealed recently by extensive reconnaissance drilling for gold carried out by Troy Resources NL.

The Shepherd Well uranium deposit (MGA 705419E 6838476N) is within Lake Noondie, 8.2 km east of the Yuinmery Homestead on RAYS ROCKS. It has an inferred resource estimated at 1.58 Mt grading at 0.37 kg/t U_3O_8 (Pickaxe Pty Ltd, 1998).

References

AHMAT, A. L., 1986, Metamorphic patterns in the greenstone belts of the Southern Cross Province, Western Australia: Western Australia Geological Survey, Report 19, p. 1–21.

ANAND, R. R., CHURCHWARD, H. M., SMITH, R. E., SMITH, K., GOZZARD, J. R., CRAIG, M. A., and MUNDAY, T. J., 1993, Classification and atlas of regolith-landform mapping units: CSIRO/AMIRA Project P240A, Exploration and Mining Restricted Report 440R (unpublished).

ANAND, R. R., and PAINE, M., 2002, Regolith geology of the Yilgarn Craton, Western Australia: implications for exploration: Australian Journal of Earth Sciences, v. 49, p. 3–162.

ARNDT, N., BRUZAK, G., and REISCHMANN, T., 2001, The oldest continental and oceanic plateaus: Geochemistry of basalts and komatiites of the Pilbara Craton, Australia, *in* Mantle plumes: their identification through time *edited by* R. E. ERNST and K. L. BUCHAN: Boulder, Colorado, Geological Society of America Special Paper 352, p. 359–387.

ARNDT, N. T., and LESHER, C. M., 1992, Fractionation of REEs by olivine and the origin of Kambalda komatiites, Western Australia: Geochimica et Cosmochimica Acta, v. 56, p. 4191–4204.

BEARD, J. S., 1976, The vegetation of the Murchison region: Vegetation Survey of Western Australia, 1:1 000 000 Series, sheet 6 and explanatory notes: Perth, University of Western Australia Press.

BEARD, J. S., 1990, Plant life of Western Australia: Perth, Kangaroo Press, 319p.

BEESON, J., GROVES, D. I., and RIDLEY, J. R., 1993, Controls on mineralization and tectonic development of the central part of the northern Yilgarn Craton: Perth, Western Australia, Minerals and Energy Research Institute of Western Australia (MERIWA), Report no. 109, 93p.

BINNS, R. A., GUNTHORPE, R. J., and GROVES, D. I., 1976, Metamorphic patterns and development of greenstone belts in the eastern Yilgarn Block, Western Australia, *in* The early history of the Earth *edited by* B. F. WINDLEY: London, John Wiley and Sons, p. 303–313.

BIOLOGICAL SURVEYS COMMITTEE, 1992, The biological survey of the Eastern Goldfields of Western Australia. Part 6. Youanmi–Leonora study area: Records of the Western Australian Museum, Supplement Number 40, 131p.

BLEWETT, R. S., CASSIDY, K. F., CHAMPION, D. C., HENSON, P. A., GOLEBY, B. S., JONES, L., and GROENEWALD, P. B., 2004a, The Wangkathaa Orogeny: an example of episodic regional 'D_2' in the late Archaean Eastern Goldfields Province, Western Australia: Precambrian Research, v. 130, p. 139–159.

BLEWETT, R. S., SHEVCHENKO, S., and BELL, B., 2004b, The North Pole Dome: a non-diapiric dome in the Archaean Pilbara Craton, Western Australia: Precambrian Research, v. 133, p. 105–120.

CAMPBELL, I. H., GRIFFITHS, R. W., and HILL, R. I., 1989, Melting in an Archaean mantle plume: heads it's basalts, tails it's komatiites: Nature, v. 339, p. 697–699.

CHEN, S. F., 2004, Geology of the Marmion and Richardson 1:100 000 sheets: Western Australia Geological Survey, 1:100 000 Geological Series Explanatory Notes, 27p.

CHEN, S. F., LIBBY, J. W., GREENFIELD, J. E., WYCHE, S., and RIGANTI, A., 2001, Geometry and kinematics of large arcuate structures formed by impingement of rigid granitoids into greenstone belts during progressive shortening: Geology, v. 29, p. 283–286.

CHEN, S. F., LIBBY, J. W., WYCHE, S., and RIGANTI, A., 2004, Kinematic nature and origin of regional-scale ductile shear zones in the central Yilgarn Craton, Western Australia: Tectonophysics, v. 394, p. 139–153.

CHEN, S. F., and PAINTER, M.G.M., in press, Sandstone, W.A. Sheet 2742: Western Australia Geological Survey, 1:100 000 Geological Series.

CHEN, S. F., RIGANTI, A., WYCHE, S., GREENFIELD, J. E., and NELSON, D. R., 2003, Lithostratigraphy and tectonic evolution of contrasting greenstone successions in the central Yilgarn Craton, Western Australia: Precambrian Research, v. 127, p. 249–266.

CHEN, S. F., and WYCHE, S., (compilers), 2001, Archaean granite–greenstones of the central Yilgarn Craton, Western Australia — a field guide: Western Australia Geological Survey, Record 2001/14, 76p.

CHEN, S. F., and WYCHE, S., 2003, Geology of the Bungalbin 1:100 000 sheet: Western Australia Geological Survey, 1:100 000 Geological Series Explanatory Notes, 27p.

CLARKE, E. de C., 1914, Notes on the geology and mining at Sandstone and Hancock's, East Murchison Goldfield: Western Australia Geological Survey, Bulletin 62, p. 11–66.

COLLERSON, K. D., CAMPBELL, L. M., WEAVER, B. L., and PALACZ, Z. A., 1991, Evidence for extreme mantle fractionation in early Archaean ultramafic rocks from northern Labrador: Nature, v. 349, p. 209–214.

COMMONWEALTH BUREAU OF METEOROLOGY, viewed 23 September 2004, <http://www.bom.gov.au>.

DALSTRA, H. J., RIDLEY, J. R., BLOEM, E. J. M., and GROVES, D. I., 1999, Metamorphic evolution of the central Southern Cross Province, Yilgarn Craton, Western Australia: Australian Journal of Earth Sciences, v. 46, p. 765–784.

EISENLOHR, B. N., GROVES, D. I., LIBBY, J., and VEARNCOMBE, J. R., 1993, The nature of large scale shear zones and their relevance to gold mineralisation, Yilgarn Block: Perth, Western Australia, Minerals and Energy Research Institute of Western Australia (MERIWA), Report no. 122, 161p.

GERDES, R. A., YOUNG, G. A., CAMERON, B. F., and BEATTIE, R. D., 1970, Sandstone and Youanmi airborne magnetic and radiometric survey, Western Australia 1968: Australia Bureau of Mineral Resources, Record 1970/2 (unpublished), 34p.

GIBSON, C. G., 1908, Report upon the auriferous deposits of Barrambie and Errolls (Cue District) and Gum Creek (Nannine District) in the Murchison Goldfield; also Wiluna (Lawlers District) in the East Murchison Goldfield: Western Australia Geological Survey, Bulletin 34, 44p.

GREENFIELD, J. E., 2001, Geology of the Lake Giles 1:100 000 sheet: Western Australia Geological Survey, 1:100 000 Geological Series Explanatory Notes, 19p.

GREENFIELD, J. E., and CHEN, S. F., 1999., Structural evolution of the Marda–Diemals area, Southern Cross Province: Western Australia Geological Survey, Annual Review 1998–99, p. 68–73.

GRIFFIN, T. J., 1990, Southern Cross Province *in* Geology and mineral resources of Western Australia: Western Australia Geological Survey, Memoir 3, p. 60–77.

GRUAU, G., CHAUVEL, C., ARNDT, N. T., and CORNICHET, J., 1990, Al-depletion in komatiites and garnet fractionation in the early Archaean mantle: Hf isotopic constraints: Geochimica et Cosmochimica Acta, v. 54, p. 3095–3101.

HALLBERG, J. A., 1976, A petrochemical study of a portion of the western Yilgarn Block: Australia, CSIRO Minerals Research Laboratories, Division of Mineralogy, Report FP13, 38p.

HALLBERG, J. A., 1987, Postcratonization mafic and ultramafic dykes of the Yilgarn Block: Australian Journal of Earth Sciences, v. 34, p. 135–149.

HOCKING, R. M., and COCKBAIN, A. E., 1990, Regolith, *in* Geology and mineral resources of Western Australia: Western Australia Geological Survey, Memoir 3, p. 591–602.

HOCKING, R. M., LANGFORD, R. L., THORNE, A. M., SANDERS, A. J., MORRIS, P. A., STRONG, C. A., and GOZZARD, J. R., 2001, A classification system for regolith in Western Australia: Western Australia Geological Survey, Record 2001/4, 22p.

HOUSE, M., 1996, An integrated geophysical study of the three-dimensional structure and tectonic evolution of the Late Archaean granitoid–greenstone terrain in the Kambalda–Widgiemooltha area, Western Australia: University of Western Australia, PhD thesis (unpublished).

KERR, A. C., and ARNDT, N. T., 2001, A note on the IUGS reclassification of high-Mg and picritic volcanic rocks: Journal of Petrology, v. 42, p. 2169–2171.

KRAPEZ, B., BROWN, S. J. A., HAND, J., BARLEY, M. E., CAS, R. A. F., 2000, Age constraints on recycled crustal and supracrustal sources of Archaean metasedimentary sequences, Eastern Goldfields Province, Western Australia: evidence from SHRIMP zircon dating: Tectonophysics, v. 322, p. 89–133.

LANE, R., MILLIGAN, P., and ROBSON, D., 2003, An airborne gravity gradiometer survey of Broken Hill, *in* Broken Hill Exploration Initiative — Abstracts from the July 2003 Conference *edited by* M. PELJO: Canberra, Geoscience Australia, Record 2003/13, p. 89–92.

MAITLAND, A. G., 1919, The gold deposits of Western Australia, *in* The mining handbook *edited by* A. G. MAITLAND: Western Australia Geological Survey, Memoir 1, p. 1–92.

MATHESON, R. S., and MILES, K. R., 1947, The mining groups of the Yilgarn Goldfield north of the Great Eastern Railway: Western Australia Geological Survey, Bulletin 101, 242p.

McDONOUGH, W. F., and SUN, S-S., 1995, The composition of the earth: Chemical Geology, v. 120, p. 223–253.

MINMET Australia Proprietary Limited, 2004, viewed 15 September 2004, <http://www.intierra.com.minmet>.

MYERS, J. S., and HOCKING, R. M., 1998, Geological map of Western Australia, 1:2 500 000 (13th edition): Western Australia Geological Survey.

NELSON, D. R., 1997, Evolution of the Archaean granite–greenstone terranes of the Eastern Goldfields, Western Australia: SHRIMP U–Pb zircon constraints: Precambrian Research, v. 83, p. 57–81.

NELSON, D. R., 1999, Compilation of geochronology data, 1998: Western Australia Geological Survey, Record 1999/2, 222p.

NELSON, D. R., 2001, Compilation of geochronology data, 2000: Western Australia Geological Survey, Record 2001/2, 205p.

NELSON, D. R., 2002, Compilation of geochronology data, 2001: Western Australia Geological Survey, Record 2002/2, 282p.

NELSON, D. R., 2004, 165364, 165365: *in* Compilation of geochronology data, October 2004 update: Western Australia Geological Survey.

NELSON, D. R., in prep., 165364, 178050, 178051, 178052, 178054, 178056, 178060, 178061, 178062: *in* Compilation of geochronology data: Western Australia Geological Survey.

PASSCHIER, C. W., and TROUW, R. A. J., 1996, Microtectonics: Springer, 289p.

PAYNE, A. L., VAN VREESWYK, A. M. E., PRINGLE, H. J. R., LEIGHTON, K. A., and HENNIG, P., 1998, An inventory and condition survey of the Sandstone–Yalgoo–Paynes Find area, Western Australia: Agriculture Western Australia, Technical Bulletin 90, 372p.

PERRING, C. S., BARNES, S. J., and HILL, R. E. T., 1996, Geochemistry of komatiites from Forrestania, Southern Cross Province, Western Australia: Evidence for crustal contamination: Lithos, v. 37, p. 181–197.

PICKAXE Proprietary Limited, 1998, Annual Report: Report to Australian Stock Exchange, 1 September 1998, 12p.

PIDGEON, R. T., and HALLBERG, J. A., 2000, Age relationships in supracrustal sequences in the northern part of the Murchison Terrane, Archaean Yilgarn Craton, Western Australia: a combined field and zircon U–Pb study: Australian Journal of Earth Sciences, v. 47, p. 153–165.

PIDGEON, R. T., and WILDE, S. A., 1990, The distribution of 3.0 Ga and 2.7 Ga volcanic episodes in the Yilgarn Craton of Western Australia: Precambrian Research, v. 48, p. 309–325.

RAMSAY, J. G., 1967, Folding and fracturing of rocks: New York, McGraw-Hill, 568p.

RIGANTI, A., 2002, Geology of the Barlee 1:100 000 sheet: Western Australia Geological Survey, 1:100 000 Geological Series Explanatory Notes, 21p.

RIGANTI, A., 2003, Geology of the Everett Creek 1:100 000 sheet: Western Australia Geological Survey, 1:100 000 Geological Series Explanatory Notes, 39p.

RIGANTI, A., and CHEN, S. F., 2002, Geology of the Jackson 1:100 000 sheet: Western Australia Geological Survey, 1:100 000 Geological Series Explanatory Notes, 51p.

SCHIØTTE, L., and CAMPBELL, I. H., 1996, Chronology of the Mount Magnet granite–greenstone terrain, Yilgarn Craton, Western Australia: implications for field based predictions of the relative timing of granitoid emplacement: Precambrian Research, v. 78, p. 237–260.

SPROULE, R. A., LESHER, C. M., AYER, J. A., THURSTON, P. C., and HERZBERG, C. T., 2002, Spatial and temporal variations in the geochemistry of komatiites and komatiitic basalts in the Abitibi greenstone belt: Precambrian Research, v. 115, p. 153–186.

STEWART, A. J., WILLIAMS, I. R., and ELIAS, M., 1983, Youanmi, W.A.: Australia BMR and Western Australia Geological Survey, 1:250 000 Geological Series Explanatory Notes, 58p.

SUN, S-S., and McDONOUGH, W.F., 1989, Chemical and isotopic systematics of oceanic basalts: implications for mantle composition and processes, *in* Magmatism in the ocean basins *edited by* A. D. SAUNDERS and M. J. NORRY: Geological Society, Special Publication 42, p. 313–345.

TALBOT, H. W. B., 1912, Geological investigations in the country lying between latitude 28° and 29°45' south, and longitude 118°15' and 120°40' east, embracing part of the North Coolgardie and East Murchison Goldfields: Western Australia Geological Survey, Bulletin 45, 61p.

TINGEY, R. J., 1985, Sandstone, W.A.: Western Australia Geological Survey, 1:250 000 Geological Series Explanatory Notes, 37p.

TROY RESOURCES NL, 2004, Annual Report: Report to Australian Stock Exchange, 22 October 2004, 65p.

TYLER, I. M., and HOCKING, R. M., 2001, Tectonic units of Western Australia (scale 1:2 500 000): Western Australia Geological Survey.

van de GRAAFF, W. J. E., CROWE, R. W. A., BUNTING, J. A., and JACKSON, M. J., 1977, Relict early Cainozoic drainage in arid Western Australia: Zeitschrift fur Geomorphologie, v. 21, p. 379–400.

WYCHE, S., 2004, Lake Mason, W.A. Sheet 2842: Western Australia Geological Survey, 1:100 000 Geological Series.

WYCHE, S., CHEN, S. F., GREENFIELD, J. E., and RIGANTI, A., 2001, Geology of the Johnston Range 1:100 000 sheet: Western Australia Geological Survey, 1:100 000 Geological Series Explanatory Notes, 31p.

WYCHE, S., NELSON, D. R., and RIGANTI, A., 2004, 4350–3130 Ma detrital zircons in the Southern Cross Granite–Greenstone Terrane, Western Australia: implications for the early evolution of the Yilgarn Craton: Australian Journal of Earth Sciences, v. 51, p. 31–45.

Appendix 1

Gazetteer of localities on Atley, Rays Rocks, and southern Sandstone

Locality	*Easting*	*Northing*
Atley Homestead	703100	6876150
Bell Chambers Well	708400	6887650
Black Range	712136	6887178
Bulchina Mine	719337	6893096
Coomb Bore	745400	6893300
Dandaraga Homestead	726500	6885300
Hancocks Mine	729500	6897800
Iron Knob Well	738200	6889300
London Bridge	727578	6899373
Maninga Marley Mine	744000	6881300
Mount Holmes (on Everett Creek)	792250	6873100
New Year Bore	725400	6905000
Nunngarra Mine	723000	6893000
Rays Rocks	708350	6798200
Sandstone	725900	6902000
Six Mile Well	728150	6890650
Waukenjerrie Hill	729200	6928700
Yuinmery Homestead	697200	6838800

Appendix 2

Correlation of old and new rock codes for Atley, Rays Rocks, and southern Sandstone

Old code	*New code*
q	zqY
g	gY
Ag	AgY
Agb	Axg-mbY
Agf	AmgssY
Agm	AgmY
Agmf	AmgmsY
Agn	AmgsnY
Ang	AmgnY
Ab	AbYSA
Aba	AmbaYSA
Abf	AmbbsYSA
Abg	Axmb-mgYSA
Abv	AbbYSA
Acc	AccbYSA
Aci	AcibYSA
Ao	AoYSA
Aog	AogYSA
Aogf	AmogsYSA
As	AsYSA
Ash	AshYSA
Au	AmuYSA
Aur	AmusrYSA

Appendix 3

Sample preparation and analysis for geochemistry

For each sample, any veined or weathered material was removed using a diamond saw in GSWA's Carlisle laboratory, and any saw marks were ground off using a carborundum lap. Samples were then thoroughly washed and dried. A maximum of 1 kg of material was crushed in a modified Nugget™ jaw crusher. For each sample, a small amount of material was crushed and rejected, then the remainder of the sample was reduced to a nominal particle size of about 0.5 cm. After crushing of each sample, the crusher was cleaned with compressed air and a wire brush; after every five samples, the crusher jaws were removed, cleaned with high-pressure water, and dried.

Approximately 250 g of crushed material was milled for approximately 90 seconds in a Tema™ tungsten carbide ring mill, producing a talcum-powder grade pulp, with approximately 50 g of powder reserved for analysis.

Analyses of either GSWA's internal Bunbury Basalt reference material (BB1) or the Kerba Granodiorite reference material (KG1) were carried out along with unknowns and duplicates of unknowns, in each batch.

Analyses undertaken at Geoscience Australia (GA) comprise major element oxides and some trace elements analysed by X-ray fluorescence (XRF) on a fused glass disc and a pressed powder pellet, following the methodology of Norrish and Hutton (1969) and Norrish and Chappell (1977). The remaining trace elements, and the rare earth elements (REE; La–Lu) were analysed by inductively coupled plasma mass spectrometry (ICP-MS) using a solution prepared by dissolving the XRF glass disc, as described by Eggins et al. (1997) and Pyke (2000). ICP-MS and XRF calibration was checked by the routine analysis of eight international reference materials, including DNC-1, DTS-1, GSP-2, RGM-1, SCO-1, W-2, BHVO-1, and AGV-1. Based on analyses of reference material, most major element oxides have a percent relative standard deviation (RSD%) of < 4, whereas trace elements and REE with concentrations > ten times the detection level have RSD% <10 (most <5). FeO and LOI (loss on ignition) were determined gravimetrically.

References

EGGINS, S. M., WOODHEAD, J. D., KINSLEY, L. P. J., MORTIMER, G. E., SYLVESTER, P., McCULLOCH, M. T., HERGT, J. M., and HANDLER,. M. R., 1997, A simple method for the precise determination of ≥40 trace elements in geological samples by ICPMS using enriched isotope internal standardisation: Chemical Geology, v. 134, p. 311–326.

NORRISH, K., and CHAPPELL, B. W., 1977, X-ray fluorescence spectrometry, *in* Physical Methods in Determinative Mineralogy (2nd edition) *edited by* J. ZUSSMAN: London, Academic Press, p. 201–272.

NORRISH, K., and HUTTON, J. T., 1969, An accurate X-ray spectrographic method for the analysis of a wide range of geological samples: Geochimica et Cosmochimica Acta, v. 33, p. 431–453.

PYKE, J., 2000, Minerals laboratory staff develop new ICP-MS preparation method: Canberra, AGSO Research Newsletter, v. 33, p. 12–14.

Appendix 4

Recorded gold production from the Sandstone area

Site	*Start date*	*End date*	*Ore treated (kt)*	*Contained metal (kg gold)*
Abundance	1905	1905	0.428	9.817
Adelaide	1903	1921	262.069	6 361.649
Agnes	1907	1908	0.153	2.077
Albion	1907	1909	0.015	2.256
Allies	1914	1915	0.049	0.118
Another shot	1904	1904	0.006	0.218
Apples	1941	1954	1.04	113.738
Apples Extended	1950	1950	0.063	0.244
Artesian	1914	1916	0.152	25.517
Aruncourt	1906	1907	0.044	2.217
Ballarat	1904	1904	0.008	0.284
Bellchambers	1938	1942	3.143	42.395
Bilbie	1903	1904	0.048	7.641
Billys Charm	1938	1939	1.223	4.291
Birthday Gift	1915	1915	0.053	0.278
Black Range	1903	1925	2.468	99.342
Black Range Gold Mine	1958	1960	0.173	25.393
Black Range Gold Mines Ltd	1942	1942	0.085	0.446
Black Range Kohinor Conl	1907	1911	6.375	234.068
Black Range Main Reef	1903	1905	0.135	6.561
Black Range South Extended	1909	1910	–	0.746
Black Range Trafalgar No 1	1935	1936	0.242	1.4
Blackstone	1909	1909	–	0.307
Bonny Note	1932	1948	1.549	31.203
Bounty	1921	1923	0.208	2.381
Breakaway	1908	1914	0.947	87.843
Bright Beauty	1904	1905	0.022	0.732
Bulchina[a]	1999	2004	–	7 152.369
Bull Oak	1907	1917	0.798	31.251
Bulletin	1910	1937	0.784	29.322
Bullion	1907	1907	0.017	0.174
Cardigan	1904	1912	0.309	42.834
Catherine	1904	1904	0.017	0.057
Chance	1911	1911	–	0.531
Chicago	1903	1904	0.023	0.305
Comedy King	1911	1954	2.883	177.928
Comrades Leases	1907	1911	4.716	107.112
Coonabar	1910	1910	–	4.638
Crown	1905	1905	0.011	0.667
Crows	1922	1922	0.03	0.721
Dalmation	1932	1933	0.295	6.772
Dead Beat	1909	1911	0.01	3.857
Digger	1920	1920	0.017	0.472
Diver	1907	1907	0.03	0.688
Doolette South	1941	1953	2.148	78.743
Doris	1916	1916	0.021	3.797
Dream	1904	1905	0.056	8.661
Dreamland	1907	1908	0.083	9.156
Duke of Windsor	1938	1942	0.66	19.425
Dulgite	1904	1905	0.254	10.23
Eclipse	1904	1940	0.706	13.935
Eileen	1907	1909	0.079	0.596
Empire Gold Prospecting Syndicate NL	1923	1923	0.8	5.634
Entente	1917	1921	1.422	31.429
Erinjerry	1906	1906	0.015	0.167
Eureka	1903	1905	0.047	2.387
Evangeline	1905	1905	0.017	0.346
Faugh A Ballagh	1908	1917	2.577	102.462
Fingall	1904	1905	0.091	2.01
Flavinius	1911	1911	–	0.105
Floater	1904	1906	0.166	9.279
Freedom	1907	1910	0.612	19.627

Appendix 4 (continued)

Site	*Start date*	*End date*	*Ore treated (kt)*	*Contained metal (kg gold)*
General Kurapatkin	1907	1908	0.029	0.367
Georgina Mines	1931	1933	0.043	5.832
Geraldtonia	1902	1903	0.043	3.891
Glanmire	1909	1909	0.021	0.238
Golden Acre	1904	1906	0.371	5.727
Golden Ball Extended	1907	1908	0.071	1.834
Golden Gate	1905	1905	0.116	1.959
Golden Key	1905	1906	0.897	43.941
Good Hope	1904	1905	0.029	0.672
Great Koh-I-Nor	1914	1916	1.912	15.574
Great Surprise	1907	1907	–	0.177
Groper	1902	1905	0.161	9.27
Hacks	1936	1954	0.198	1.874
Hancocks	1993	1997	419.422	252.343
Hard To Get	1915	1915	–	0.277
Hatter	1905	1905	0.025	2.982
Havilah	1905	1929	49.273	1 053.517
Hill View	1939	1943	0.201	3.888
Home Rule	1911	1911	0.041	0.626
Horseshoe	1904	1908	0.238	7.938
Indomitable	1908	1909	0.1	0.586
Irishman	1910	1911	0.674	13.47
Iron Duke	1959	1959	0.113	0.269
Jewel	1904	1904	0.004	0.026
Jumble	1904	1906	0.096	2.689
Jumbo	1914	1917	0.136	16.261
Just-In-Time	1904	1904	0.043	1.076
Karridale	1905	1905	0.028	0.341
King	1982	1982	0.05	0.122
Kingoonyar	1904	1906	1.429	57.554
Kohinor	1904	1906	0.337	34.91
Kohinor North	1907	1915	1.782	38.208
Kohinor North Extended	1923	1924	0.095	0.839
Lady Ellen	1905	1914	0.653	98.927
Lady Jackson	1904	1906	0.047	0.576
Lady Jennifer	1959	1959	0.024	0.17
Lady Mary	1911	1911	0.013	6.112
Lady Maude	1906	1906	0.023	0.487
Lady Rini	1936	1937	0.708	4.311
Lady Seddon	1910	1914	1.053	22.768
Leap Year	1908	1909	0.051	0.766
Little Nell	1905	1906	0.05	0.364
Lone Hand	1912	1912	0.025	1.613
Lord William	1904	1904	0.027	0.348
Lucky Dip	1923	1923	0.014	0.246
Lucky Mine	1939	1939	0.28	0.697
Macs Addition	1909	1914	0.252	14.097
Magnum Bonum	1905	1905	–	0.185
Maid Marion	1907	1907	0.379	15.33
Maninga Marley	1904	1914	7.469	281.633
Maninga Marley North	1906	1914	3.594	130.011
Margaret	1913	1933	2.783	37.825
Mary	1908	1909	0.071	11.187
May King	1905	1909	0.266	4.68
Missing Link	1907	1912	0.438	19.446
Mulgarrie	1905	1905	0.025	0.107
Muriel Chapman	1904	1904	0.106	1.601
Myrtle	1914	1915	0.075	3.546
Mystery	1908	1918	4.495	106.475
Nancys Reward	1916	1921	0.885	36.61
New Jumbo	1918	1918	0.032	0.058
New Sensation	1907	1909	0.583	28.146
Nous Verrous	1922	1926	0.742	17.894
Nungarra Junction	1909	1915	1.496	23.928
Nunngarra	1907	1911	1.406	9.972

Appendix 4 (continued)

Site	*Start date*	*End date*	*Ore treated (kt)*	*Contained metal (kg gold)*
Olga	1982	1982	0.156	0.558
Orion	1909	1910	–	9.029
Oroya East	1922	1927	0.909	52.135
Oroya Extended	1909	1910	0.287	6.938
Orsova	1917	1917	0.046	0.408
Phoenix	1906	1906	0.082	0.486
Poseidon	1907	1907	0.03	3.711
Pyx	1913	1919	0.968	23.172
Queen Of The Range	1903	1904	0.197	2.085
Rainbow	1931	1932	0.026	9.262
Rambler	1914	1914	–	23.454
Redmond	1905	1905	0.035	0.579
Reindeer	1904	1906	0.086	2.538
Royal Flush	1907	1908	0.211	7.507
Royal Oak Mining Conl	1913	1915	1.862	31.312
Sandridge	1907	1911	26.771	471.471
Sandstone	1904	1993	379.023	6 508.536
Sandstone Development G M Co Ltd	1907	1908	0.883	3.136
Sceptic	1906	1906	–	0.117
Sensation	1910	1914	0.139	2.274
Shipmate	1919	1919	0.009	0.466
Sonny Boy	1935	1945	0.749	32.923
Sonny James	1947	1949	0.026	0.377
Squib	1905	1908	0.42	16.857
Storekeeper	1909	1909	–	0.291
Surprise North	1909	1909	–	0.207
Swede	1911	1911	0.037	0.272
Tekoa	1905	1905	0.015	0.479
Titanic	1914	1914	0.022	0.055
Trafalgar	1912	1915	2.484	68.924
Two Mile	1936	1938	0.24	0.896
Two Ps	1913	1913	0.037	0.466
Undaunted	1904	1904	0.081	1.432
Undaunted East	1904	1906	0.659	19.279
Undaunted East Extended	1905	1906	0.28	5.64
Vanguard	1912	1912	0.065	2.212
Venture	1908	1908	0.043	0.256
Venus	1907	1907	0.037	0.102
Victory	1910	1910	–	0.077
Wanderie	1904	1916	2.629	77.682
Wanderie No 1 North	1905	1908	0.822	18.842
Wanderie No 1 West	1904	1910	2.758	44.358
Wanderie No 2 East	1904	1904	0.008	0.015
Wanderie North	1910	1910	0.116	1.594
Wanderie North Extended	1909	1909	–	0.686
Wanganui	1904	1904	–	0.341
Waratah	1925	1928	0.422	9.973
Welcome	1904	1907	0.376	10.322
Wha G Ms Ltd	1908	1909	2.605	49.228
Wild Dog	1905	1905	0.008	0.166
Winora	1963	1963	0.203	0.232
Wirraminna	1903	1941	0.587	4.092
Wirraminna Central	1905	1906	0.414	5.689
Wirraminna South	1906	1906	0.052	1.138
Wonoka	1906	1913	9.026	141.432
Worker	1904	1909	1.225	44.248
Total				**25 120.227**

Reference

[a] MINMET Australia Proprietary Limited, 2004, viewed 15 September 2004, <http://www.intierra.com.minmet>.

All other data are from the Western Australian Department of Industry and Resources' mines and mineral deposits information (MINEDEX) database as of September 2004

Appendix 5

Gold resources in the Sandstone area

Site	*Resource category*	*Tonnage (Mt)*	*Grade (g/t)*	*Contained metal (kg gold)*	*Source*
Bellchambers	Indicated	0.16	2.7	432	Gold Mines of Australia, 1997
Bull Oak	Indicated	0.39	1.5	585	Herald Resources Ltd, 1998
Eureka–Sandstone	Indicated	0.112	1.6	179.2	Herald Resources Ltd, 2003
Havilah	Indicated	0.285	1.7	484.5	Herald Resources Ltd, 2003
Havilah	Inferred	0.041	2.1	86.1	Herald Resources Ltd, 2003
Ladybird	Indicated	0.118	2.5	295	Herald Resources Ltd, 2003
Ladybird	Inferred	0.04	2.1	84	Herald Resources Ltd, 2003
Lord Henry and Lord Nelson	Inferred	3.673	2.7	9 922	Troy Resources NL, 2004
Maninga Marley	Indicated	0.08	3.1	248	Herald Resources Ltd, 2000
Oroya–Sandstone	Indicated	0.063	5.3	333.9	Herald Resources Ltd, 1997
Piper	Inferred	0.08	1.79	143.2	Troy Resources NL, 2003
Plum Pudding	Indicated	0.05	1.6	80	Herald Resources Ltd, 1999
Sandstone North	Indicated	0.077	2	154	Herald Resources Ltd, 1999
Shillington	Inferred	0.13	1.5	195	Herald Resources Ltd, 2000
Two Mile Hill	Indicated	0.487	1.6	779.2	Herald Resources Ltd, 2002
Two Mile Hill	Inferred	0.102	2.6	265.2	Herald Resources Ltd, 2002
Vanguard–Sandstone	Indicated	0.105	1.5	157.5	Herald Resources Ltd, 1999
Vanguard–Sandstone	Inferred	0.225	1.6	360	Herald Resources Ltd, 1999
Total				**14 783.8**	

References

GOLD MINES OF AUSTRALIA Limited, 1997, Annual Report: Report to Australian Stock Exchange, 6 November 1997, 72p.

HERALD RESOURCES Limited, 1997, Annual Report: Report to Australian Stock Exchange, 30 October 1997, 56p.

HERALD RESOURCES Limited, 1998, Annual Report: Report to Australian Stock Exchange, 26 October 1998, 52p.

HERALD RESOURCES Limited, 1999, Annual Report: Report to Australian Stock Exchange, 20 October 1999, 52p.

HERALD RESOURCES Limited, 2000, Annual Report: Report to Australian Stock Exchange, 27 October 2000, 64p.

HERALD RESOURCES Limited, 2002, Annual Report: Report to Australian Stock Exchange, 24 October 2002, 66p.

HERALD RESOURCES Limited, 2003, Annual Report: Report to Australian Stock Exchange; 23 October 2003, 64p.

TROY RESOURCES NL, 2003, Annual Report: Report to Australian Stock Exchange, 27 October 2003, 66p.

TROY RESOURCES NL, 2004, Annual Report: Report to Australian Stock Exchange, 22 October 2004, 65p.

The ATLEY, RAYS ROCKS, and southern SANDSTONE 1:100 000-scale geological map sheets in the central Yilgarn Craton contain the Sandstone greenstone belt, and parts of the Unaly Hill and East Youanmi greenstone belts. The economically significant Sandstone greenstone belt has a triangular geometry, and contains widespread ultramafic rocks in the south. The Archaean greenstone rock types, lithostratigraphy, geochemistry, geophysical modelling results, tectonic history, and metamorphic features of the Sandstone greenstone belt are described in detail in these Explanatory Notes. Other Archaean greenstones, granitic rock types, Cainozoic regolith deposits, and gold mineralization are also described briefly.

These Explanatory Notes are published in digital format (PDF) and are available online at: www.doir.wa.gov.au/gswa/onlinepublications. Laser-printed copies can be ordered from the Information Centre for the cost of printing and binding.

Further details of geological publications and maps produced by the Geological Survey of Western Australia are available from:

Information Centre
Department of Industry and Resources
100 Plain Street
East Perth, WA 6004
Phone: (08) 9222 3459 Fax: (08) 9222 3444

www.doir.wa.gov.au/gswa/onlinepublications

CHEN

Geology of the Atley, Rays Rocks, and southern Sandstone 1:100 000 sheets

EXPLANATORY NOTES

RAYS ROCKS

AUSTRALIA 1:100 000 GEOLOGICAL SERIES

GEOLOGICAL SURVEY OF WESTERN AUSTRALIA

SHEET 2740

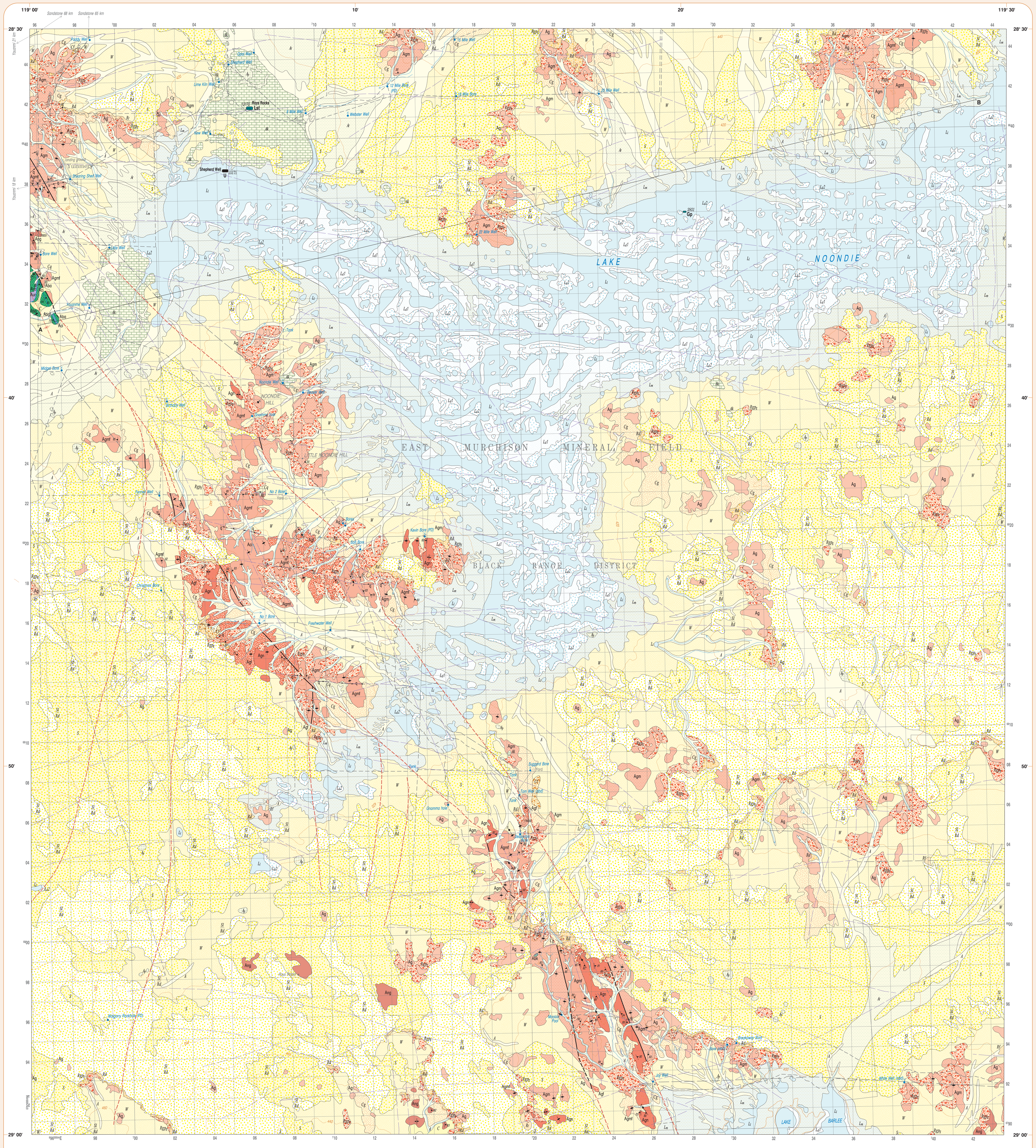

DIAGRAMMATIC SECTION

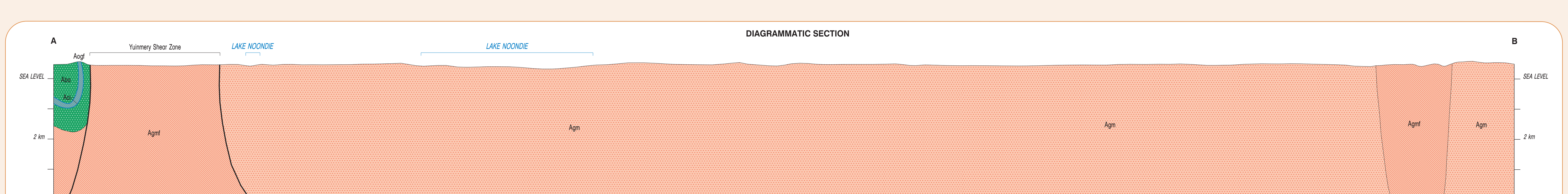

PHANEROZOIC

CAINOZOIC

C | Cf | Cg | Cq | W

A | Af | Ap | Ak | Ll | Ld1 | Lm

Colluvial units

C Mixed gravel and debris from different rock types as proximal talus; includes sand and silt
Cf Ferruginous gravel and reworked lateritic duricrust
Cg Quartzofeldspathic gravel, sand, and silt derived from granitic rock
Cq Quartz-vein debris

Sheetwash unit

W Clay, silt, and sand; locally ferruginous

Alluvial units

A Clay, sand, and gravel in drainage systems
Af Clay, sand, and gravel within floodplain
Ap Clay and silt in claypans
Ak Calcrete developed in and adjacent to alluvial channels and drainage

Lacustrine units

Ll Saline playa lake deposits
Ld1 Dune and lake deposits; active systems within and adjacent to playa lakes; non-vegetated or poorly vegetated
Lm Mixed dune, evaporite, sheetwash, and alluvial deposits adjacent to playa lakes

Ld2 | S | Sl

Lacustrine unit

Ld2 Stabilized sand dunes within and adjacent to playa lakes; typically vegetated

Sandplain units

S Residual and eolian sand
Sl Yellow sand with minor ferruginous pisoliths, silcrete, silt, and clay

Rd | Rf | Rgpg

Residual or relict units

Rd Siliceous and ferruginous duricrust, undivided
Rf Ferruginous duricrust and pisoliths
Rgpg Quartzofeldspathic sand and quartz gravel over granitic rock with sparse granitic rock outcrop

ARCHAEAN

YILGARN CRATON

q — Quartz vein

Ag | Agf | Agm | Agmf | Agn

Ag Granitic rock, undivided; includes deeply weathered granitic rock
Agf Strongly foliated granitic rock; typically deeply weathered
Agm Fine- to coarse-grained monzogranite; massive to weakly foliated, locally porphyritic
Agmf Strongly foliated, fine- to coarse-grained monzogranite; locally gneissic; *c.* 2718 Ma[1] near Tom Well
Agn Granitic rock with locally prominent gneissic banding; strongly foliated

Ang — Granitic gneiss; banded quartz–feldspar–biotite orthogneiss; *c.* 2681 Ma[1] near Yuinmery Homestead

Acc | Aci

Acc Banded chert; includes minor banded iron-formation; metamorphosed
Aci Metamorphosed banded iron-formation and minor banded chert

Aogf — Strongly foliated metagabbro; medium to coarse grained

Aba | Abk

Aba Fine- to medium-grained amphibolite, typically strongly foliated
Abk Komatiitic basalt with pyroxene-spinifex texture; metamorphosed

Aur — Tremolite–chlorite(–talc) schist

INTERPRETED BEDROCK GEOLOGY

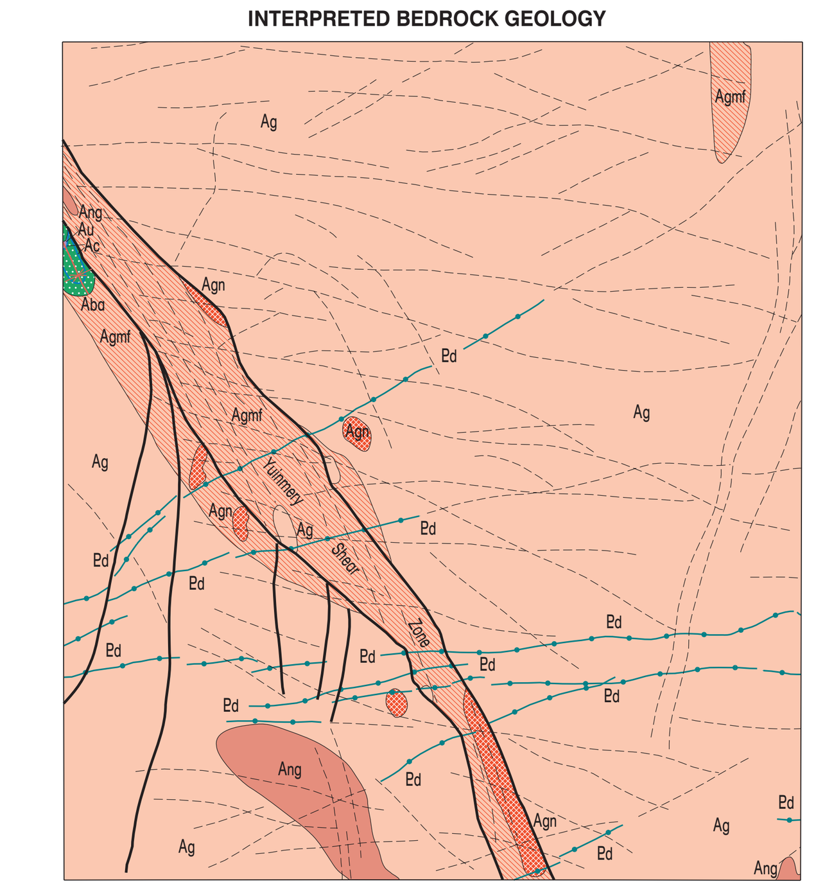

SCALE 1:500 000

0 5 10 15 20

Kilometres

Ꝑd — Mafic dyke

Ag | Agmf | Agn

Ag Granitic rock, mainly monzogranite
Agmf Foliated granitic rock, mainly monzogranite
Agn Gneissic granitic rock

Ang — Granitic gneiss
Ac — Banded iron-formation and chert
Aba — Amphibolite dominant
Au — Metamorphosed ultramafic rock

YILGARN CRATON

Fault or shear zone boundary
Fold axis
Foliation trend
Fracture pattern

For further details, refer to main reference

Geological boundary
exposed
Fault or shear
exposed
concealed
concealed, interpreted from aeromagnetic data
Fold, showing axial trace
syncline; exposed, concealed
Bedding, showing strike and dip
inclined — 64
Way-up indicator
pillow structure
Metamorphic foliation, showing strike and dip
inclined — 30
vertical
Gneissic banding, showing strike and dip
inclined — 84
vertical
Stretching lineation, showing trend and plunge
inclined — 38
Joint, showing strike and dip
vertical
Aeromagnetic lineament
Isotopic age determination site with identification number — 178051

Road; unsealed
Major track
Track
Fence, generally with track
Homestead — Yuinmery
Building
Yard — Yard
Rock — Rays Rocks
Breakaway
Sand dune
Contour line, 20 metre interval — 420

Watercourse with ephemeral pool or waterhole
Pool — Pool
Gnamma hole, rockhole — Gnamma hole, Rockhole
Bore, well — Bore, Well
Windpump
Tank — Tank
Abandoned — (abd)
Position doubtful — (PD)

Abandoned mine or deposit — Rays Rocks
Opencut

MINERAL OCCURRENCES

MINERALIZATION STYLES*

Regolith hosted

MINERAL AND ROCK COMMODITY GROUPS

Energy
Industrial mineral

MINERAL AND ROCK COMMODITIES

Gypsum — Gp
Limestone — Lst
Uranium — U

OPERATING STATUS AND SITE IDENTIFICATION NUMBER

Abandoned mine — e.g. *13170*
Mineral deposit — e.g. 13171
Mineral occurrence or prospect — e.g. *3831*

Mineral occurrences and numbers are from the GSWA WAMIN database.
*Larger symbols represent mines or deposits also in the DoIR MINEDEX database.

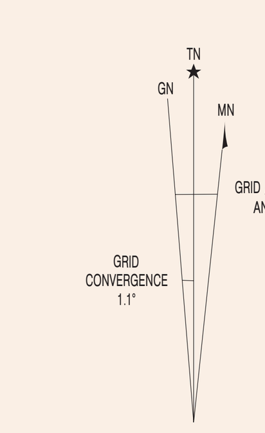

True north, grid north and magnetic north are shown diagrammatically for the centre of the map. Magnetic north is correct for 2003 and moves easterly by about 0.1° in 1 year.

SHEET INDEX

WINDIMURRA 2641	ATLEY 2741 YOUANMI	EVERETT CREEK 2841	MUNJEROO 2941	WILDARA 3041 LEONORA	WEEBO 3141
YOUANMI 2640	SH 50-4 RAYS ROCKS 2740	RICHARDSON 2840	MOUNT ALEXANDER 2940	SH 51-1 WILBAH 3040	LEONORA 3140
MALGAR 2639	BARLEE 2739 BARLEE	MARMION 2839	MOUNT MASON 2939	BALLARD 3039 MENZIES	MELITA 3139
ROSS 2638	SH 50-8 JOHNSTON RANGE 2738	LAKE GILES 2838	MULLINE 2938	SH 51-5 RIVERINA 3038	MENZIES 3138

1:100 000 maps shown in black
1:250 000 maps shown in brown

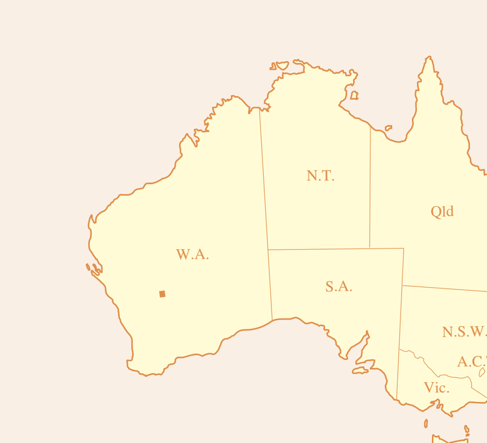

Geology by S. F. Chen 2002

Geochronology by:
(1) D. R. Nelson, in prep., GSWA Record 2004/2.

Edited by G. Hall and G. Loan

Cartography by P. Taylor, K. Greenberg, and B. Williams

Mineralization and rock commodity information from non-confidential data held in the WAMIN database, GSWA, at 12 September 2003.

Topography from the Department of Land Information Sheet SH 50-4, 2740, with modifications from geological field survey

Plotted by the Geological Survey of Western Australia. Digital and hard copies of this map are available from the Information Centre, Department of Industry and Resources, 100 Plain Street, East Perth, WA, 6004. Phone (08) 9222 3459, Fax (08) 9222 3444
Web www.doir.wa.gov.au Email geological.survey@doir.wa.gov.au

The recommended reference for this map is:
CHEN, S. F., 2003, Rays Rocks, W.A. Sheet 2740 Western Australia Geological Survey, 1:100 000 Geological Series

Department of Industry and Resources

Geological Survey of Western Australia

CLIVE BROWN, M.L.A.
MINISTER FOR STATE DEVELOPMENT

JIM LIMERICK
DIRECTOR GENERAL

TIM GRIFFIN
DIRECTOR

SCALE 1:100 000

1000 0 1 2 3 4 5 6 7 8 9 10

Metres — Kilometres

UNIVERSAL TRANSVERSE MERCATOR PROJECTION
HORIZONTAL DATUM: GEOCENTRIC DATUM OF AUSTRALIA 1994
VERTICAL DATUM: AUSTRALIAN HEIGHT DATUM

Grid lines indicate 1000 metre interval of the Map Grid Australia Zone 50

The Map Grid Australia (MGA) is based on the Geocentric Datum of Australia 1994 (GDA94)
GDA94 positions are compatible within one metre of the datum WGS84 positions

RAYS ROCKS

SHEET 2740 FIRST EDITION 2003
Version 1 — December 2003

AUSTRALIA 1 : 100 000 GEOLOGICAL SERIES

GEOLOGICAL SURVEY OF WESTERN AUSTRALIA

ATLEY

SHEET 2741

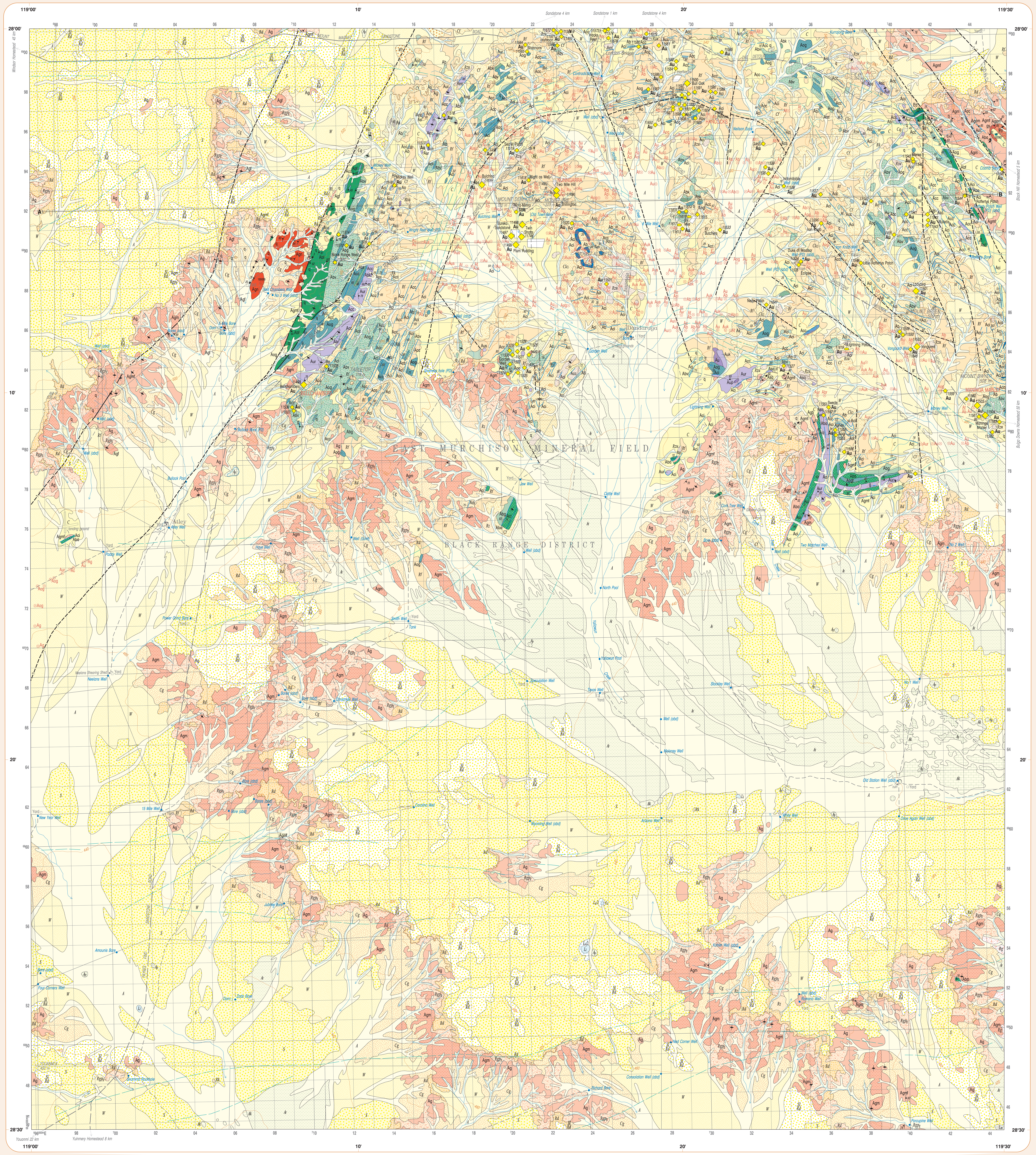

DIAGRAMMATIC SECTION

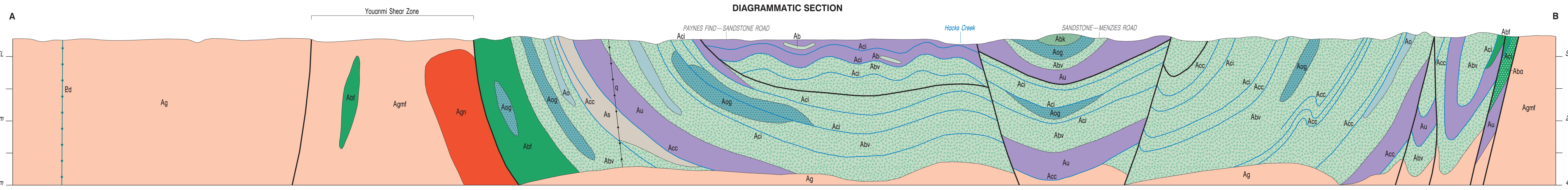

PHANEROZOIC — CAINOZOIC

Colluvial units

- *C* Mixed gravel and debris from different rock types; includes sand and silt; locally ferruginous
- *Cf* Ferruginous gravel and reworked duricrust
- *Cg* Quartzofeldspathic gravel, sand, and silt derived from granitoid rock
- *Clci* Talus mainly derived from banded iron-formation and chert; locally cemented
- *Cq* Quartz-vein debris

Sheetwash units

- *W* Clay, silt, and sand; locally ferruginous
- *Wf* Ferruginous grit; includes clay, silt, and sand

Alluvial units

- *A* Clay, silt, sand, and gravel in drainage systems
- *Af* Clay, silt, sand, and gravel within floodplain
- *Ap* Clay and silt in claypans
- *Ak* Calcrete developed in and adjacent to alluvial channels

Lacustrine units

- *Ll* Saline playa lake deposits
- *Lm* Mixed sand dune, evaporite, and alluvial deposits adjacent to playa lakes

Lacustrine unit

- *Ld2* Stabilized sand dunes adjacent to playa lakes; typically vegetated

Sandplain units

- *S* Residual and eolian sand
- *Sl* Yellow sand with minor ferruginous pisoliths, silcrete, silt, and clay

Residual or relict units

- *Rd* Siliceous and ferruginous duricrust
- *Rf* Ferruginous duricrust and pisoliths
- *Rg* Quartzofeldspathic sand; commonly over granitoid rock
- *Rgpg* Quartzofeldspathic sand and quartz gravel over granitoid rock, with sparse granitoid outcrop
- *Rk* Calcrete
- *Rz* Silcrete
- *Rzu* Siliceous caprock over ultramafic rock

PROTEROZOIC

- Ꝑd Mafic dyke; includes dolerite and gabbro

ARCHAEAN — YILGARN CRATON

- q Quartz vein
- g Granitoid dyke
- gy Granophyre

- Ag Granitoid rock, undivided; includes deeply weathered rock
- Agb Granitoid rock interleaved with minor mafic rock
- *c.* 2686 Ma[1 2] Agcm **COOMB BORE MONZOGRANITE:** medium- to coarse-grained monzogranite; includes minor syenogranite and granodiorite
- Agf Strongly foliated granitoid rock; typically deeply weathered
- Agm Fine- to coarse-grained monzogranite; massive to weakly foliated
- Agmf Strongly foliated, fine- to coarse-grained monzogranite; locally gneissic
- Agn Gneissic granitoid rock; fine to coarse grained, strongly foliated monzogranite to syenogranite; *c.* 2667 Ma[1] near Bell Chambers Well

- As Metasedimentary rock, undivided; typically deeply weathered
- Asq Quartz-rich metasedimentary rocks, mainly quartzite
- Acc Banded chert and ferruginous chert; includes minor banded iron-formation; metamorphosed
- Aci Metamorphosed banded iron-formation and minor banded chert

- Af Fine-grained felsic rock, metamorphosed; commonly weathered; *c.* 2731 Ma[2] in Bulchina opencut

- Ao Medium- and coarse-grained mafic rock; typically deeply weathered
- Aog Medium- to coarse-grained metagabbro; massive to weakly deformed
- Aogf Strongly foliated metagabbro; medium to coarse grained

- Ab Metamorphosed fine-grained mafic rock, undivided; metamorphosed; typically deeply weathered
- Aba Amphibolite; fine to medium grained, typically strongly foliated
- Abf Foliated to amphibolitic metabasalt; fine to medium grained
- Abg Mafic rock interleaved with minor granitoid rock; metamorphosed
- Abk Pyroxene spinifex-textured komatiitic basalt; metamorphosed
- Abr Tremolite- and chlorite-rich rock, with relict pyroxene spinifex texture; moderately to strongly foliated
- Abt Metamorphosed mafic tuff; well bedded
- Abv Metabasalt; fine grained, massive to weakly foliated

- Au Metamorphosed ultramafic rock, undivided; typically deeply weathered
- Auk Metakomatiite, with relict olivine spinifex texture
- Aup Peridotite; metamorphosed and locally serpentinized
- Aur Tremolite–chlorite(–talc) schist
- Aus Serpentinite

Geological boundary
- exposed
Fault
- exposed
- concealed
- concealed, interpreted from aeromagnetic data
Fold, showing axial trace and generalized plunge direction
- syncline; exposed, concealed
Small-scale fold axis, showing trend and plunge
- anticline
- syncline
- antiform
- synform
Bedding, showing strike and dip
- inclined
- vertical
Way-up indicator
- pillow structure
Foliation, showing strike and dip
- inclined
- vertical
- trend of foliation
Mineral lineation, showing trend and plunge
- inclined
Fracture, joint, or extension vein, showing strike and dip
- inclined
- vertical
Aeromagnetic lineament
Isotopic age determination site with identification number — 123456

Road, sealed
Road, unsealed
Major track
Track
Fence, generally with track
Abandoned railway
Homestead — Atley
Locality — Nunngarra
Building
Yard — Yard
Microwave repeater station
Horizontal control; major, minor
Breakaway
Sand dune
Contour line, 20 metre interval — 240

Watercourse with ephemeral pool or waterhole
Pool — Pool
Gnamma hole, rockhole — Gnamma hole, Rockhole
Soak — Soak
Bore, well — Bore, Well
Windpump
Dam, tank — Dam, Tank
Abandoned — (abd)
Position doubtful — (PD)

Mining centre — HANCOCKS
Mine or deposit name — Bulchina
Battery or treatment plant, abandoned
Opencut
Tailings or stockpile
Subsurface data from drillhole, costean, shallow shaft, or pit — Au

MINERAL OCCURRENCES

MINERALIZATION STYLES*

- Vein and hydrothermal mineralization
- Mineralization in the regolith

MINERAL AND ROCK COMMODITY GROUPS

- Precious metal

MINERAL AND ROCK COMMODITIES

Gold .... Au

OPERATING STATUS AND SITE IDENTIFICATION NUMBER

Operating mine	e.g. 11493
Abandoned mine	e.g. *11506*
Mineral occurrence or prospect	e.g. *3465*

Mineral occurrences and numbers are from the GSWA WAMIN database.
*Larger symbols represent mines or deposits also in the DoIR MINEDEX database

INTERPRETED BEDROCK GEOLOGY

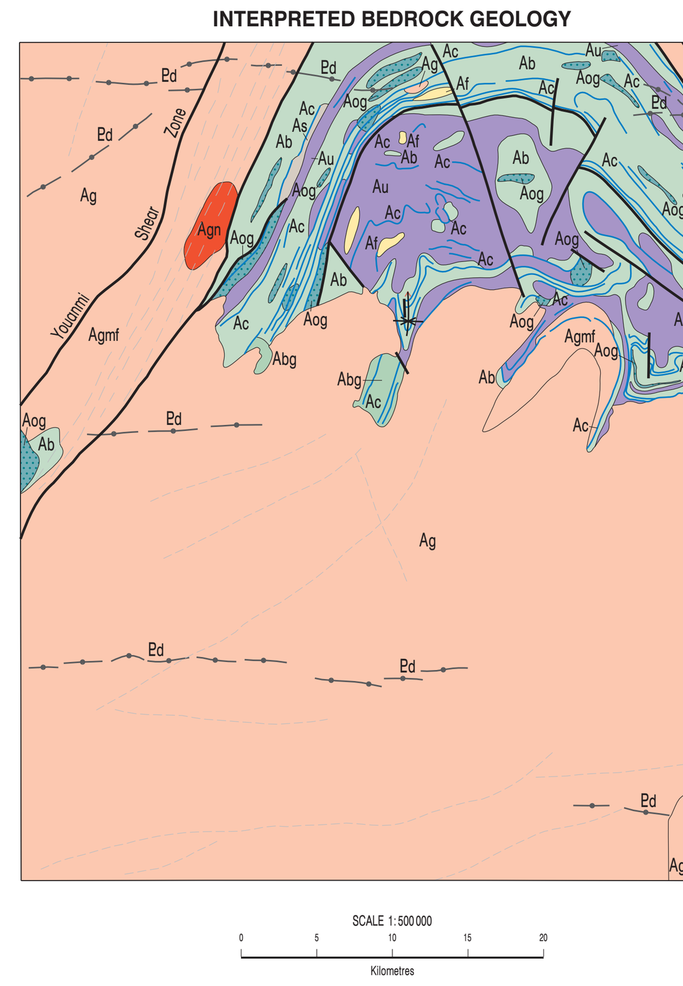

- Ꝑd Mafic dyke
- gy Granophyre
- Ag Granitoid rock
- Agcm Coomb Bore Monzogranite
- Agmf Foliated granitoid rock, mainly monzogranite
- Agn Gneissic granitoid rock
- As Clastic sedimentary rock dominant
- Ac Banded iron-formation and chert
- Af Felsic volcanic and volcaniclastic rocks
- Aog Metagabbro dominant
- Ab Metabasalt dominant
- Abg Mafic and ultramafic rocks with minor granitoid; metamorphosed
- Au Metamorphosed ultramafic rocks dominant

YILGARN CRATON

- Fault
- Fold axis
- Foliation trend
- Fracture pattern

For further details, refer to main reference

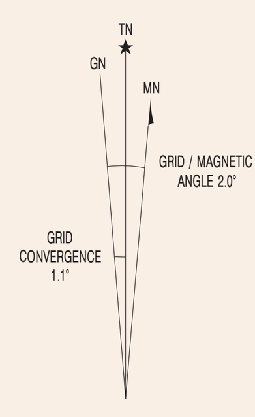

True north, grid north and magnetic north are shown diagrammatically for the centre of the map. Magnetic north is correct for 2002 and moves easterly by about 0.1° in 1 year.

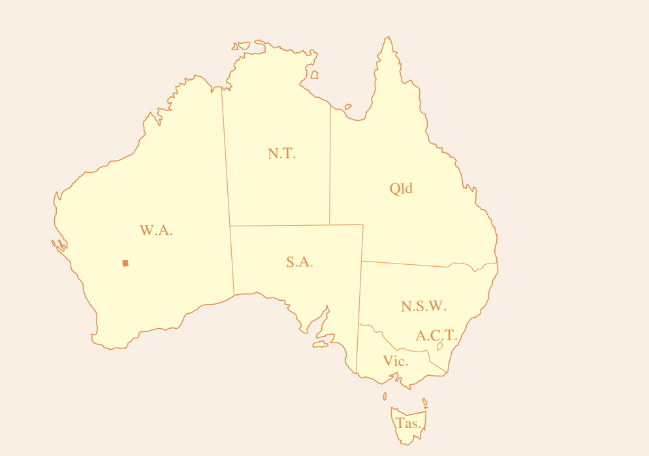

Geology by S. F. Chen 2001–2002

Geochronology by:
(1) D. R. Nelson, 2002, GSWA Record 2002/2, p. 219–224.
(2) D. R. Nelson, in prep., GSWA Record 2003/2.

Edited by C. Strong and G. Loan

Cartography by D. Ladbrook and K. Greenberg

Mineralization and rock commodity information from non-confidential data held in the WAMIN database, GSWA, at 3 June 2003. Data points filtered for clarity on the plotted product; full set of data points available in digital data

Topography from the Department of Land Administration Sheet SH 50-4, 2741 with modifications from geological field survey

Plotted by the Geological Survey of Western Australia. Digital and hard copies of this map are available from the Information Centre, Department of Industry and Resources, 100 Plain Street, East Perth, WA, 6004. Phone (08) 9222 3459, Fax (08) 9222 3444
Web www.doir.wa.gov.au Email geological_survey@doir.wa.gov.au

The recommended reference for this map is:
CHEN, S. F., 2003, Atley, W.A. Sheet 2741: Western Australia Geological Survey, 1:100 000 Geological Series.

SHEET INDEX

NOWTHANNA 2643	YOUNO DOWNS 2743 SANDSTONE	MONTAGU 2843	YEELIRRIE 2943	MOUNT KEITH 3043 SIR SAMUEL	WANGGANNOO 3143
WOODLEY 2642	SG 50-16 SANDSTONE 2742	LAKE MASON 2842	DEPOT SPRINGS 2942	SG 51-13 SIR SAMUEL 3042	DARLOT 3142
WINDIMURRA 2641	ATLEY 2741 YOUANMI	EVERETT CREEK 2841	MUNJEROO 2941	WILDARA 3041 LEONORA	WEEBO 3141
YOUANMI 2640	SH 50-4 RAYS ROCKS 2740	RICHARDSON 2840	MOUNT ALEXANDER 2940	SH 51-1 WILBAH 3040	LEONORA 3140

1:100 000 maps shown in black
1:250 000 maps shown in brown

Department of Industry and Resources

CLIVE BROWN, M.L.A.
MINISTER FOR STATE DEVELOPMENT

JIM LIMERICK
DIRECTOR GENERAL

Geological Survey of Western Australia

TIM GRIFFIN
DIRECTOR

SCALE 1:100 000

1000 Metres 0 1 2 3 4 5 6 7 8 9 10 Kilometres

UNIVERSAL TRANSVERSE MERCATOR PROJECTION
HORIZONTAL DATUM: GEOCENTRIC DATUM OF AUSTRALIA 1994
VERTICAL DATUM: AUSTRALIAN HEIGHT DATUM

Grid lines indicate 1000 metre interval of the Map Grid Australia Zone 50

The Map Grid Australia (MGA) is based on the Geocentric Datum of Australia 1994 (GDA94)
GDA94 positions are compatible within one metre of the datum WGS84 positions

ATLEY

SHEET 2741 FIRST EDITION 2003
Version 1 — June 2003

SANDSTONE

AUSTRALIA 1 : 100 000 GEOLOGICAL SERIES | **GEOLOGICAL SURVEY OF WESTERN AUSTRALIA** | **SHEET 2742**

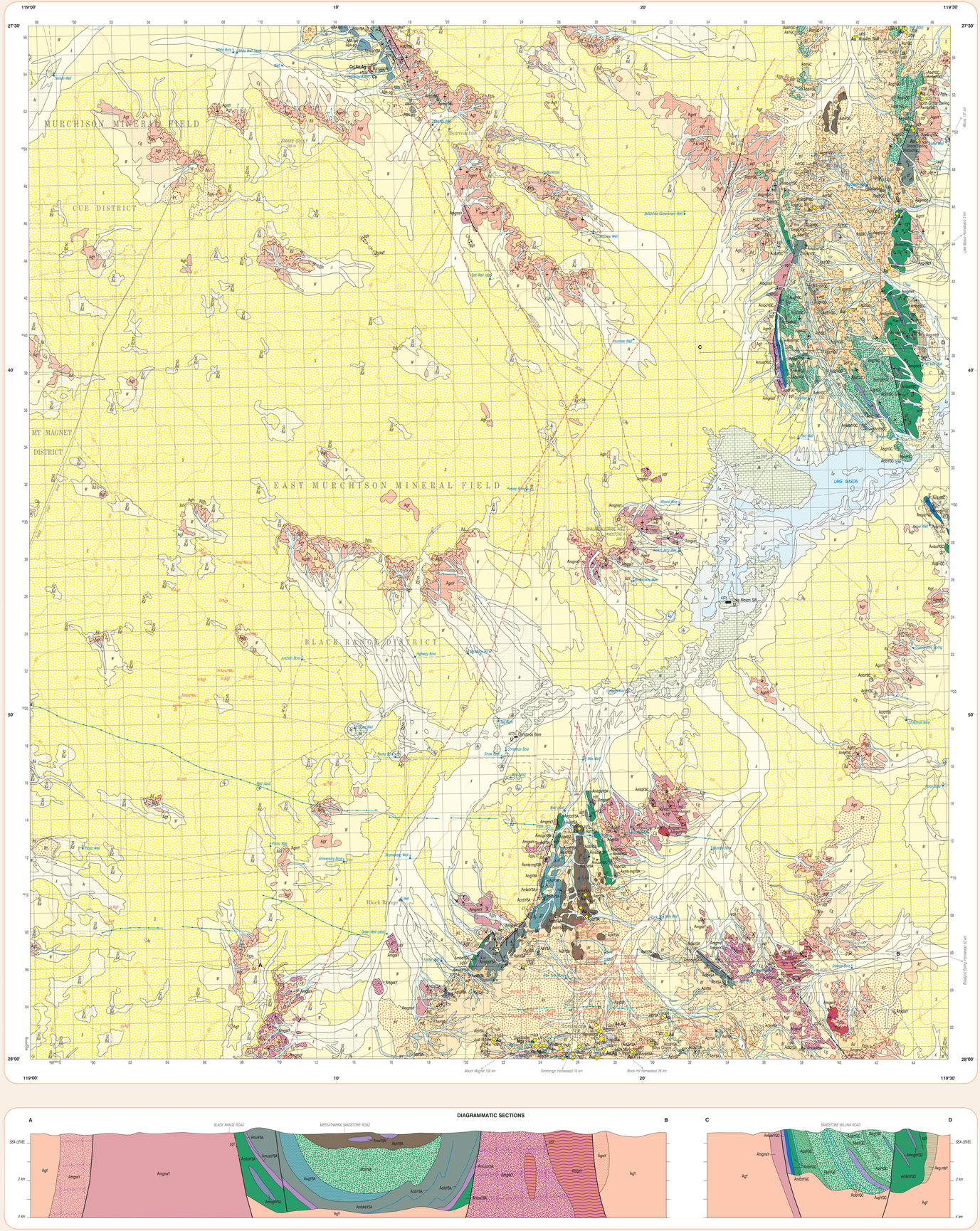

DIAGRAMMATIC SECTIONS

INTERPRETED BEDROCK GEOLOGY

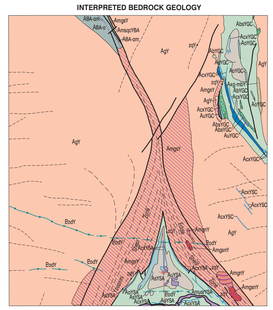

Boulder greenstone belt
Bonnievale greenstone belt
Sandstone greenstone belt
Gum Creek greenstone belt
Southern Cross Granite–Greenstone Terrane
Murchison Granite–Greenstone Terrane
YILGARN CRATON

Fault
Foliation trend
Fracture pattern
Fold axis
For further details, refer to main reference

SHEET INDEX

Search for current GSWA map products online (www.doir.wa.gov.au/astockshop)

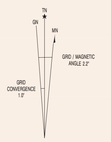

True north, grid north and magnetic north are shown diagrammatically for the centre of the map. Magnetic north is correct for 2005 and moves easterly by about 0.1° in 1 year.

DATA DIRECTORY

Theme	Data Source	Data Currency	Agency
Geology	GSWA	2002 – 2003	Dept of Industry and Resources
Structural data	WAROX	NOV 2004	Dept of Industry and Resources
Mineral occurrences (non-confidential)	MINEDEX	NOV 2004	Dept of Industry and Resources
	WAMIN	NOV 2004	Dept of Industry and Resources
Cadastre	TENGRAPH	NOV 2004	Dept of Industry and Resources
Horizontal control	GEOMAR	NOV 2004	Dept of Land Information
Topographic nomenclature	GEONOMA	2004	Dept of Land Information
Topography	DLI (modified by GSWA field survey)	2004	Dept of Land Information

Department of Industry and Resources

ALAN CARPENTER, M.L.A. — MINISTER FOR STATE DEVELOPMENT
JIM LIMERICK — DIRECTOR GENERAL

Geological Survey of Western Australia

TIM GRIFFIN — DIRECTOR

SCALE 1:100 000

1000 Metres 0 1 2 3 4 5 6 7 8 9 10 Kilometres

UNIVERSAL TRANSVERSE MERCATOR PROJECTION
HORIZONTAL DATUM: GEOCENTRIC DATUM OF AUSTRALIA 1994
VERTICAL DATUM: AUSTRALIAN HEIGHT DATUM
Grid lines indicate 1000 metre interval of the Map Grid Australia Zone 50

GDA

The Map Grid Australia (MGA) is based on the Geocentric Datum of Australia 1994 (GDA94). GDA94 positions are compatible within one metre of the datum WGS84 positions

Reference points to align maps based on the previous datum, AGD84, have been plotted near the map corners

Geology by S. F. Chen 2002–2003 and M. G. M. Pointer 2002

Geochronology by:
(1) D. R. Nelson, in prep., GSWA geochronology dataset, GSWA 178360, 178061, 178062

Edited by G. Lazo and A. Thomson

Cartography by P. Blackhouse, P. Taylor, and B. Williams

Published by the Geological Survey of Western Australia. Digital and hard copies of this map are available from the Information Centre, Department of Industry and Resources, 100 Plain Street, East Perth, WA, 6004. Phone (08) 9222 3459. Fax (08) 9222 3444
Web: www.doir.wa.gov.au Email: geological.survey@doir.wa.gov.au

The recommended reference for this map is:
CHEN, S. F. and PAINTER, M. G. M., 2005, Sandstone, W.A. Sheet 2742: Western Australia Geological Survey, 1:100 000 Geological Series.

PHANEROZOIC

CAINOZOIC

Colluvial units
- C — Colluvium, undivided; includes gravel, sand, and silt; locally ferruginous
- Cf — Ferruginous gravel and reworked ferruginous duricrust
- Cg — Quartz/lithopathic gravel, sand, and silt, commonly derived from granitic rock and associated weathering products
- Clc — Talus mainly derived from bonded iron-formation and chert; locally cemented
- Cq — Quartz-vein debris

Sheetwash units
- W — Clay, silt, and sand; locally ferruginous gravel
- Wf — Clay, silt, and sand with abundant ferruginous grit

Alluvial units
- A — Clay, silt, sand, and gravel in channels and on floodplains
- a — Clay, silt, sand, and gravel on floodplains
- Ap — Clay and silt in claypans
- Ak — Calcrete and carbonate-cemented alluvium in channels and drainage

Lacustrine units
- Lu1 — Dune and lake deposits; active systems within and adjacent to playa lakes; non-vegetated or poorly vegetated
- Lm — Mixed dune, evaporite, sheetwash, and alluvial deposits, typically adjacent to playa lakes
- Le — Saline and gypsiferous evaporite deposits; clay, silt, and sand in playa lakes

Lacustrine unit
- Lu2 — Stabilized dunes within and adjacent to playa lakes; typically vegetated

Sandplain units
- S — Residual and eolian sand with minor silt and clay; dunes locally common
- Sl — Yellow sand with minor ferruginous and siliceous pisoliths, silt, and clay

Residual or relict units
- Rd — Siliceous and ferruginous duricrust, undivided
- Rf — Ferruginous duricrust and pisoliths
- Rgh — Quartz/lithopathic sand and quartz gravel over granitic rock, with sparse granitic rock outcrop
- Rz — Silcrete
- Rza — Silica outcrop over ultramafic rock

PROTEROZOIC

- Bodr — Mafic to ultramafic dyke; interpreted from aeromagnetic data; maybe subsurface
- zqf — Quartz vein
- gf — Granitic dyke
- pgmf — Pegmatite vein

- Amgmgf — Strongly foliated, fine- to coarse-grained metamorphosed granitic rock; locally gneissic; c. 2687 Ma[1] southwest of Wizard Bore
- Amgrgf — Granitic gneiss; bonded quartz±lithopathic orthogneiss; c. 2693 Ma[1] north-northeast of Sandstone
- Amgmgf — Metagranitic rock with locally prominent gneissic bonding; typically strongly foliated
- Amgsgf — Strongly foliated metagranitic rock; typically deeply weathered
- Agf — Granitic rock, undivided; includes deeply weathered granitic rock
- Avg-mbf — Massive to moderately foliated granitic rock interleaved with minor foliated metamafic rock
- Agmpf — Fine- to coarse-grained monzogranite, locally porphyritic; massive to weakly foliated; c. 2664 Ma[1] southwest of Wizard Bore
- Agmpf — Porphyritic monzogranite; fine to coarse grained, commonly with feldspar megacrysts

- AcctrYMU — Bonded chert and ferruginous chert; minor bonded iron-formation; metamorphosed
- AmbdrYMU — Amphibolite, fine to medium grained, typically foliated
- AmuYMU — Metamorphosed ultramafic rock, undivided (subsurface only)

- AmsqzYBA — Quartz–chlorite schist, and minor foliated metasedimentary rock
- AcbYBA — Bonded iron-formation and minor bonded chert; metamorphosed

- ABA-c — **Boorambie intrusion**: medium- to coarse-grained, layered mafic rock; metamorphosed; typically deeply weathered
- ABA-og — Layered gabbro, with minor pyroxenite and anorthosite; metamorphosed
- ABA-om — Mingelletite; metamorphosed

- AmsqzYSC — Quartz-rich metasedimentary rock, mainly quartzite; metamorphosed
- AsYSC — Sedimentary rock, undivided; metamorphosed; weathered
- AcbYSC — Bonded iron-formation and minor bonded chert; metamorphosed

- AsYSA — Sedimentary rock, undivided; metamorphosed; typically deeply weathered (subsurface only)
- AshYSA — Shale and siltstone; minor sandstone and volcaniclastic rock; metamorphosed; typically weathered
- AcctrYSA — Bonded chert and ferruginous chert; minor bonded iron-formation; metamorphosed
- AcbYSA — Bonded iron-formation and minor bonded chert; metamorphosed

- AmsgrYSA — Strongly foliated metagabbro
- AcrYSA — Mafic intrusive rock; typically medium to coarse grained; metamorphosed; deeply weathered
- AogYSA — Gabbro, medium to coarse grained; massive to weakly deformed; metamorphosed

- Asmb-mgYSA — Foliated metamafic rock, interleaved with minor foliated granitic rock
- AmbpYSA — Amphibolite; fine to medium grained, commonly foliated; local foliated metabasalt
- AmbdrYSA — Foliated metabasalt; fine to medium grained; local amphibolite
- AbYSA — Fine- to very fine-grained mafic rock, undivided; metamorphosed; commonly deeply weathered
- AbtYSA — Basalt, massive to weakly foliated; metamorphosed (in section only, interpreted from AbYSA)

- AmuYSA — Metamorphosed ultramafic rock, undivided; typically deeply weathered
- AmuatrYSA — Tremolite–chlorite(–talc) schist
- AmuurYSA — Foliated medium- to coarse-grained pyroxenite

- AshYGC — Sedimentary rock, undivided; metamorphosed; typically deeply weathered
- AsmYGC — Shale and siltstone; metamorphosed; typically weathered
- AcctrYGC — Bonded chert and ferruginous chert; minor bonded iron-formation; metamorphosed
- AcbYGC — Bonded iron-formation and minor bonded chert; metamorphosed

- AmsgrYGC — Strongly foliated metagabbro
- AcrYGC — Mafic intrusive rock; typically medium to coarse grained; metamorphosed; deeply weathered
- AogYGC — Gabbro, medium to coarse grained; massive to weakly deformed; metamorphosed

- Asmb-mgYGC — Foliated metamafic rock, interleaved with minor massive to moderately foliated granitic rock
- AmbpYGC — Amphibolite; fine to medium grained, commonly foliated; local foliated metabasalt
- AmbdrYGC — Foliated metabasalt; fine to medium grained; local amphibolite
- AmbarYGC — Tremolite- and chlorite-rich rock; local relict pyroxene spinifex texture; moderately to strongly foliated
- AbYGC — Fine- to very fine-grained mafic rock, undivided; metamorphosed; commonly deeply weathered
- AbtrYGC — Basalt; massive to weakly foliated; metamorphosed
- AbchYGC — Pyroxene spinifex-textured basalt; minor basalt; metamorphosed

- AmuarYGC — Tremolite–chlorite(–talc) schist
- AugYGC — Peridotite; metamorphosed and serpentinized

MINERAL OCCURRENCES

MINERALIZATION STYLES*
- Vein and hydrothermal
- Regolith hosted

MINERAL AND ROCK COMMODITY GROUPS
- Precious metal
- Base metal
- Energy
- Industrial mineral

MINERAL AND ROCK COMMODITIES

Copper	Cu
Gold	Au
Magnesite	Mgs
Silver	Ag
Uranium	U

OPERATING STATUS AND SITE IDENTIFICATION NUMBER

Operating mine	e.g. 17425
Abandoned mine	e.g. 17422
Mineral deposit	e.g. 4276
Mineral occurrence or prospect	e.g. 4279

Mineral occurrences and numbers are from the GSWA MINARN database.
*Longer symbols represent mines or deposits also in the DoIR MINEDEX database.

Geological boundary

Fault
- exposed
- concealed
- concealed, interpreted from aeromagnetic data

Fold, showing axial trace
- syncline, exposed, concealed
- Small-scale fold axis, showing trend and plunge
- unspecified
- anticline
- Bedding, showing strike and dip
- inclined
- vertical
- overturned
- Way-up indicator
- pillow structure
- Metamorphic foliation, showing strike and dip
- inclined
- vertical
- Gneissic banding, showing strike and dip
- inclined
- vertical
- Cleavage, showing strike and dip
- inclined
- Shear-sense indicator
- showing dip of foliation
- dextral
- inclined
- sinistral
- inclined
- vertical
- Lineation, unspecified, showing trend and plunge
- inclined
- Mineral lineation, showing trend and plunge
- inclined
- Axis of crenulation, showing trend and plunge
- inclined
- Mineral alignment, showing trend and plunge
- inclined
- Fracture, joint, or extension vein, showing strike and dip
- inclined
- vertical
- Aeromagnetic lineament
- Isotopic age determination site with identification number (TRIAD)
- Road, sealed
- Road, unsealed
- Track
- Fence, generally with trock
- Townsite, population less than 1000 — Sandstone
- Homestead — Black Range
- Building
- Yard
- Horizontal control, major, minor
- Breakaway
- Sand dune
- Contour line, 20 metre intervcl — 420
- Watercourse
- Rockhole — Rockhole
- Spring — Spring
- Pipeline — pipeline
- Bore, well — Bore, Well
- Tank — Tank
- Windpump
- Abandoned, position doubtful — (dbd) (PD)
- Mineral field boundary
- Mineral field district boundary — Christmas Bore
- Mine, abandoned mine, or deposit (names are filtered for clarity)
- Opencut or quarry
- Tailings or stockpile
- Mineral exploration drillhole showing subsurface data — IS AbYSA